The overturning circulation in a changing Arctic

Anais Magali Bretones

Thesis for the degree of Philosophiae Doctor (PhD)
University of Bergen, Norway
2023

UNIVERSITY OF BERGEN

The overturning circulation in a changing Arctic

Anais Magali Bretones

Thesis for the degree of Philosophiae Doctor (PhD)
at the University of Bergen

Date of defense: 22.11.2023

Year: 2023

Title: The overturning circulation in a changing Arctic

Name: Anais Magali Bretones

Print: Skipnes Kommunikasjon / University of Bergen

Acknowledgements

Firstly, I express my deep gratitude to my supervisor, **Kerim**, who played an essential role in my scientific and personal growth. I am immensely thankful for the freedom you granted me in the direction of my research and for encouraging me to maintain a healthy work-life balance. Thank you for encouraging me to learn Norwegian and enjoy my leisure time, especially during good weather.

I would also like to extend my gratitude to my co-supervisor, **Mari**, for the invaluable support she provided me during the initial stages of my PhD. Regular meetings and constructive feedback have been critical in shaping my ideas and writing my first paper. I also thank **Aleksi** for always being available to answer my numerous queries. Finally, I cannot thank **Marius** enough for providing continuous feedback during the final end sprint and for cranking up my motivation.

I have also been blessed with collaborations with amazing early-career scientists. I thank in particular **Ida** for helping me to get started with the EC-Earth-PISM data, **Ailin** for showing interest in my early results, and my friends and co-authors **Morven*** and **Yvan*** for their valuable insights and encouragement.

Meanwhile, I would not have come this far without **Laura**. I thank you deeply for your kindness and scientific support, despite a very different field of research. And to my close group of friends, who have been a source of constant support and happiness over the years. Our trips to Sotra, Voss, Rosendal, Hardangervidda, Sogndal, Spain, Fennel, and the mountains around Bergen have been essential for my mental well-being.

I am grateful to my great colleagues, flatmates, Su&W and weekend-in-the-office buddies, to the indestructible frokost team, the BKK volunteers and the climbing community in general, to the runnaholics, and to all the party people out there, who have made me feel at home in Bergen. I especially thank **Karita***, who inspired me and helped me to organize myself even before I officially started my PhD, and until the end. I also thank **Andreas**, my Landåslien flatmates (**Fran**, **Lander** and **Meike**), **Nadine**, **Augustin**, **Helene***, and **Stefanie*** for introducing me to the institute and life in Norway. I am also grateful to **Alexios**, **Elina**,

Kim, **Sonja**, **Paul**, **Idunn**, **Axel**, **Xabier**, **Jakob**, and **Liza** & Miko for animating the second and slow (COVID) part of my PhD. In the final year, I am thankful to **Danielle**, **Kristine**, **Julien**, **Inès**, **Artem**, **Mats**, **Sandro**, **Konstanze**, **Therese**, **Johanne**, **Vår**, **Heather***, **Guillaume***, and **Léo** for spicing my life up. Finally, I give a big thanks to my friends and colleagues who took the time to read and comment on my thesis in a record time (*), and also to everyone else who offered to read it.

I would also like to thank the staff at the cantina for providing delicious food, smiles, and hugs. The foosball table installed by the MET office was also a critical addition during my breaks towards the end. Lastly, I would like to thank my family for their persistent support, allowing me to stay in Bergen for five years without any complaints (well, not too many!).

Abstract in English

Dense water formation happens in the open water Arctic Ocean as a result of strong air-sea fluxes. By substantially reducing air-sea exchanges, the sea ice determines the regions of dense water formation; however, the sea ice is retreating fast under increased greenhouse gas emissions. While recent studies indicate that the Arctic could be an important source of dense water for the Atlantic Meridional Overturning Circulation (AMOC), it is unclear how the changes in dense-water formation under sea-ice retreat impact the overturning. This can be explained by the lack of studies looking at the overturning in the Arctic.

In Paper I, we present a method to study the northernmost extension of the AMOC in a model using a tripolar grid and apply it to a simulation of EC-Earth-PISM forced with a high emission scenario (RCP8.5) to investigate the effect of the winter sea-ice retreat on the circulation. With this new method, we capture the Arctic overturning north of the Greenland-Scotland Ridge, and name it the Arctic Meridional Overturning Circulation (ArMOC). We show that the sea-ice retreat leads to a northward shift in dense-water formation sites and a transient enhancement of the ArMOC until 2100. We further suggest that the ArMOC strengthening reduces the overall weakening of the AMOC in a future warming climate.

To account for model variability, we extend the analysis of Paper I to eight CMIP6 models forced with a similar high-emission scenario (SSP5-8.5) in Paper II. Using water mass transformation calculations based on the outcrop of dense layers and associated surface fluxes during winter, we show that the ArMOC strengthens consistently with the increase in dense-water formation north of the Greenland-Scotland Ridge. However, there is a large model spread in the timing and amplitude of the ArMOC strengthening, which reflects on the heat transport into the Arctic. In addition, the ArMOC starts weakening before the year 2050 in the majority of the models, in contrast to Paper I.

In Paper III, we further investigate the relation between sea ice and overturning by analyzing a simulation reproducing a rapid sea-ice retreat consistent with a past abrupt warming event from the last glacial period. The release of freshwater in the North Atlantic and Nordic Seas forces a cold state with winter sea ice covering the entire North Atlantic, and the termination of the freshwater forcing triggers the transition toward warmer condition and an

ice-free Nordic Seas. In this simulation, the appearance of deep convection as sea ice retreats strengthens the AMOC and activates an estuarine (salinity-driven) overturning circulation that enhances the stratification and temporarily inhibits convection.

Based on the results of the three papers, I conclude that the ArMOC depends on dense-water formation and Arctic stratification, both of which are tightly linked to the sea-ice cover. I suggest further investigations of the mechanism leading to an ArMOC enhancement, since it impacts the heat transport into the Arctic, and therefore, the sea-ice reduction, and could delay the AMOC weakening. In addition, these results highlight the need for an improved representation of the Arctic stratification in models.

Abstract in Norwegian

Ved å begrense varmeutvekslingen mellom hav og atmosfære bestemmer sjøisen området for dannelse av dypvann i Arktis. Under økte klimagassutslipp trekker sjøisen seg nordover. Mens nyere studier tyder på at Arktis kan være en viktig kilde til dypvann som mater den nedre grenen av den Nord-Atlantiske omveltningssirkulasjonen (AMOC), er det uklart hvordan redusert sjøis-dekke vil påvirke omveltningen. Dette kan forklares med mangelen på studier som ser på Arktis sitt bidrag til omveltningssirkulasjonen.

I Paper I presenterer vi en metode for å studere den nordligste forlengelsen av AMOC i en modell med et tripolart modell-grid. Metoden brukes på en simulering av EC-Earth-PISM med et høyutslippsscenario (RCP8.5) for å undersøke effekten av redusert sjøis på sirkulasjonen. Med den nye metoden fanger vi opp den arktiske omveltningen nord for Grønland-Skottland-ryggen og gir denne navnet Arctic Meridional Overturning Circulation (ArMOC). Vi viser at sjøisens tilbaketrekning fører til en forflytning av områder med dypvannsdannelse nordover og en forbigående styrking av ArMOC frem til 2100. Vi foreslår videre at styrkingen av ArMOC reduserer den generelle svekkelsen av AMOC i et fremtidig varmere klima.

For å ta høyde for modellforskjeller utvider vi analysen i Paper I til åtte CMIP6-modeller med et lignende høyutslippsscenario (SSP5-8.5) som i Paper I. Vi viser at ArMOC styrker seg konsekvent med økningen av dypvannsdannelse nord for Grønland-Skottland-ryggen, evaluert ved hjelp av vannmassetransformasjons beregninger. Det er imidlertid store modellforskjeller i timingen og magnituden til styrkningen av ArMOC, noe som gjenspeiles i varmetransporten inn i Arktis. I motsetning til Paper I, begynner ArMOC å svekkes før år 2050 i flertallet av modellene.

I Paper III undersøker vi videre forholdet mellom sjøis og omveltning ved å analysere en simulering som gjenskaper en rask tilbaketrekning av sjøis i samsvar med en tidligere brå oppvarming under den siste istiden. Utslipp av ferskvann i Nord-Atlanteren og den nordiske hav tvinger fram en kald tilstand med vinter-sjøis som dekker hele Nord-Atlanteren, og terminering av ferskvannspådrivet utløser overgangen mot varmere tilstander og et isfritt Nordisk hav. I denne simuleringen styrkes utseendet til dyp konveksjonen når havis trekker seg tilbake, AMOC styrkes og det aktiverer en estuarin (saltholdighetsdrevet) omveltningssirkulasjon som

forsterker stratifiseringen og midlertidig hemmer konveksjon.

Basert på resultatene fra de tre artiklene som utgjør denne doktorgradsoppgaven, konkluderer jeg med at ArMOC er avhengig av dypvannsdannelse og den arktiske stratifiseringen, som igjen er tett knyttet til sjøisen. Jeg foreslår ytterligere undersøkelser av mekanismen som fører til en ArMOC-styrking, fordi dette påvirker varmetransporten inn i Arktis og dermed også reduksjonen av sjøis. I tillegg fremhever resultatene behovet for en forbedret representasjon av den arktiske stratifiseringen i modeller.

List of publications

1. Anaïs Bretones, Kerim H. Nisancioglu, Mari F. Jensen, Ailin Brakstad, Shuting Yang, *Transient increase in Arctic deep-water formation and ocean circulation under sea-ice retreat*, Journal of Climate, **35(1)**, 109-124, 2022.

2. Anaïs Bretones, Aleksi Nummelin, Kerim H. Nisancioglu, Morven Muilwijk, *Arctic Overturning Circulation (ArMOC) strengthening in CMIP6 models*, Submitted to Journal of Climate.

3. Anaïs Bretones, Chuncheng Guo, Yvan Romé, Kerim H. Nisancioglu, *Arctic circulation changes at the transition from a Heinrich stadial to a Greenland interstadial*, Manuscript prepared for submission to Climate of the Past.

Contents

Chapter 1

Introduction

1.1 From the Atlantic to the Arctic: motivations

In the North Atlantic, the Atlantic meridional overturning circulation (*AMOC*) refers to the northward transport of relatively warm water in the upper ocean (*Atlantic water*) and the southward transport of colder water at depth (*North Atlantic deep water*). Because of the difference in temperature of these two water masses, the overturning is associated with a net northward heat transport contributing to about 70% of the global oceanic heat transport (*Ganachaud and Wunsch*, 2003). Key elements of the northern limb of the Atlantic overturning circulation are shown in Figure 1.1.

Fluctuations in the AMOC have been linked to multidecadal changes in sea surface temperatures across the North Atlantic, a phenomenon known as Atlantic Multidecadal Variability (*Zhang et al.*, 2019). Consequently, AMOC variations have far-reaching consequences for Arctic sea ice and surface air temperature over Europe, North America, and Asia on these time scales. Meanwhile, reconstructions of AMOC strength, based on proxy records, indicate large variations of the AMOC in the past (*Caesar et al.*, 2021) and in particular during abrupt climate shifts of the last glacial period (*Lynch-Stieglitz*, 2017). Further, the AMOC has been considered as one of the potential drivers behind these abrupt climate shifts (*Rahmstorf*, 2002). Therefore, the structure, variability, and driving mechanisms of the AMOC have garnered substantial scientific attention over the past several decades (*Buckley and Marshall*, 2016; *Zhang et al.*, 2019; *Johnson et al.*, 2019; *Jackson and Petit*, 2023).

The importance of the AMOC has motivated the deployment of several mooring arrays across the Atlantic, providing continuous observations of the overturning at specific latitudes. The first array was deployed in 2004 at 26°N to monitor the heat transport associated with the Gulf Stream (RAPID program; *Cunningham*, 2008). However, modeling studies suggest that

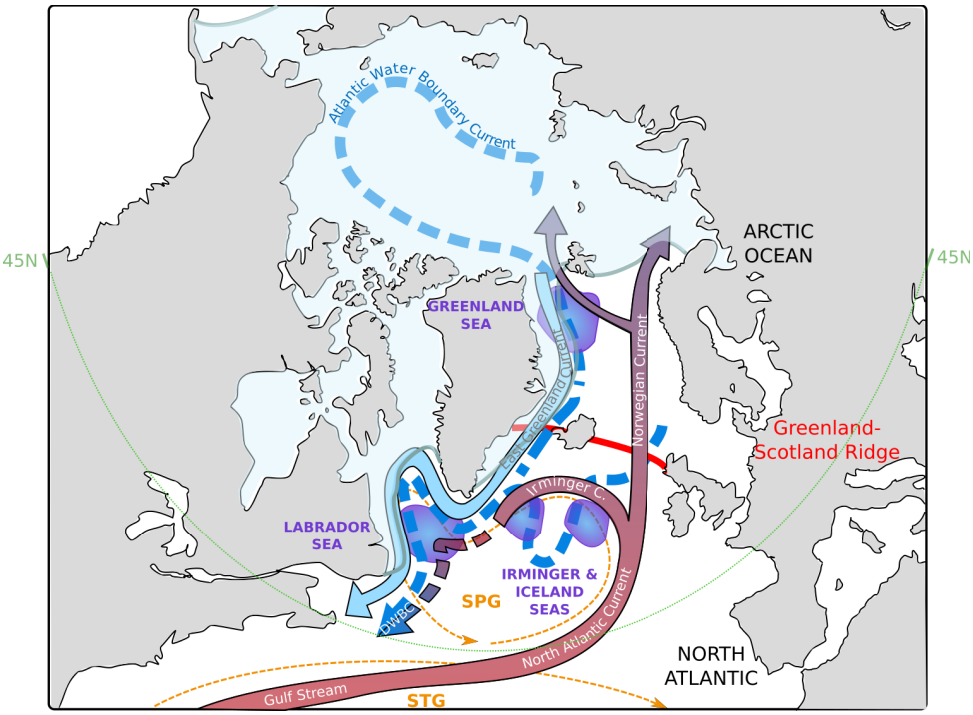

Figure 1.1: Main surface (plain arrows) and deep (dashed arrows) currents in the North Atlantic and Arctic Ocean. The colors of the arrows indicate different water characteristics: warm and saline (red), cold and saline (blue), and cold and fresh (light blue). In the North Atlantic, the currents are associated with horizontal wind-driven circulations: the Subtropical (STG) and Subpolar (SPG) gyres. In addition, light blue coloring indicates the approximate position of the winter sea-ice cover and the purple-blue-filled circles show regions of high water-mass transformation.

the overturning variability varies with latitude, with a shift at 40°N, suggesting a change in the forcing mechanisms (*Bingham et al.*, 2007). Therefore, an array was deployed in 2014 in the subpolar region (Overturning in the Subpolar North Atlantic Program, OSNAP; *Lozier et al.*, 2019) across the Labrador Sea (OSNAP-West) and between Greenland and Scotland (OSNAP-east). Estimates of the mean Arctic overturning circulation (*Eldevik and Nilsen*, 2013; *Tsubouchi et al.*, 2023) were also made possible since the mid-1990s by the systematic monitoring of volume transport across the Greenland-Scotland Ridge (*Østerhus et al.*, 2019) and across the Bering Strait (*Woodgate*, 2018). While these arrays play a fundamental role in the study of ocean overturning, the observation period is still too short to disentangle trends from interannual or decadal variability. Consequently, climate models remain key in our understanding of overturning changes in a warming climate.

The underlying mechanisms of AMOC variability depend on both timescale and region (*Buckley and Marshall*, 2016; *Kostov et al.*, 2021). On seasonal to interannual timescales, AMOC

variability is primarily the response to local wind forcing, while the transformation of water-masses toward higher densities (*dense-water formation*) becomes more important on decadal, and higher, timescales. At high latitudes, dense-water formation is associated with the production of North Atlantic deep water and has canonically been thought to take place through deep convection in the Labrador and Greenland Seas (*Buckley and Marshall*, 2016; *Johnson et al.*, 2019). However, recent observations from the OSNAP array suggest that Labrador Sea convection contributes minimally to the strength of the Atlantic meridional overturning circulation and that the source waters of the AMOC lower limb mainly originate from the transformation of Atlantic water north of the OSNAP array (*Lozier et al.*, 2019). This transformation takes place both in the Irminger and Iceland Seas (*Petit et al.*, 2020) and in the Nordic Seas (*Chafik et al.*, 2019), but model results also suggest a substantial contribution from the Arctic basins (*Zhang and Thomas*, 2021).

For the future, climate models project a weakened overturning circulation in the North Atlantic under increased greenhouse gas emissions (*Weijer et al.*, 2020; *Asbjørnsen and Årthun*, 2023). Moreove, certain studies suggest the possibility of a tipping point and the potential for an AMOC collapse (*Ditlevsen and Ditlevsen*, 2023). However, the likelihood of this occurrence is presently a subject of ongoing debate and intensive investigation. Meanwhile, present and future overturning changes in the Arctic domain remain largely unexplored (*Bitz et al.*, 2006; *Eldevik and Nilsen*, 2013; *Haine*, 2021), despite climate change being most pronounced in this region (*Rantanen et al.*, 2022).

In this dissertation, I will investigate the overturning circulation north of the Greenland Scotland Ridge, an overturning hereby referred to as the Arctic meridional overturning circulation (ArMOC). The Arctic region has a unique hydrography, as detailed in Section 1.2, including the interplay of Atlantic water transformation and circulation with sea ice processes, as discussed in Section 1.3. While rapid and profound changes are projected in the Arctic under global warming (see Section 1.2), there are examples from the last glacial period where changes of comparable magnitude are thought to have been influenced in a significant way by the overturning circulation (see Section 1.5).

1.2 The Arctic Ocean and its water masses

In this work, I define the Arctic Ocean as the seas and basins located between the Greenland-Scotland Ridge (GSR) and the Bering Strait (Fig. 1.2). The term Arctic Ocean is often used to refer to the Arctic basins (Eurasian and Canadian basins), and sometimes includes the contiguous shelf seas (Beaufort, Chukchi, East Siberian, Laptev, Kara, and Barents Seas). Including also the Nordic Seas (Norwegian, Greenland, and Iceland Seas), the region has been

Figure 1.2: Map of the Arctic Ocean restyled after *Rudels and Quadfasel* (1991). The light blue and dark blue contour lines indicate the 500 m and 2000 m isobaths. Both the Bering Strait and the Nares Strait are shallower than 500 m. The GSR presents deeper sections between the Faroe and Shetland islands (Faroe Shetland Channel, 850 m) and in the west between Greenland and Iceland (Denmark Strait, 650 m).

referred to as the Arctic Mediterranean Sea by *Aagaard et al.* (1985). These different terms are used to unify regions sharing similar hydrography, bathymetry, or processes. However, the hydrography is dependent on the climatic conditions and has likely varied through time. For example, some parts of the Arctic basins may have a hydrography resembling the Atlantic's hydrography in the future (see Section 1.3), and conversely, the Nordic Seas might have looked more like the Arctic basins during cold periods of the last glacial (*Dokken et al.*, 2013). On the other hand, the GSR is a clear limit between the wide and deep Atlantic Ocean, and the patchwork of seas, narrow passages, and ridges present farther north. This topographic barrier has been limiting exchange between the Atlantic and the Arctic Mediterranean for at least 12 Ma before present (*Uenzelmann-Neben and Gruetzner*, 2018) and roughly coincides with the Arctic Circle (66°N). Here, I use the GSR as the southern limit of the Arctic Ocean in the Atlantic.

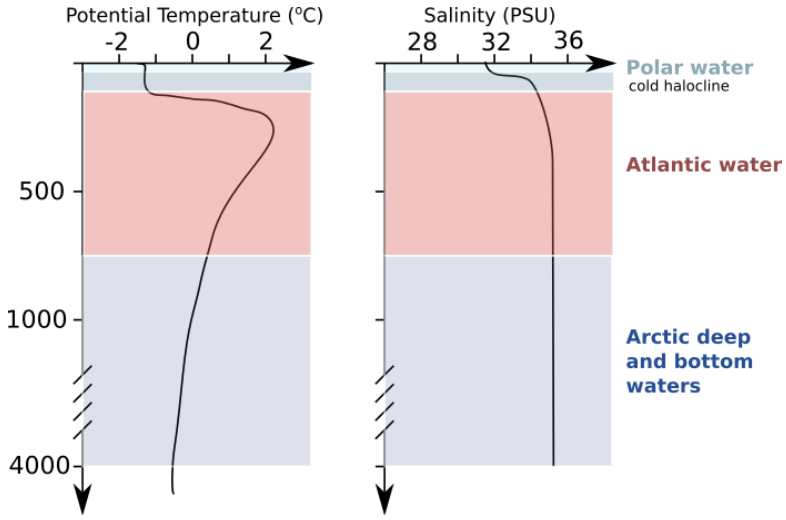

Figure 1.3: Sketch of the typical water column structure in the Arctic basins (Canadian and Eurasian basins) based on *Bluhm et al.* (2015): a cold and fresh layer (Polar water) is separated from a warm and saline intermediate layer (Atlantic water) by a cold layer with a strong gradient of salinity (the cold halocline). Below 600 m, the ocean is filled with relatively cold and saline water (Arctic deep and bottom waters).

In contrast to the tropics, precipitation exceeds evaporation in the polar regions, resulting in anomalously fresh surface water. This effect is amplified in the Arctic Ocean since it is surrounded by a large catchment area for precipitation, discharging additional freshwater through river runoff (*Rudels and Carmack*, 2022; *Nummelin et al.*, 2017). As a result of reduced insolation at high latitudes, the Arctic Ocean is anomalously cold: an effect that is amplified by the presence of sea ice reflecting solar radiation. This imbalance in freshwater and heat is partly compensated by the exchange with the Atlantic Ocean (see Fig. 1.1 and Section 1.3).

The Arctic Ocean is characterized by its three largest water masses (*Haine*, 2021). The Atlantic water is limited to the top 700 m in the Arctic Ocean due to the GSR limiting the inflow. Meanwhile, the Atlantic water is relatively warm ($> 0°$C; *Rudels*, 2015) and thus lighter (more *buoyant*) than the underlying Arctic deep and bottom waters.
In the Arctic basins, the Atlantic water is replaced by a fresh and highly buoyant layer of Polar water at the surface (Fig. 1.3). The Polar water is the product of Atlantic water mixing with freshwater from the large rivers runoff in the Arctic as well as meltwater from the Greenland ice sheet and seasonal sea ice. The cold temperature of the Polar water ($< 0°$C; *Rudels*, 2015) is maintained by the contact with perennial sea-ice cover, and it is isolated from the underlying Atlantic water by a similarly cold layer presenting a strong salinity gradient: the *cold halocline*.

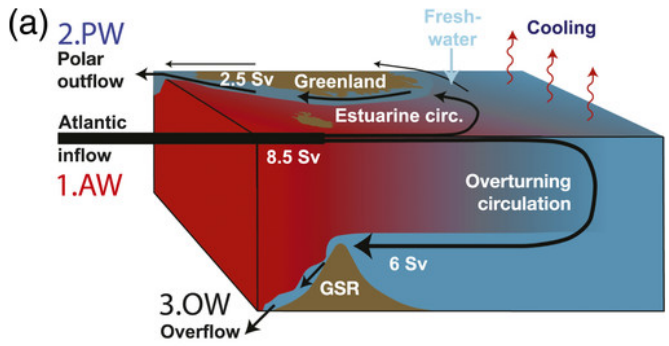

Figure 1.4: The overturning circulation and estuarine circulation in the Arctic as seen by *Eldevik and Nilsen* (2013). In this system, 8.5 Sv of Atlantic water enters the Arctic Ocean. 6 Sv of this inflow densifies through cooling and exits the Arctic as Overflow water (overturning circulation) while 2.5 Sv is mixed with freshwater and returns south via the East Greenland Current (estuarine circulation).

The salinity gradient results in strong layering in density (*stratification*), which is a fundamental characteristic of the Arctic Ocean. In addition, the export of cold and fresh Polar water through the East Greenland Current (Fig. 1.1) promotes sea-ice formation along its way by isolating the sea ice from the warm Atlantic water.

If the stratification were to break, it would lead to sea-ice retreat, by exposing the surface layers to the warm Atlantic water (*Polyakov et al.*, 2017; *Dokken et al.*, 2013). The hydrography of the different basins in the Arctic and the presence of sea ice are thus tightly linked to the freshwater input to the Arctic Ocean as well as the circulation and inflow of warm Atlantic water.

1.3 The Arctic overturning circulation

The mean circulation in the Arctic and exchange with the Atlantic Ocean can be described through the concept of double estuarine circulation (*Carmack and Wassmann*, 2006; *Rudels*, 2010; *Eldevik and Nilsen*, 2013; Fig. 1.4). In the double estuarine circulation, the circulation is divided into two cells: the estuarine circulation and the ("anti-estuarine") overturning circulation. These two cells present opposing directions of circulation, each driven by different buoyancy forcing mechanisms.

The estuarine circulation is a salinity-driven cell, usually seen as a horizontal circulation. It is sometimes referred to as estuarine overturning circulation (*Wilson and Straneo*, 2015; *Gräwe et al.*, 2016; *Muchowski et al.*, 2023) as it also has a small vertical signature. In this cell,

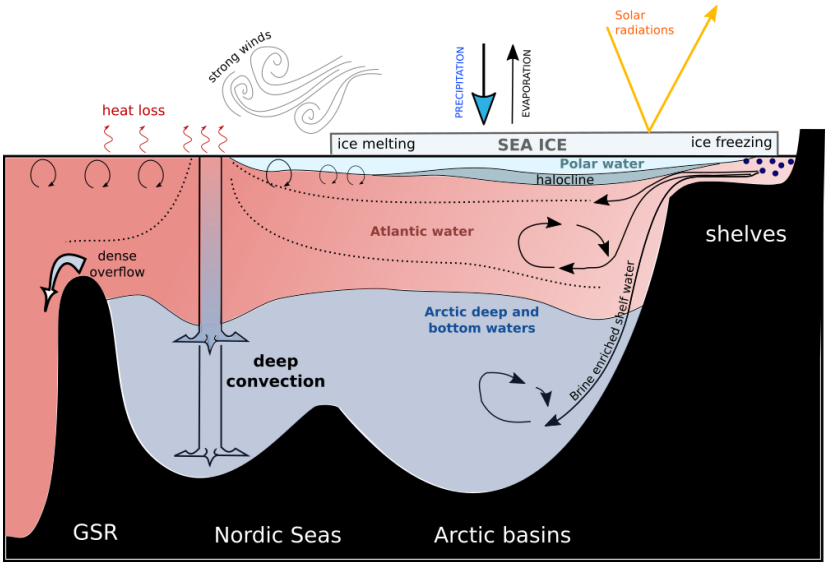

Figure 1.5: Sketch presenting key physical processes occurring in the Arctic Ocean (inspired by *Aagaard et al.*, 1985) and setting the hydrography of the different regions: the Polar water is the result of high freshwater flux to the Arctic (precipitation-evaporation and river runoff) and limited mixing with the Atlantic water due to the presence of the halocline and sea ice, while the Arctic bottom water comes from the densification of Atlantic water (through deep convection and entrainment by brine enriched shelf water). Some of the Arctic bottom water exits the Arctic Ocean as dense overflow while the rest remains trapped by the GSR.

the Atlantic water enters the Arctic Ocean through the Norwegian Atlantic Current (Fig. 1.1) and mixes with colder and fresher waters close to Svalbard and in the Barents Sea. The resulting water mass (Polar water) is more buoyant and is then exported southward at the surface within the East Greenland Current (Fig. 1.1). In depth space, this circulation appears anti-clockwise with a relative upward motion of the Atlantic water.

The overturning circulation is a thermally-driven cell, which has both horizontal and vertical components. Referred to as the Arctic overturning and ArMOC in Section 1.1, this cell corresponds to the northernmost extension of the AMOC and constitutes the central focus of interest in this dissertation. Within this circulation cell, Atlantic water undergoes a process of densification and downward motion as it traverses the Arctic Ocean (Fig. 1.1). The densification of Atlantic water occurs through two processes: heat loss and entrainment by brine-enriched shelf water (Fig. 1.5).

During winter, the heat loss to the atmosphere is stronger, especially in the presence of powerful and cold winds originating from the land or sea-ice cover. In the case of strong cooling and weak stratification, larger-scale mixing is initiated, referred to as deep convection. Deep convection involves an entrainment of Atlantic water, sometimes all the way to the sea floor, and has been observed in the North Atlantic (Labrador Sea; *Våge et al.*, 2009), in the Nordic Seas (Greenland Sea; *Brakstad et al.*, 2019), and more sporadically in the Irminger Sea (*de Jong and de Steur*, 2016).

In the Arctic basins, the perennial sea-ice cover reduces air-sea interactions and mechanical mixing induced by wind, consequently inhibiting the occurrence of deep convection. However, the Arctic shelves are places of high sea-ice production where winds maintain open water conditions by exporting the sea ice formed. The salt expelled (*brine*) as sea ice forms becomes substantial and results in the formation of denser water. This water is entrained down the slope toward the deeper basins, mixing with the relatively warm Atlantic water.

The dense water formed contributes to renewing the Arctic deep and bottom waters and feeds the Atlantic Water Boundary Current (Fig. 1.1). It is exported southward through the Fram Strait before it finally exits the Arctic as dense overflow water at the GSR (Fig. 1.4). The ArMOC's strength at the GSR was estimated to be approximately 6 Sv by *Østerhus et al.* (2019).

1.4 The changing Arctic

The Arctic is currently warming four times as fast as the global mean (*Rantanen et al.*, 2022) and is transitioning to a new, warmer, seasonally ice-free climate state (*Landrum and*

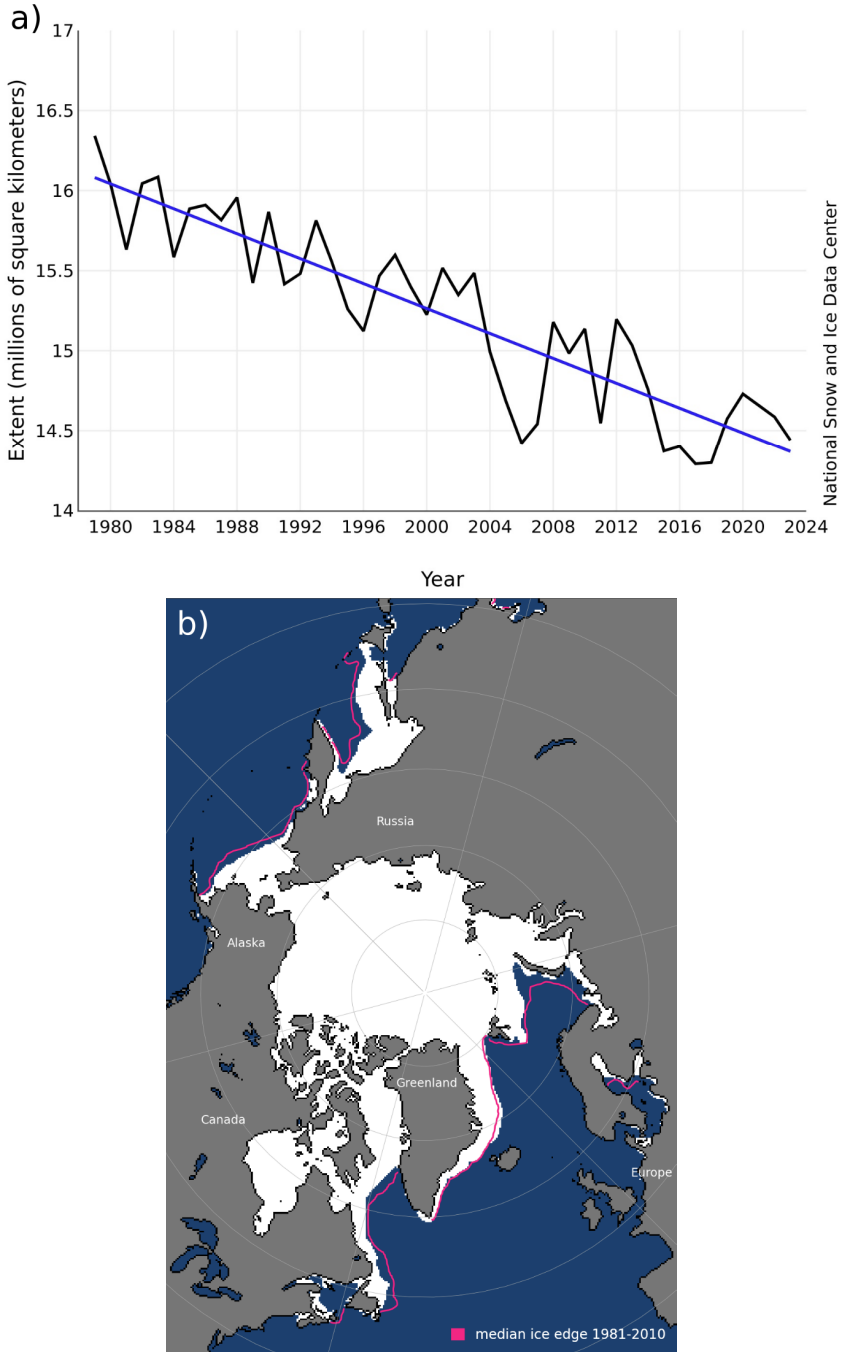

Figure 1.6: Average March sea-ice extent from 1979 to 2023 (a) and map of the mean sea-ice extent in March 2023 (b). The pink line indicates the 1981 to 2010 average. Credit: National Snow & Ice Data Center (Boulder, Colorado)

Holland, 2020). The changing Arctic climate has possible implications for the structure and strength of the Arctic overturning circulation (*Shu et al.*, 2022) and small biases in climate models can have great implications for future projections. In addition to changes to the circulation, a reduction of the sea-ice cover will greatly affect marine ecosystems and fauna (*Ingvaldsen et al.*, 2021).

A retreating sea-ice cover is a visible manifestation of ongoing Arctic climate change. The sea-ice reduction over the last four decades can be quantified and visualized thanks to the development of satellite remote sensing. Services, such as those of the National Snow & Ice Data Center, provide daily updates and basic analysis of the state of Arctic sea-ice cover (`http://nsidc.org/arcticseaicenews/`). Based on these data, it has been found that the Arctic sea ice cover has decreased in all seasons and all regions since satellite observations started in 1979 (*Comiso et al.*, 2017; *Onarheim et al.*, 2018). Figure 1.6 shows for example the mean sea-ice extent in March 2023 compared with the mean sea-ice edge since 1981. As reported in previous studies (e.g., *Onarheim et al.*, 2018), we see a clear retreat of the winter sea-ice edge in the Barents Sea, especially in the direction of the Kara Sea. In addition, two areas north of Svalbard, at the boundary between the Barents Sea and the Eurasian Basin, are now free of sea ice (e.g., *Onarheim et al.*, 2014). The sea-ice retreat is currently more dramatic during summer than winter. Overall, the winter (maximum) and summer (minimum) sea-ice extent have been reducing at a rate of 2.5% and 10.8% per decade, respectively, between 1979 and 2016 (*Comiso et al.*, 2017). Moreover, the shrinking of the sea-ice cover has been accompanied by a reduction in the presence of thicker multiyear sea ice. (*Lindsay and Schweiger*, 2015; *Kwok*, 2018) report a reduction of the annual mean sea-ice thickness of 65% in the Arctic basins during the period from 1975 to 2012. Under further emissions, these trends are expected to continue. Ultimately, the Arctic is expected to become seasonally free of sea ice before the year 2050, according to the Coupled Intercomparison Model Phase 6 (CMIP6) models that best capture the observed sea-ice retreat (*Notz and SIMIP Community*, 2020). It should be emphasized that the sea-ice cover in both summer and winter is exposed to large natural variability on interannual to multidecadal timescales (*Laxon et al.*, 2003; *Barnhart et al.*, 2016; *Årthun et al.*, 2019; *Wettstein and Deser*, 2014; *Ding et al.*, 2017). This variability translates into large uncertainty in the timing of ice-free conditions (*Årthun et al.*, 2021).

The retreat of the sea-ice edge observed in Figure 1.6 is reminiscent of the location of the warm surface currents in the Arctic Ocean (Fig. 1.1), and several studies have related the retreating winter sea-ice cover in the Barents Sea to enhanced ocean heat transport into the region (e.g., *Årthun et al.*, 2012; *Smedsrud et al.*, 2013). Observations from recent decades indicate that the ocean heat transport toward the Arctic has increased (*Tsubouchi et al.*, 2020; *Smedsrud et al.*, 2022) and this increased influence of Atlantic water in the region has been termed an "Atlantification" of the Arctic Ocean (*Årthun et al.*, 2012; *Polyakov*

et al., 2017). Model studies furthermore suggest that the Atlantification of the Arctic is expected to continue in the future (*Muilwijk et al.*, 2023). One of the main manifestations of Atlantification is a weakening of the water column stability in the Barents Sea (*Lind et al.*, 2018) and Eurasian Basin (*Polyakov et al.*, 2017). A continued Atlantification of the Arctic could therefore potentially lead to a breakdown of the water column structure presented in Figure 1.3 with implications for ocean convection and water mass transformation.

The ongoing sea-ice retreat along the margins of the Arctic Ocean also leads to further cooling and modification of the warm Atlantic waters (*Våge et al.*, 2018; *Pérez-Hernández et al.*, 2019). As the transition towards a seasonally ice-free Arctic Ocean continues, enhanced water mass transformation can thus be expected, leading to a possible strengthening of the Arctic overturning circulation (e.g., *Bitz et al.*, 2006; *Brodeau and Koenigk*, 2016; *Lique and Thomas*, 2018). The Arctic overturning circulation could therefore be a stabilizing factor in a weakening AMOC, highlighting the importance of understanding its drivers and its response to climate change.

1.5 Past abrupt warming in the Arctic

The current warming rate experienced by portions of the Arctic (1°C per decade; *Jansen et al.*, 2020) is comparable to the natural abrupt climate transitions that occurred during the last glacial period and known as Dansgaard–Oeschger (D-O) events (Fig. 1.7). The footprint of D-O events was first identified in Greenland ice cores (*Bond et al.*, 1993) and are associated with rapid sea-ice retreat (*Dokken et al.*, 2013). Understanding the mechanisms at play during these past rapid climate shifts can give us insight into the current and projected Arctic sea-ice retreat (*Jansen et al.*, 2020).

D-O events happened regularly between 60-27 kyr before present and resulted in major disruptions of the North Atlantic climate. A D-O cycle lasts between 400 and 2600 years (*Wolff et al.*, 2010) and is composed of a cold and relatively stable phase (the *stadial*), an abrupt warming (the D-O transition or D-O event) to a relatively warm phase (the *interstadial*), followed by a more or less abrupt cooling back to stadial conditions (*Lohmann and Ditlevsen*, 2019). The D-O warming is characterized by a sustained temperature increase of about 1°C per decade (see periods stressed in red in Fig. 1.7) and can lead to a maximum temperature increase of 16.5°C on the Greenland ice sheet (D-O 10, *Kindler et al.*, 2014). Proxy-based studies indicate that the temperature oscillations in Greenland are tightly linked to the advance and retreat of the sea-ice cover (*Hoff et al.*, 2016). In particular, *Dokken et al.* (2013) highlight the presence of an extensive sea-ice cover in the Nordic Seas during the stadials, based on the presence of a cold halocline, contrasting with sea-ice free conditions during the

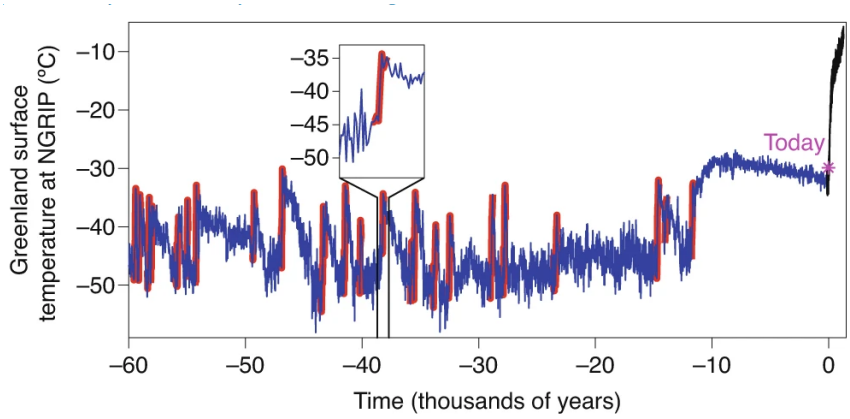

Figure 1.7: Past and future temperatures at the NGRIP deep ice coring site in Greenland, with a close-up on the transition from the Heinrich stadial 4 to the Greenland interstadial 8 at 38 ky before present (*Jansen et al.*, 2020). The red lines stress the periods of abrupt warming (1° per decade, or more, sustained for at least 40 years).

interstadials. *Dokken et al.* (2013) further show that there is a gradual warming of the subsurface in the Nordic Seas during the stadial period, followed by a warm overshoot at the onset of the interstadial period. As a result of a weakening of the water column stratification, sea ice could retreat abruptly and lead to the release of the accumulated subsurface heat (*Bassis et al.*, 2017).

The changes in the sea-ice cover have also been associated with changes in dense-water formation (*Li and Born*, 2019; *Sadatzki et al.*, 2019), which in turn modulates the AMOC strength. In fact, the AMOC has long been proposed as the main driver of the D-O oscillations (*Rahmstorf*, 2002). In this scenario, an AMOC strengthening (resp. weakening) results in increasing (resp. decreasing) heat transport into the North Atlantic and Nordic Seas, thereby accelerating sea ice melting (resp. growth) and heat loss to the atmosphere. Proxy data suggest the existence of several AMOC modes during the last glacial period (*Böhm et al.*, 2015): a strong AMOC mode associated with dense-water formation in the Nordic Seas during the interstadial periods; a shallow and weak AMOC mode during the stadial periods; and an off-mode associated with periods of large iceberg discharges called Heinrich events (*Heinrich*, 1988).

The transition from a strong to a weak AMOC mode, hence from warm interstadial to cold stadial, has been linked to anomalous freshwater fluxes associated with episodes of ice-sheet retreat and enhanced calving (*Birchfield et al.*, 1994). When directed at dense-water formation regions, an anomalous freshwater flux could indeed suppress convection (*Roche et al.*, 2010) and as a result, induce an AMOC weakening. In climate models, freshwater hosing experiments have emerged as an efficient way to trigger abrupt climate

transitions (*Manabe and Stouffer*, 1995). The amount of freshwater needed to obtain a significant AMOC weakening is strongly model dependent (*Kageyama et al.*, 2010) and only a few models manage to obtain the observed climatic response with realistic values for the freshwater (*Obase and Abe-Ouchi*, 2019; *Romé et al.*, 2022). In addition, it was shown that the AMOC weakening precedes the arrival of icebergs and the required surface freshening by 1000 years (*Marcott et al.*, 2011), which questions the input of freshwater as a mechanism to explain the observed abrupt transitions of the last glacial.

In this dissertation, I do not have the ambition to determine the main driver of D-O cyles, instead, I study the mechanisms at play during one D-O event, focusing on the interactions between sea ice and the overturning circulation, with particular attention to the Arctic. Studies focusing on the Arctic overturning changes accompanying the transition are lacking. Evaluating the overturning locally could be all the more interesting in a transition from Heinrich stadial to interstadial since Heinrich stadials are associated with a strongly reduced AMOC. In addition, the anomalous freshwater fluxes could also impact the estuarine circulation.

Given that the D-O events are the largest and most abrupt climate shifts as of yet recorded in the Arctic, they could also shed light on the current accelerating trends of sea ice retreat and rapid warming currently observed in the Arctic.

Chapter 2

Objectives and methods

2.1 Objectives

The main objective of this thesis is to provide new insights into the overturning circulation in the Arctic, and in particular, its dependency on the sea-ice cover. To this end, I will endeavor to answer the following questions:

- How can we assess the overturning in the North Atlantic and Arctic regions? (Paper I)
- How does the Arctic overturning change under future sea-ice retreat and what are its main drivers in climate models? (Papers I&II)
- Are there similarities between future and past circulation in the Arctic under rapid sea-ice retreat? (Paper III)
- What are the effects of enhanced freshwater flux on the Arctic overturning? (Papers I&III)

2.2 Data

To answer the objectives of this thesis, we use climate model simulations of present and future climate change (Papers I&II) and of climate change during the transition from stadial to interstadial conditions (Paper III). These simulations were carried out with earth system models from eight families of models: EC-Earth (EC-Earth-PISM in Paper I, EC-Earth3 in Paper II), NorESM (NorESM2-MM in Paper II, NorESM1-F in Paper III), IPSL-CM6, UKESM1-0-LL, ACCESS-ESM1-5, CanESM5, and MRI-ESM2-0.

Model name	Ocean component	horizontal resolution	vertical resolution	Sea-ice component	reference
EC-Earth2.3	NEMO3.6	60 km	75 levels	NEMO-LIM2	*Hazeleger et al.* (2012)
EC-Earth-PISM	NEMO3.6	60 km	75 levels	NEMO-LIM2	*Madsen et al.* (2022)
CanESM5	NEMO3.4.1	60 km	45 levels	NEMO-LIM2	*Swart et al.* (2019)
EC-Earth3	NEMO3.6	60 km	75 levels	NEMO-LIM3	*Döscher et al.* (2022)
MRI-ESM2-0	MRI.COM4.4	55 km	61 levels	MRI-COM4.4	*Yukimoto et al.* (2019)
UKESM1-0-LL	NEMO-HadGEM3-GO6.0	61 km	75 levels	CICE-HadGEM3-GSI8	*Sellar et al.* (2020)
ACCESS-ESM1-5	ACCESS-CM2	51 km	50 levels	CICE4.1	*Ziehn et al.* (2020)
CNRM-CM6-1	NEMO3.6	60 km	75 levels	GELATO 6.1	*Voldoire et al.* (2019)
IPSL-CM6A-LR	NEMO3.6	60 km	75 levels	NEMO-LIM3	*Lurton et al.* (2020)
NorESM2-MM	BLOM	43 km	70 levels*	CICE5.2.1	*Seland et al.* (2020)
NorESM1-F	BLOM	43 km	53 levels*	CICE4	*Guo et al.* (2019a)

Table 2.1: Characteristics of the model simulations used in Paper I, Paper II and Paper III. The horizontal resolution corresponds to the mean distance between the grid cells in the Arctic.

Section 2.2.1 and Section 2.2.2 give more insights into the simulation's differences and their credibility.

2.2.1 Model simulations

In Papers I and II, we use model simulations from the Coupled Model Intercomparison Project phase 5 (CMIP5; *Taylor et al.*, 2012) and phase 6 (CMIP6; *Eyring et al.*, 2016) archives, respectively. The models were configured in accordance with the protocols of the 5^{th} or the 6^{th} phase of the Coupled Model Intercomparison Project, which represent the current state-of-the-art in terms of climate projections. The models were forced with pre-industrial atmospheric forcing conditions until the years 2006 (Paper I) or 2014 (Paper II), and with high-emission scenarios on-wards (RCP8.5 in Paper I, ssp5-8.5 in Paper II) to ensure a subsequent sea-ice retreat. This choice of RCP and SSP scenarios, as opposed to a $4\times CO_2$ experiment for example, allows for a more realistic representation of the timing of sea-ice changes in response to increasing emissions, aligning better with observed climate trends.

In Paper I, the model (EC-Earth2.3; *Hazeleger et al.*, 2012) is coupled to a dynamic Greenland ice sheet model (PISM) and run until 2300 to evaluate the impact of additional freshwater flux resulting from the ice sheet melting. In addition, the length of the simulation has the advantage of capturing the entire transition to perennially ice-free conditions in the Arctic. In Paper I, using only one model is valuable to formulate and define feedback mechanisms in the Arctic.

In contrast, using several earth system models in Paper II allows us to test the robustness of the overturning response to sea-ice retreat. The selection of models was constrained by the grid of the models (tripolar grid) and the availability of the *horizontal mass transport* variable at the time of the study. The tripolar grid is a pre-condition for the method used to evaluate the Arctic overturning, as elaborated upon in Section 2.2.3. In addition, it allows for a higher horizontal resolution in the Arctic (*Murray*, 1996).

Out of the eight models considered, five models use a variation of NEMO as the ocean model (Table 2.2), implying similar vertical mixing schemes (turbulent kinetic energy scheme; *Madec et al.*, 1998); however, they present different horizontal resolution in the ocean and different sea-ice component. Some more diversity is obtained with MRI-ESM2-0, ACCESS-ESM1-5, and NorESM2-MM which have different ocean components, vertical and horizontal resolutions, and sea-ice components. In addition, ACCESS-ESM1-5 and NorESM2-MM use the K-Profile Parameterization vertical mixing scheme. Overall, these models exhibit a wide range of behavior in terms of e.g., overturning strength and Arctic sea-ice extent (Table 2.2.2; section 2.2.2), reflecting the diversity observed within the CMIP6 dataset (*Weijer et al.*, 2020;

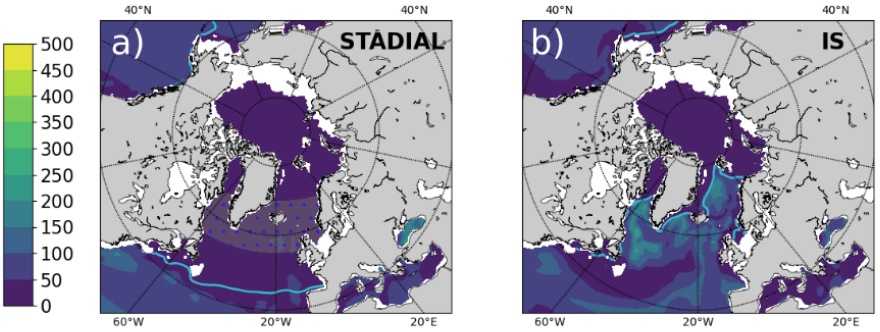

Figure 2.1: Winter (March) sea-ice extent and mixed-layer depth during the stadial (a) and interstadial (b) period. The stadial period shows the equilibrium conditions 350 yrs after the start of the freshwater forcing and the interstadial period the return to the MIS3 initial conditions, 150 yrs after the termination of the freshwater forcing. The region where the freshwater was injected is indicated with blue dots.

Notz and SIMIP Community, 2020; *Asbjørnsen and Årthun*, 2023).

In Paper III, a 800 yrs freshwater hosing experiment was conducted employing a fast version of NorESM1-M (CMIP5 version of NorESM; *Bentsen et al.*, 2013) with the aim of replicating an abrupt warming event that bears resemblance to Dansgaard-Oeschger (DO) events. In NorESM-F, (*Guo et al.*, 2019a) improved the model's efficiency by increasing the model year per day (< 40 to 90) to allow for a multi-millennial experiment, and (*Guo et al.*, 2019b) forced the model for 500 yrs with a background climate representative of the Marine Isotope Phase 3 (MIS3) to reach a relatively warm climate state (interstadial). Here, the experiment was branched off from the MIS3 equilibrium experiment and forced for 500 yrs with a freshwater flux of 0.33 Sv (1 Sv$= 1 \times 10^6 \mathrm{m^3 s^{-1}}$); evenly distributed between 50°N and 70°N) leading to a full stadial-like state with extensive sea-ice cover (Fig. 2.1a). The freshwater flux was tuned to obtain a weaker AMOC and extensive winter sea-ice cover in line with stadial conditions. Freshwater forcing of the same order of magnitude and in the same region are commonly been used to obtain an AMOC shutdown (0.22 Sv, *Van Meerbeeck et al.*, 2009; 0.3 Sv, *Kageyama et al.*, 2010; 0.1 Sv *Manabe and Stouffer*, 1997). After the freshwater forcing interruption, the simulation is prolonged for another 300 yrs which results in the recovery of the interstadial conditions (Fig. 2.1b). The recovery phase intends to reproduce a stadial-to-interstadial transition and can therefore be compared with proxy records, which is a distinct advantage inherent to paleoclimate studies.

2.2.2 Model evaluation

models	AMOC 26	AMOC decline	March SI	ISR	BO
EC-Earth2.3	×	×	14.94	×	×
CanESM5	12.29	-49%	15.94	×	×
EC-Earth3	17.37	×	15.22	6.6	2.8
MRI-ESM2-0	17.34	×	14.24	6.7	3.9
UKESM1-0-LL	16.42	-43%	16.34	×	×
ACCESS-ESM1-5	19.01	-33%	14.5	×	×
CNRM-CM6-1	16.30	-55%	15.75	×	×
ISPL-CM6A-LR	12.35	-38%	15.12	6.5	4.7
NorESM2-LM	20.55	-52%	14.04	3.7	1.8
CMIP6 MMM	17.7		15.46	×	×
std deviations	0.8		2.01		
Observations	17.4		14.35	3.4	2.6
std deviations	0.4		0.54	1.4	0.9

Table 2.2: Mean maximum overturning strength at 26°N (in Sverdrup) for the time period 2005-2014 and percent decline in 2081–2100 compared to the historical (1850–2014) mean (*Weijer et al.*, 2020), mean sea-ice extent in March and September (million km^2) over the period 1979-1998 (*Notz and SIMIP Community*, 2020) and transport across the Iceland-Scotland Ridge (ISR) and Barents sea opening (BO) for the period 1986-2005 (*Madonna and Sandø*, 2022). The models that do not use NEMO are highlighted in bold and missing values are indicated with a cross. Multimodel mean (MMM) includes 27 models for the AMOC at 26°N and 40 models for the March sea-ice extent

The state-of-the-art climate models are known to struggle to represent the key characteristics of the Arctic Ocean (*Heuzé et al.*, 2023; *Khosravi et al.*, 2022). In particular, CMIP6 models do not represent well the Arctic stratification (*Muilwijk et al.*, 2023), they have too cold and deep intermediate Atlantic Water layers, and their bottom water masses are too warm (*Heuzé et al.*, 2023). In this context, I list below some key results highlighting the strengths and weaknesses of the models used in this dissertation and CMIP models in general, focusing on the AMOC, dense-water formation, and sea-ice extent.

There is a positive bias in sea-ice extent in CMIP models that increased from CMIP5 to CMIP6 (*Shen et al.*, 2021). However, the CMIP6 model spread in sea-ice extent captures the observational estimate and the sensitivity of the sea-ice cover to warming is closer to the observed values compared to the CMIP5 models (*Davy and Outten*, 2020; *Notz and SIMIP Community*, 2020). In our subset of models (Table 2.2.2), the models that do not use NEMO as an ocean model have less sea ice in winter.

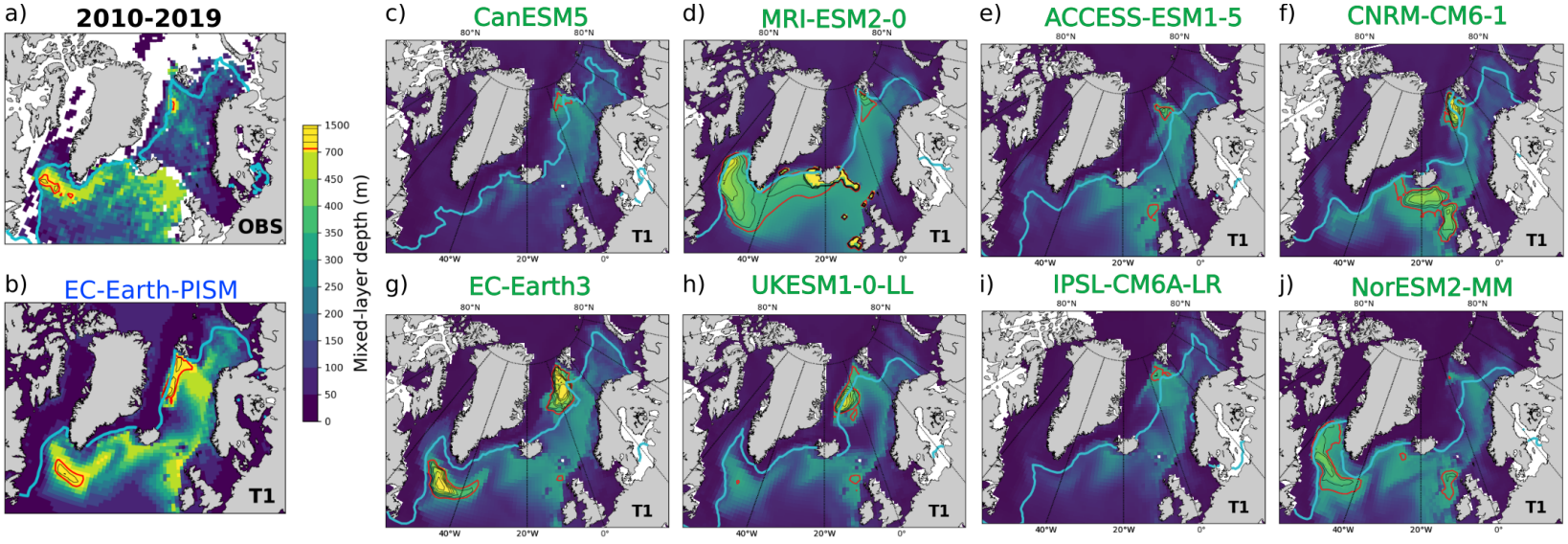

Figure 2.2: Winter mixed layer depth and sea ice extent (blue line) for the time period 2010–19. The red contour lines highlight the regions with an 800-m-deep mixed layer. In (a), the sea ice extent was obtained from the National Snow and Ice Data Center (NSIDC) and the mixed-layer depth was computed using observations from the dataset combined by *Huang et al.* (2020). Mixed-layer depth were computed following *de Boyer Montégut et al.* (2004) and averaged for three winter months (February-April) in a&b. In c-j, the mixed-layer depths are outputs from the model for the March only.

There are big variations within CMIP6 models regarding the strength and location of deep convection (Fig. 2.2). Some models have no, or very weak, deep convection in the Labrador, Iceland, and Irminger Seas (CanESM5, IPSL-CM6A-LR and CNRM-CM6-1). Except MRI-ESM2-0 and NorESM2-MM, all of the models present the highest mixed-layer depth value in the Greenland Sea, with the maximum varying between 1000 m (IPSL-CM6A-LR) and 1900 m (EC-Earth3). The CMIP5 and CMIP6 models have also been criticized for not realistically representing dense-water formation (*Heuzé et al.*, 2013; *Heuzé*, 2021). Meanwhile, *Jackson and Petit* (2023) evaluated the contribution of watermass transformation in different regions from surface fluxes and found similarities with observations. In most models, the watermass transformation in the Labrador Sea is only contributing for 1–5 Sv to the overturning with the exception of NorESM2-MM which presents overly strong values. Meanwhile, there is no dense watermass transformation in the Labrador Sea in CanESM5.

The representation of the AMOC has been improved in the transition from CMIP5 to CMIP6 with in particular an ensemble mean overturning strength at 26°N, falling within one standard error of the observed mean for the time period 2004-2018 (*Weijer et al.*, 2020); however the spread among models remains large (9.6 Sv to 23 Sv for 27 models; 12.29 Sv to 20.55 Sv for our subset of models, Table 2.2.2). *Weijer et al.* (2020) highlight a linear relationship between the mean overturning strength and the AMOC weakening in 12 out of 16 models, with ACCESS-ESM1-5 being an outlier in this regard.

Studies of volume and heat transport across the Arctic gateways (GSR, *Heuzé and Årthun*, 2019; *Madonna and Sandø*, 2022; Bering Strait, *Woodgate*, 2018) and within the Arctic (Fram Strait, *Muilwijk et al.*, 2018; Barents Sea opening, *Smedsrud et al.*, 2013; *Muilwijk et al.*, 2018) have also stressed large bias and spread in CMIP5 and CMIP6 models in the Arctic. However, no multi-model studies have looked into the Arctic overturning.

EC-Earth2.3 has a cold and fresh bias in the Arctic in the 20^{th} century, as well as an excessively extensive and thick sea-ice cover (*Koenigk et al.*, 2013). EC-Earth-PISM also has a too extensive sea-ice cover (Fig. 2.2b). During the pre-industrial period, the coupling with the dynamic ice sheet induces a freshwater flux increase of about 18% which only results in small differences in temperature and salinity compared with the uncoupled simulation (*Madsen et al.*, 2022). EC-Earth-PISM (and EC-Earth2.3) simulates relatively well the deep-convection regions, represented by the depth of the mixed layer in the North Atlantic and Nordic Seas during the period 2020-2019 (Fig. 2.2b). Under increased emissions ($4\times CO_2$ forcing), *Madsen et al.* (2022) find that the freshwater flux from the Greenland ice sheet increases by 55% and results in cooler near-surface air temperature in the Arctic, more sea ice and a weaker ocean circulation.

From NorESM1-M to NorESM-F, the strength of the AMOC and the distribution of sea ice

were improved, owing to code developments in the ocean, atmosphere, and biogeochemistry components. Additionally, the acceleration of the model's computational speed was evaluated to have only a minor impact on the simulated climate (*Guo et al.*, 2019a).

A detailed assessment of NorESM1-F in simulating pre-industrial conditions and MIS3 climate have been conducted by *Guo et al.* (2019a) and *Guo et al.* (2019b). Compared to the pre-industrial conditions, the MIS3 interstadial-like climate is characterized by 2 m thicker multiyear Arctic sea ice, a (19%) stronger AMOC, and 2.9°C cooler mean surface temperature (*Guo et al.*, 2019b).

Although uncertainties persist in Arctic modeling, these climate models represent our most advanced tools for studying the Arctic overturning. They prove indispensable for conducting mechanistic analyses and will therefore be used in this dissertation to identify possible changes and feedback mechanisms.

2.3 Methods

2.3.1 Meridional overturning streamfunction

To visualize and quantify the meridional overturning circulation, I use the overturning streamfunction Ψ (units: $\mathrm{m^3\,s^{-1}} = 1\times10^{-6}$ Sv), which is a function of the latitude λ and the depth z:

$$\Psi(\lambda, z) = \int_{z}^{0}\int_{\phi_A}^{\phi_E} v(\phi', \lambda, z')\frac{2\pi \mathrm{R}_T}{360}\,\mathrm{d}\phi'\,\mathrm{d}z' \quad (\mathrm{m^3\,s^{-1}}) \tag{2.1}$$

By integrating the meridional velocities v across the Atlantic Ocean at each depth, and performing a cumulative sum of that integration from the surface to the bottom, we get information about the location of the mean northward and southward flows in the water column. Figure 2.3b presents the result of these computations performed at every latitude from 30°S to 85°N by *Johnson et al.* (2019) using output from an ocean state estimate. The upper positive cell corresponds to the part of the overturning circulation that involves the formation of North Atlantic deep water and that I am focusing on in this dissertation. This representation shows a circulation involving 15-20 Sv of water located in the top 3000 m with a return flow below 1000 m depth.

The integration can also be done along layers of same density (*isopycnals*) instead of following fixed-depth levels (Ψ_σ, Fig.2.3a) since the water also experiences a change in density as it

overturns.In this case, the streamlines indicate a transformation of water from low density in the tropics (potential density of 33 kg m^{-3}) to high density in the North Atlantic (>37.38 kg m^{-3}). This streamfunction presents higher volume transport as the densification of a water parcel does not always involve sinking. As a consequence, some of the density-space overturning circulation is associated with the horizontal (gyre) circulation and is therefore not captured in depth-space (*Zhang and Thomas*, 2021).

The overturning in depth and density space diverge substantially in the subpolar region (*Johnson et al.*, 2019). Ψ_σ is preferred in this region as water slowly transformed within the gyre represents a substantial fraction of the North Atlantic Deep Water. *Zhang* (2010) therefore recommend using the streamfunction in density space when studying the connectivity between the subpolar overturning with the overturning at lower latitudes. In this dissertation I keep using the streamfunction in depth space, in addition to the streamfunction in density space, since my foremost interest lies in the vertical motion of water initiated by strong heat loss.

Figure 2.3a and b show that there is a circulation in the Arctic that involves further densification of 2-4 Sv of Atlantic Water (37.65-37.75 kg m^{-3}; a) but no sinking of the water masses (b). These values are smaller than what observations suggest (6 Sv; *Østerhus et al.*, 2019). However, the meridional overturning streamfunction is not well adapted to study this region of the ocean (*Bitz et al.*, 2006). In fact, integrating velocities along lines of same latitude is problematic beyond 70°N: regions that are far apart are then combined (see Fig. 2.3c). The meridional streamfunction is therefore not appropriate to assess the Arctic overturning characteristics in ocean models.

The models used in this dissertation were chosen based on their ocean grid (Fig. 2.4) to work around this issue. Referred to as tripolar grid, the grids present a flattening of the latitudes close to the pole. Therefore, it is possible to integrate the (pseudo-)meridional velocity v from the west to the east along pseudo-latitude in the Atlantic (red, blue, and green regions in Fig. 2.4) and $-v$ from the east to the west in the Arctic (purple region). By doing this we ensure that we capture the circulation within the Arctic up to the Siberian shelf in a physically correct manner (*Bitz et al.*, 2006).

2.3.2 Dense-water formation

Dense-water formation at high northern latitudes is key to the state of the overturning circulation (*Chafik et al.*, 2019; *Lozier et al.*, 2019; *Zhang and Thomas*, 2021). In Paper I, dense-water formation location and strength are estimated qualitatively based on the mixed-layer depth in March. The mixed-layer depth is quantified as the depth where the density

$\rho = \rho(T_0 - \Delta T, S_0)$ is reached, where T_0 and S_0 are the temperature and salinity at the surface, respectively, and $\Delta T = 0.2°$C following *Huang et al.* (2020). The regions that have a mixed layer deeper than 800 m are then defined as dense-water formation regions. This method is motivated by good agreement with observations for the period 2010-2019 (Fig. 2.2a&b).

In Paper II, we use the water-mass transformation (WMT) framework, based on surface fluxes (heat and freshwater) to be able to quantify and compare dense-water formation within models. Previous studies have shown good correlations between surface-forced WMT and the overturning in density space in the North Atlantic and Nordic Seas (*Jackson and Petit*, 2023; *Årthun*, 2023; *Desbruyères et al.*, 2019).

As a first step, we compute the surface density flux D following (*Langehaug et al.*, 2012):

$$D = -\beta \; Q_F \; S + \frac{-\alpha Q_H}{c_p} \quad (\mathrm{kg\,m^{-2}\,s^{-1}}) \tag{2.2}$$

Here, Q_F represents the freshwater flux (including precipitation-evaporation, river runoff, and sea-ice and iceberg melt) and Q_H is the net heat flux out of the ocean. $Q_F < 0$ (evaporation>precipitation) and $Q_H > 0$ (heat loss to the atmosphere) imply a positive density flux (D>0).

A water mass transformation function F (in units of Sv) can then be computed for each potential density σ by integrating the density flux D over the area A where the layer of density σ outcrops, such that:

$$F(\sigma) = \frac{1}{\Delta T} \int_{year} \int_{A} D \; \delta(\sigma - \sigma') \; \mathrm{d}A \; \mathrm{d}t \quad (\mathrm{kg\,m^{-2}\,s^{-1}}) \tag{2.3}$$

With $\Delta T = \int_{year} \mathrm{d}t$ and δ the Dirac Delta function such that $\delta(\sigma - \sigma')$ equals 1 when $\sigma = \sigma'$ and 0 otherwise and A the area where this condition is met.

In Paper II, we compute F over the winter months only (January, February, and March) and integrate it over the largest densities ($\sigma > 35$) in an attempt to isolate dense-water formation processes. Moreover, we compute F at each pseudo-latitude to enable a regional comparison with the overturning strength.

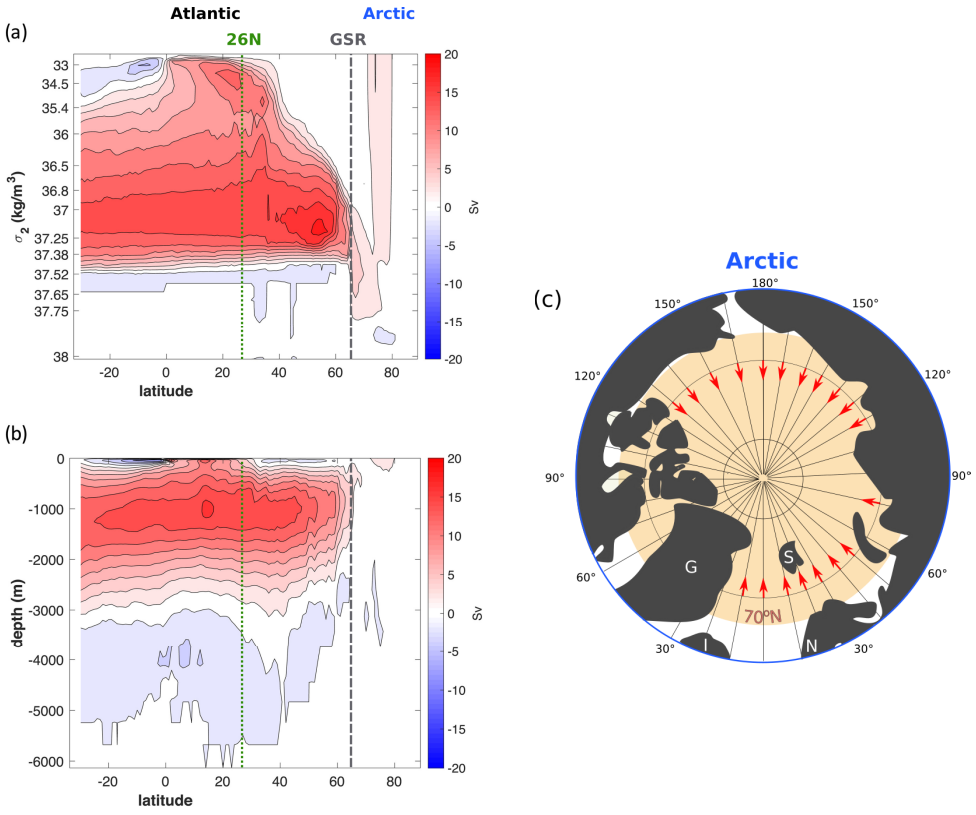

Figure 2.3: Atlantic meridional overturning streamfunction as a function of latitude and density (a) and depth (b), calculated by *Johnson et al.* (2019) from the Estimating the Circulation and Climate of the Ocean dataset. Positive values (red) indicate a clockwise circulation. I have highlighted the 26°N latitude, where the AMOC strength is often measured, and the latitude of the Greenland-Scotland Ridge (GSR) In (c), a map stresses the issue arising north of 70°N (orange region): the integration of positive meridional velocities along a line of same latitude (red arrows) mixes regions that are far apart (ie, the Nordic and Barents seas with the Siberian shelf).

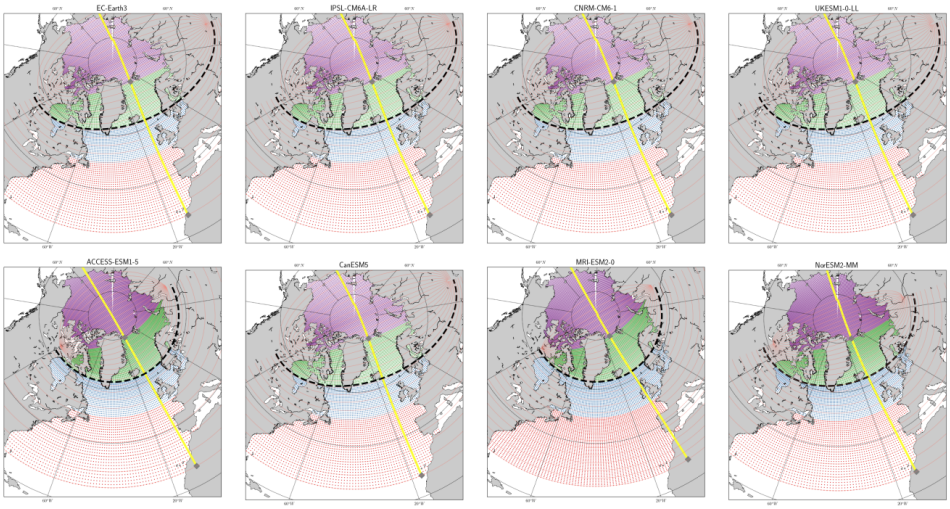

Figure 2.4: Geometry of the (tripolar) grid of the models used in this dissertation and axis used to project the overturning (yellow line). The latitudes flatten close to the pole and are referred to as pseudo-latitude. The position of the Greenland-Scotland Ridge (GSR) is stressed on the maps by the dashed line and the colors indicate regions used in Paper II: the Subtropical gyre (red), Subpolar gyre (blue), Nordic Seas (green), and Arctic basins (purple) regions.

Chapter 3

Summary of papers

Paper I: Transient increase in Arctic Deep-Water formation and ocean circulation under sea-ice retreat

Model simulations have shown that the retreat of the winter sea ice in the Arctic could be accompanied by a northward shift and a reduction of deep convection. However, increasing freshwater flux from the Greenland ice sheet melting, not included in models, could also interfere with deep convection. In Paper I, we test how deep convection evolves under sea-ice retreat in a long simulation of an earth system model (EC-Earth2.3) coupled with a dynamic Greenland ice sheet (PISM). Forced with a high emission scenario (RCP8.5), the model presents the following changes: the ocean becomes free of winter sea ice by 2175 and the Greenland ice sheet produces 300 Sv of freshwater through melting and calving between the year 2100 and 2300. We study deep convection changes accompanying the winter sea-ice retreat by analyzing mixed-layer depth maps from six snapshots, from 1975 to 2175. In addition, we investigate the consequences on the local overturning circulation by computing the overturning streamfunction across the Nordic Seas and Arctic basins. We find that deep convection follows the winter sea-ice edge until it reaches the Nansen Basin, around the year 2100. During the same time, there is an enhancement and a northward expansion of the

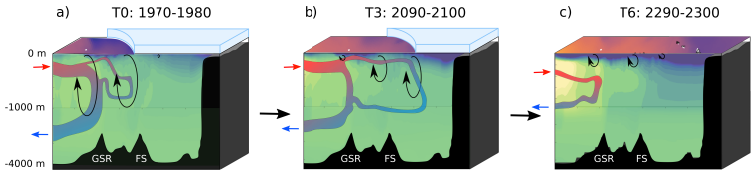

Figure 3.1: Schematic showing the ArMOC development in relation to deep convection changes under winter sea-ice retreat.

overturning north of the Greenland-Scotland Ridge. We propose to rename the circulation north of the ridge ArMOC (Arctic Meridional Overturning Circulation) to encourage studying this circulation on its own, as it presents different trends compared to the AMOC. After 2100, deep convection stops following the sea-ice edge because the ocean is too stratified in the Arctic basins. This phenomenon is amplified by the increase in freshwater flux (precipitation and Greenland meltwater). Because of the deep convection interruption, the ArMOC weakens and eventually collapses (Fig. 3.1).

Paper II: Arctic Overturning circulation (ArMOC) strengthening in CMIP6 models

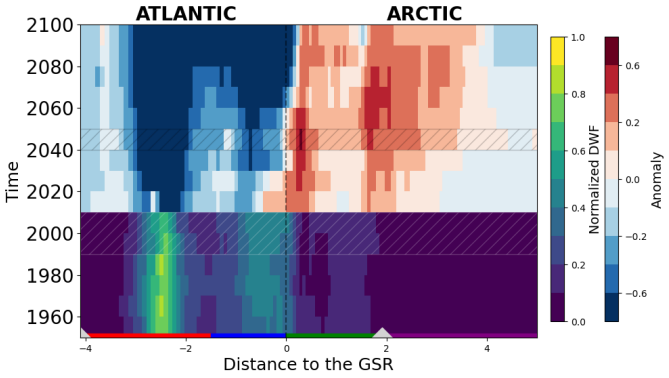

Figure 3.2: Dense water formation anomalies (DWF) in the North Atlantic and Arctic Ocean from the year 2010 to 2100.

We showed in Paper I that there is a transitory enhancement of the ArMOC in EC-Earth-PISM (CMIP5 model) due to an increase in deep convection north of the Greenland-Scotland Ridge as the winter sea ice retreats. We further test this mechanism by analyzing simulations from eight different CMIP6 models. Forced with a similar high emission scenario (ssp5-8.5), the models also present an ArMOC strengthening. However, the multi-model mean suggests that the strengthening stops before 2050, thus 50 yrs earlier than previously found (PI). In addition, half of the models present a substantial increase in dense-water formation north of the Greenland-Scotland Ridge. The increase propagates poleward (Fig. 3.2), reminding the northward shift in deep convection from Paper I. Moreover, the same models present a stronger ArMOC strengthening and heat transport increase into the Arctic basins. We conclude that the amplitude and timing of the ArMOC strengthening is model-dependent. In particular, models that sustain and enhance heat loss to the atmosphere in the Arctic Ocean have a stronger ArMOC strengthening. Representing the ArMOC and its forcing mechanism

correctly seems fundamental as it also affects the heat transport increase into the Arctic basins, and therefore the sea-ice cover.

Paper III: Arctic circulation changes at the transition from a Heinrich stadial to a Greenland interstadial

Paper III investigates local overturning changes accompanying an abrupt warming event consistent in amplitude with past climatic oscillations known as Dansgaard–Oeschger (DO) events. The AMOC is believed to play an important role in driving DO events, by providing the heat that rapidly melts the sea ice and warms the Arctic atmosphere. However, we find that the AMOC influence is partly inhibited by the development of a strong and deep estuarine overturning circulation in the simulation used. The estuarine overturning is also activated by the sea-ice retreat and enhanced mixing; however, it acts to repress convection and the northward expansion of the overturning circulation. Its formation south and then north of the Greenland-Ridge results in a sea-ice retreat and warming in two phases. The ArMOC develops only after the estuarine cell has disappeared, and does not contribute to the sea-ice retreat.

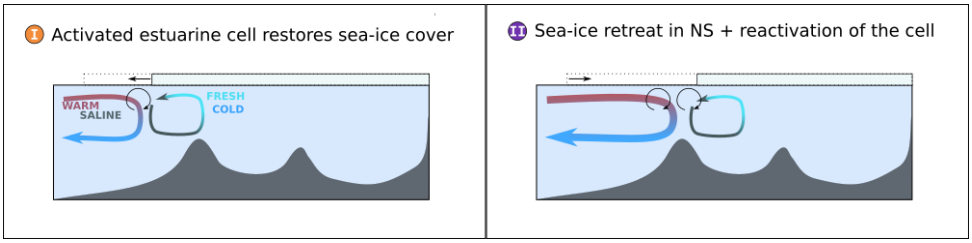

Figure 3.3: Sketch presenting the development of an estuarine cell in the North Atlantic (a) and Nordic Seas (b) as the sea-ice retreats. The overturning cells are both enhanced by convection at the sea-ice edge, but the estuarine cell reduces the convection by restoring the stratification.

Main conclusions

- In models using a tripolar grid, the overturning streamfunction can be extended to the Arctic Ocean and captures the Arctic overturning (named Arctic Meridional Overturning Circulation, ArMOC) **(Paper I)** and an estuarine circulation under glacial conditions **(Paper III)**. However, it does not capture the present estuarine circulation.
- As opposed to the AMOC, the deep circulation north of the GSR depends on dense-water formation and can shut down **(Papers I&III)**

- A northward shift in dense-water formation enhances the ArMOC under future sea-ice retreat **(Papers I&II)**
- The enhanced ArMOC is associated with increased heat transport to the Arctic basins **(Paper II)**
- The large freshwater content in the Arctic basins limits the dense-water formation shift and the ArMOC strengthening, independent of meltwater fluxes from the Greenland ice sheet **(Paper I)**
- Anomalously fresh conditions in the Arctic Ocean lead to the formation of a strong estuarine cell that delays the sea-ice retreat under a warming event **(Paper III)**

Chapter 4

Scientific results

Paper I

4.1 Transient Increase in Arctic Deep-Water Formation and Ocean Circulation under Sea Ice Retreat

Anaïs Bretones, Kerim H. Nisancioglu, Mari F. Jensen, Ailin Brakstad, Shuting Yang

Journal of Climate, **246/106492**, (2022)

Transient Increase in Arctic Deep-Water Formation and Ocean Circulation under Sea Ice Retreat

ANAÏS BRETONES,[a,b] KERIM H. NISANCIOGLU,[a,b,c] MARI F. JENSEN,[a,b] AILIN BRAKSTAD,[b,d] AND SHUTING YANG[e]

[a] *Department of Earth Science, University of Bergen, Bergen, Norway*
[b] *Bjerknes Centre for Climate Research, Bergen, Norway*
[c] *Centre for Earth Evolution and Dynamics, Department of Geosciences, University of Oslo, Oslo, Norway*
[d] *Geophysical Institute, University of Bergen, Bergen, Norway*
[e] *Danish Meteorological Institute, Copenhagen, Denmark*

(Manuscript received 23 February 2021, in final form 22 September 2021)

ABSTRACT: While a rapid sea ice retreat in the Arctic has become ubiquitous, the potential weakening of the Atlantic meridional overturning circulation (AMOC) in response to global warming is still under debate. As deep mixing occurs in the open ocean close to the sea ice edge, the strength and vertical extent of the AMOC is likely to respond to ongoing and future sea ice retreat. Here, we investigate the link between changes in Arctic sea ice cover and AMOC strength in a long simulation with the EC-Earth–Parallel Ice Sheet Model (PISM) climate model under the emission scenario RCP8.5. The extended duration of the experiment (years 1850–2300) captures the disappearance of summer sea ice in 2060 and the removal of winter sea ice in 2165. By introducing a new metric, the Arctic meridional overturning circulation (ArMOC), we document changes beyond the Greenland–Scotland ridge and into the central Arctic. We find an ArMOC strengthening as the areas of deep mixing move north, following the retreating winter sea ice edge into the Nansen Basin. At the same time, mixing in the Labrador and Greenland Seas reduces and the AMOC weakens. As the winter sea ice edge retreats farther into the regions with high surface freshwater content in the central Arctic Basin, the mixing becomes shallower and the ArMOC weakens. Our results suggest that the location of deep-water formation plays a decisive role in the structure and strength of the ArMOC; however, the intermittent strengthening of the ArMOC and convection north of the Greenland–Scotland ridge cannot compensate for the progressive weakening of the AMOC.

KEYWORDS: Ocean; Arctic; Deep convection; Meridional overturning circulation; Ice loss/growth

1. Introduction

Arctic sea ice cover has retreated at an unprecedented rate in the last decades as a consequence of rising greenhouse gases (Nghiem et al. 2007; Notz and Stroeve 2016; Stroeve and Notz 2018). As a consequence of the warming, the deep convection in the Labrador Sea is weakening (Yang et al. 2016). Under further emissions, these trends are expected to continue, ultimately resulting in a seasonally ice-free Arctic (Notz and Community 2020) with a potential shut down of North Atlantic deep-water formation (Jahn and Holland 2013; Brodeau and Koenigk 2016). On a larger scale and related to the reduction in North Atlantic deep-water formation, a weakening of the Atlantic meridional overturning circulation (AMOC) is found in most climate models (Cheng et al. 2013). However, little is known about potential changes in the deep circulation and overturning in the Nordic seas and Arctic Ocean.

Winter in the high latitudes is characterized by strong heat fluxes from the relatively warm ocean to the much colder atmosphere, destabilizing the upper ocean. Depending on the intensity of these fluxes, and the background ocean stratification, the surface cooling is either followed by sea ice formation, inhibiting further ocean heat loss, or compensated by mixing with deeper and relatively warmer ocean water. In the North Atlantic, the high salinity of the upper ocean results in a weak stratification that allows for deep mixing during winter as the surface cools. In contrast, in the Arctic Basin (including the Canadian and Eurasian Basins) there is a fresh surface layer fed by continental river runoff and maintained by the presence of sea ice that currently inhibits open-ocean convection. However, the ongoing warming of the Arctic and the resulting acceleration of the hydrological cycle (Rawlins et al. 2010) and winter sea ice decrease are expected to impact the Arctic stratification (Nummelin et al. 2015; Davis et al. 2016). This might impact the potential for open-ocean convection in the Arctic Basin in the future.

Observations over the past 20 years show that mixing at the end of the winter can reach a depth of 1000 m in areas of the Labrador Sea (Våge et al. 2009; Yashayaev and Loder 2017), the Irminger Sea (de Jong and de Steur 2016), and the Greenland Sea (Brakstad et al. 2019). These deep-water formation sites are the main sources of dense water contributing to the renewal of North Atlantic Deep Water and, thus, setting the strength of the AMOC. However, the convection strength varies in time. While deep convection can disappear for a few years, as in the Labrador Sea during the Great Salinity Anomaly in the 1960s (e.g., Kim et al. 2020), it can also be absent for longer time periods, as for the last interglacial

Denotes content that is immediately available upon publication as open access.

Corresponding author: Anaïs Bretones, anais.bretones@uib.no

DOI: 10.1175/JCLI-D-21-0152.1

(Hillaire-Marcel et al. 2001). Under future global warming, deep convection in the North Atlantic and the AMOC is predicted to weaken (Cheng et al. 2013; Jahn and Holland 2013). This raises concerns, as the intensity of the convection and the production of dense water influences how much heat and carbon are stored in the deep ocean. In particular, changes in deep-water formation have previously been associated with major climate shifts, such as the Heinrich events (Broecker et al. 1992) and the Young Dryas (Fairbanks 1990).

In contrast to studies focusing on the shutdown of Labrador Sea deep-water formation under increased freshwater fluxes into the subpolar gyre, Lique et al. (2018) link deep-water formation changes, in particular enhanced convection in the Arctic, to winter sea ice retreat. Under $4 \times CO_2$ forcing in the High-Resolution Global Environmental Model (HiGEM), the authors find a northward shift of the deep mixing regions (defined by a mixed layer deeper than 400 m), corresponding to the northward retreat of sea ice. The simulated sea ice retreat is found to be associated with a change in surface circulation, bringing more salty Atlantic water into the Eurasian Basin and weakening the upper ocean stratification. Under this configuration, enhanced air–sea buoyancy fluxes, facilitated by the retreat of the sea ice, deepen the mixed layer.

The findings of Lique et al. (2018) shed new light on an earlier study by Bitz et al. (2006) with the Community Climate System Model, version 3 (CCSM3). Using a transect crossing the Arctic region to compute the overturning circulation, Bitz et al. (2006) find a strengthening of the overturning north of the Greenland–Scotland ridge in an experiment with a doubling of CO_2. The enhanced circulation is linked to increased sea ice production in the Arctic Ocean, from the Siberian Shelf to the Canadian Archipelago. Studying the simulated ocean ideal age, Bitz et al. (2006) identify anomalously young water on the Siberian shelf, indicating strengthened convection, possibly impacting the Arctic overturning. The authors do not assess changes to the depth of the mixed layer in the new ice-free open ocean regions. However, it is plausible that enhanced deep convection in these regions could be an alternative explanation for the simulated strengthened Arctic overturning.

Rather than applying an instant doubling or quadrupling of atmospheric CO_2 as in Lique et al. (2018) and Bitz et al. (2006), Brodeau and Koenigk (2016) apply an emission scenario with gradually increasing CO_2 (RCP8.5), to observe how the deep convection in the Arctic follows the retreating winter sea ice. They forecast a shutdown of the deep convection in the Labrador Sea and Iceland–Scotland area by the early 2020s using an ensemble of 12 simulations with EC-Earth3. Starting at this time, convection in the Nordic seas weakens, and by 2060 it is replaced by convection in the Arctic Ocean. This evolution is consistent with the northward shift of deep-water formation suggested by Lique and Thomas (2018). However, in all the aforementioned studies, the model simulations end before the winter sea ice is completely gone; making it impossible to investigate if deep convection develops further into the Canadian and Eurasian Basins, and how it relates to the Arctic overturning. Moreover, these previous studies do not account for the impact of increasing freshwater fluxes from the Greenland ice sheet that can inhibit convection (Fichefet et al. 2003). Depending on where the freshwater is transported and stored, increased freshwater fluxes could have major impacts on deep-water formation and overturning circulation by strengthening upper ocean stratification and inhibiting deep convection (Smith and Gregory 2009; Böning et al. 2016).

Here, we study the northward shift of deep convection and its link to winter sea ice retreat under the RCP8.5 scenario using a long simulation with EC-Earth coupled with a dynamic Greenland ice sheet. By introducing a new metric for the overturning circulation in the central Arctic Ocean, we discuss the impact of enhanced Arctic overturning on the large-scale AMOC. Moreover, the exceptional length of the coupled EC-Earth experiment results in a year round ice-free Arctic, making it possible to study the long term fate of Arctic deep-water formation and overturning.

2. Methods

In this study, we analyze a projection from the EC-Earth–Parallel Ice Sheet Model (PISM), a state-of-the-art climate model with a dynamical ice sheet module for the Greenland ice sheet (Madsen et al. 2020, manuscript submitted to *Climate Dyn.*). EC-Earth-PISM is built on the climate model EC-Earth, version 2.3 (Hazeleger et al. 2012, herein referred to as EC-Earth2.3), which is coupled with (PISM (Bueler and Brown 2009; Winkelmann et al. 2011) for the Greenland ice sheet. EC-Earth2.3 is a model developed by the EC-Earth consortium with contributions to phase 5 of the Coupled Model Intercomparison Project (CMIP5). It consists of the ECMWF's Integrated Forecast System (IFS) model cycle 31r1 (https://www.ecmwf.int/en/publications/ifs-documentation) with updated physical parameterizations, the Nucleus for European Modeling of the Ocean version 2.2 (NEMO2; Madec 2008) developed by L'Institut Pierre-Simon Laplace (IPSL) embedded with the Louvain-la-Neuve Sea Ice Model, version 2 (LIM2; Fichefet and Maqueda 1997), and the Ocean Atmosphere Sea Ice Soil coupler, version 3 (OASIS3; Valcke 2006).

In EC-Earth-PISM, the atmosphere is modified to represent surface processes over the ice sheet. The coupling with the PISM ice sheet model involves an exchange of information between the atmospheric component of EC-Earth2.3 and PISM without anomaly or flux corrections. The simulated monthly surface temperature and mass balance over the Greenland ice sheet are passed on to PISM and drive the dynamics and thermodynamics of the ice sheet. In exchange, the simulated ice mass changes in PISM are returned to EC-Earth2.3 as changes to ice extent and ice topography influencing the atmospheric circulation (Madsen et al. 2020, manuscript submitted to *Climate Dyn.*), and as freshwater fluxes influencing the ocean circulation. Thus, the model simulates the climate induced changes to the Greenland ice sheet, as well as their resulting coupled feedbacks. In particular, Madsen et al. (2020, manuscript submitted to *Climate Dyn.*) found that under a $4 \times CO_2$ increase, freshwater fluxes from the Greenland ice sheet increase by 65% when EC-Earth is coupled with PISM. In fact, surface melting is enhanced by the snow–albedo feedback in EC-Earth-PISM. In addition, the EC-Earth-PISM has a fresher top layer in the Arctic, a more extensive winter sea ice

TABLE 1. Characteristics of the scenario simulations used in this study. Note that the uncoupled simulation stops at 2100, limiting the possibilities for comparison between the two simulations. Every figure is based on the EC-Earth-PISM simulation (boldface text), except Figs. 1 and 9, which also show the EC-Earth simulation (gray lines).

Model name	Model versions	Emission scenario	Scenario simulation	Reference
EC-Earth	EC-Earth2.3	RCP8.5	2006–2100	Hazeleger et al. (2012), Koenigk et al. (2013)
EC-Earth-PISM	**EC-Earth2.3 coupled with PISM (dynamic Greenland ice sheet)**	**Representative&Extended Concentration Pathway 8.5 (RCP&ECP8.5)**	**2006–2300**	Madsen et al. (2020, manuscript submitted to *Climate Dyn.*)

cover, weaker overturning at 26°N and cooler surface air temperature after the equilibrium is reached.

Following the EC-Earth2.3 configuration for CMIP5, EC-Earth-PISM has a horizontal spectral resolution of T159 in the atmosphere with physical processes on a linear reduced Gaussian of about 125 km × 125 km, and 62 vertical layers. For the ocean, the horizontal resolution is about 1° with 42 vertical levels, and a horizontal refinement to one-third of a degree near the equator resolving equatorial planetary waves. PISM uses a regular polar-stereographic grid at 20-km resolution.

The EC-Earth-PISM experiment analyzed in this study is a long climate change simulation following the CMIP5 protocol (Taylor et al. 2012) for the historical period (1850–2005), and the representative concentration pathway 8.5 scenario for the future projection period (2006–2300). This scenario is based on an increase in emissions leading to a radiative forcing of 8.5 W m^{-2} by 2100. Following 2100, the emissions are stable for 50 years before they are considerably reduced from 2150 to 2250, resulting in a stabilization of the radiative forcing at 12.5 W m^{-2} from 2250 to 2300 (van Vuuren et al. 2011).

The experiment started from a multicentury control run with preindustrial boundary conditions, for which the global mean surface temperature and the Greenland ice sheet remain in a quasi-stable state (Madsen et al. 2020, manuscript submitted to *Climate Dyn.*). The experiment continues after 2300 for another 900 years until the year 3200, while keeping the radiative forcing constant at the 2250 level (12.5 W m^{-2}). In this study we focus on the period 1950–2300, investigating changes in ocean circulation and deep convection during Arctic sea ice retreat and Greenland ice melt. For comparison, we include the CMIP5 historical and RCP8.5 experiment (from 1850 to 2100) with EC-Earth2.3 (referred to as EC-Earth) without the coupling to the PISM ice sheet model. Table 1 summarizes the differences between the two simulations used in this study.

3. Results

a. Sea ice decrease

As the EC-Earth-PISM experiment continues after the year 2100, it captures the disappearance of Arctic sea ice in both summer and winter. Figure 1 shows the evolution of the sea ice extent, defined as the area with a concentration of sea ice higher than 15%, in September (summer) and March (winter) from 1950 to 2300. The summer sea ice reduction accelerates around year 2040, resulting in an ice-free ocean (sea ice extent < 1 M km^2, where M = 10^6) in the summer from year 2060. A similar abrupt reduction of the winter sea ice occurs in year 2135, leaving the Arctic Ocean perennially ice free from year 2165.

The abrupt summer reduction in sea ice is similar for the experiment without the dynamic Greenland ice sheet (gray lines in Fig. 1). Until 2100, the winter sea ice extent decreases at the same rate in EC-Earth-PISM and EC-Earth. This suggests that the coupling with a dynamic ice sheet does not modify the timing of the sea ice reduction, at least until 2100. However, note that the ice volume change of Greenland, resulting in enhanced freshwater fluxes to the ocean in the coupled experiment, is relatively low before 2100 (gray line, Fig. 2). Unfortunately, the shorter length of the uncoupled (EC-Earth) experiment does not allow us to study how the increasing freshwater fluxes from Greenland influence the winter sea ice reduction after 2100. However, in the complementary 4 × CO_2 forcing experiment with EC-Earth-PISM, Madsen et al. (2020, manuscript submitted to *Climate Dyn.*) found a more extensive winter sea ice cover at equilibrium.

As this study primarily focuses on processes occurring during sea ice retreat, we mainly focus on three time periods

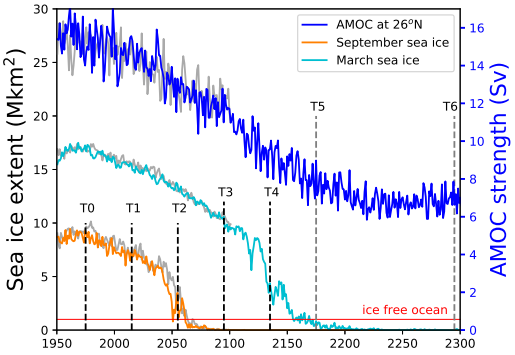

FIG. 1. Time series of the AMOC index (maximum transport at 26°N) and Arctic sea ice extent in March (light blue) and September (orange) from 1950 to 2300 for EC-Earth-PISM. Superimposed in gray from 1950 to 2100 are the same variables for the run that does not include the dynamic Greenland ice sheet. The red line indicates ice-free ocean conditions (sea ice extent < 1 M km^2, M = 10^6). The main time periods used in this analysis are indicated with dotted lines centered on each time period. T0 is used in Fig. 7 and T1 is used in Fig. 4, while T0, T2, T3, and T4 are used in Figs. 3, 6, 8, 10, and 12, and T3, T4, and T5 are used in Fig. 11.

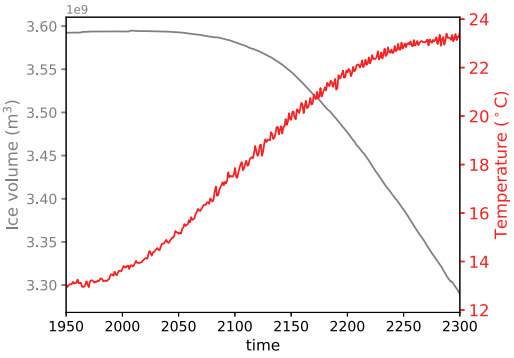

FIG. 2. Global mean annual surface air temperature (red) and Greenland ice volume (gray) in the EC-Earth-PISM simulation under the RCP8.5 emission scenario. The Greenland ice volume change results in freshwater fluxes to the ocean (see Fig. A1).

evenly spaced from 2050 to 2140: 2050–60 (T2), 2090–2100 (T3), and 2130–40 (T4), with results from each period averaged over 10 years. These are compared with the time period 1970–80, which is referred to as the historical period (T0). In addition, the period 2010–19 (T1) is used in section 3b to compare the model run with observed mixed layer properties, and the periods 2170–80 (T5) and 2290–2300 (T6) are used in section 3f to investigate the long-term evolution of an ice-free Arctic Ocean. Note, however, that the time periods T4, T5, and T6 are outside the range of the uncoupled EC-Earth simulation.

Each time period is distinct, with the mean position of the summer and winter sea ice edge progressing further into the central Arctic Ocean as the climate warms (Fig. 3). From T0 to T2, the summer sea ice edge retreats from the Barents, Kara, and Laptev Seas, as well as the Chukchi and East Siberian Seas (orange line, Fig. 3b). As shown in the time series of sea ice extent, the remaining summer sea ice is gone by the end of T2, leaving the Arctic Ocean ice free during summer for both T3 and T4 (Figs. 3c,d). On the other hand, winter sea ice (blue line) prevails in all four time periods. From T0 to T2, the winter sea ice edge retreats from most of the Barents Sea (Fig. 3b). A small reduction is found in the Greenland and Iceland Seas, but the sea ice edge still reaches Svalbard, Iceland, and the southern coast of Greenland. During T3, the retreat is visible in the Labrador Sea, along the east coast of Greenland, around Svalbard, and farther north in the Kara Sea and into the Eurasian Basin (Fig. 3c). During T4 the retreat accelerates with the opening of a large passage connecting the Greenland, Barents, and Kara Seas with the Chukchi Sea (Fig. 3d). Although the winter sea ice area does not change much from the historical period T0 to T2 or T3, it should be noted that the sea ice thins considerably. While the sea ice is up to 8 m thick during T0, it does not exceed 1.5 m during T3 (Fig. 3), which is explained by the lack of multiyear ice as the sea ice disappears completely during summer (Fig. 1). Finally, the winter sea ice retreat is accompanied by a warming of the surface ocean.

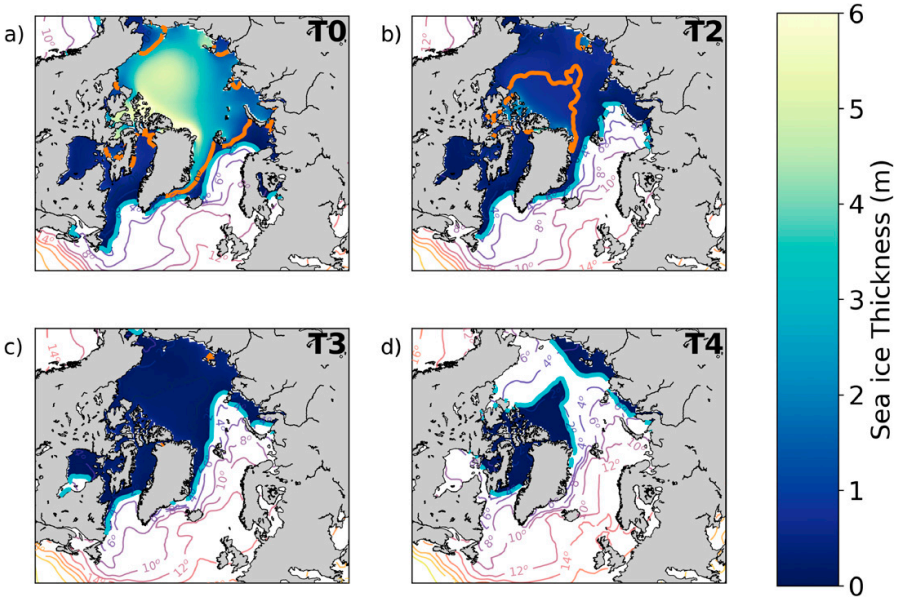

FIG. 3. Yearly mean sea ice thickness (shading; see color bar) and sea surface temperature (contour lines) for (a) T0: 1970–80, (b) T2: 2050–60, (c) T3: 2090–2100, and (d) T4: 2130–40 in the EC-Earth-PISM simulation. The blue line indicates the sea ice edge in March (winter) and the orange line marks the sea ice edge in September (summer). The sea ice edge corresponds to the 15% sea ice concentration contour line.

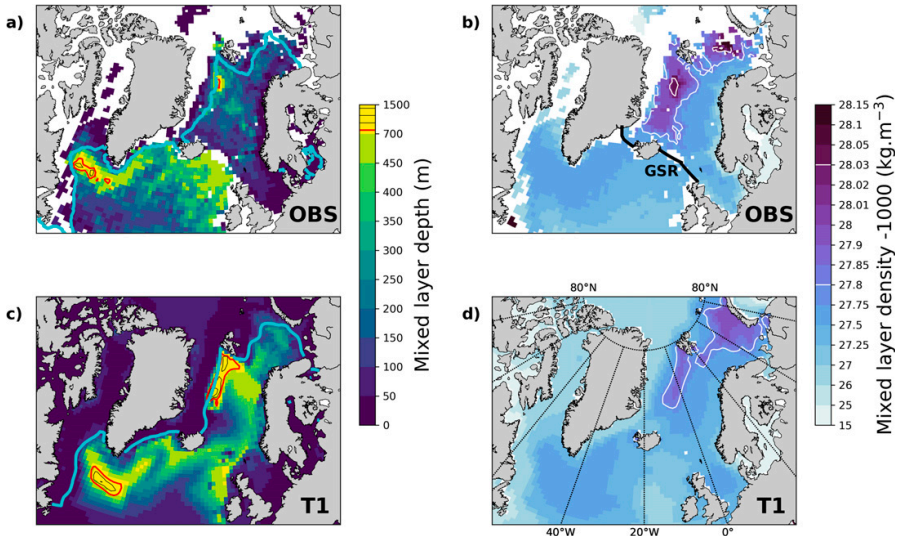

FIG. 4. Mixed layer depth with (a),(c) sea ice extent (blue line) and (b),(d) mixed layer density averaged over three winter months (February–April) for the time period T1: 2010–19. The red contour lines highlight the regions with an 800-m-deep mixed layer. The white contour lines indicate densities of 1027.8 and 1028.03 kg m^3. The sea ice extent in (a) was obtained from the National Snow and Ice Data Center (NSIDC). Mixed layer properties in (a) and (b) are based on observations, while (c) and (d) are EC-Earth-PISM model outputs.

In particular, the Barents Sea experiences a warming of 6°C from T0 to T3. At the same time, the warming in the Labrador Sea, where the sea ice edge retreat is smaller, is limited to 2°C.

b. Deep convection regions at present (T1)

The changing sea ice cover during the model simulation affects both the strength and position of wintertime convection. Before we investigate these changes further, we evaluate to what extent EC-Earth-PISM captures deep convection at present by comparing simulated mixed layer depth and density to observations for the period 2010–19 (Fig. 4). Both the observed and simulated mixed layer depth is identified as the depth where the density reaches $\rho(T_0 - \Delta T, S_0)$ where T_0 and S_0 are the surface temperature and salinity, respectively, and $\Delta T = 0.2$°C following de Boyer Montégut et al. (2004) and Holte et al. (2017). The corresponding mixed layer density is estimated as the average potential density over the extent of the mixed layer. Modeled mixed layer depths were computed using monthly averages of temperature and salinity. Observed mixed layer properties based on Argo float profiles were collected from Holte et al. (2017) south of the Greenland–Scotland ridge (indicated by the black line in Fig. 4b). Mixed layer estimates north of the ridge were obtained using observations from the dataset combined by Huang et al. (2020). This dataset includes shipboard hydrographic profiles and was used to achieve a good spatial coverage in the Barents and Nordic seas (in regions with limited Argo float data). All mixed layer properties are estimated for individual profiles before they are averaged over February, March, and April, which is when the deepest convection typically occurs. Averaging over a 3-month period also increases the number of observations, hence the reliability of the observational mixed layer climatology. Finally, we interpolate the observations onto our model grid for comparison with the modeled mixed layer depth.

The Labrador Sea and Greenland Sea stand out with observed mixed layers deeper than 1000 and 800 m, respectively (Fig. 4a). In EC-Earth-PISM, the deepest mixed layers are found in the same two regions (Fig. 4c); however, these convective regions are broader, especially in the Greenland Sea where the area of deep mixing extends south to the Iceland Sea. On average, EC-Earth-PISM tends to have deeper mixed layers, with a larger area depicting a mixed layer exceeding 500-m depth (e.g., east of the Greenland Sea or south of the Greenland–Scotland ridge). For the purpose of this study, we divide the North Atlantic and Arctic deep-water formation sites into four regions (Fig. 5): the Labrador Sea (between 60° and 35°W), the Iceland–Scotland region (south of Iceland and along the Greenland–Scotland ridge, as in Brodeau and Koenigk 2016), the western Nordic seas (Greenland and Iceland Seas) and the Nansen Basin (north of the Barents Sea). The deep-water formation sites are defined as areas with a mixed layer deeper than 800 m (red contour line in Figs. 4c and 6).

The deep convection sites in the western Nordic and Labrador Seas are associated with high mixed layer densities. Both the pattern and magnitude of the mixed layer density are well represented by the EC-Earth-PISM simulation (Figs. 4b,d), especially in the western Nordic seas (see the white contour indicating a mixed layer density of 1027.8 kg m^{-3}). One exception is the lack of the very dense mixed layers in the central

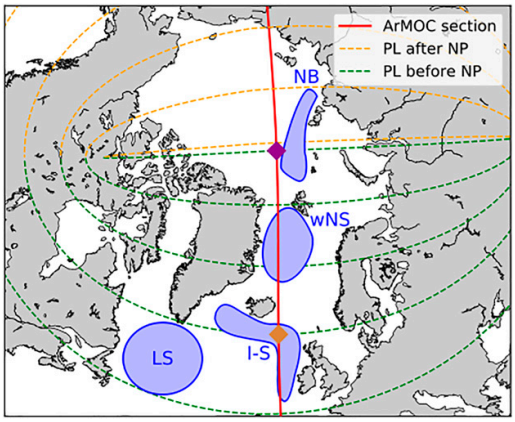

FIG. 5. Location of the dense-water formation regions used in this paper: Labrador Sea (LS), Iceland–Scotland (I-S), western Nordic seas (wNS), and Nansen Basin (NB). The red line indicates the section used in Figs. 8 and 10 and the purple and brown diamonds the position of the triangles in these same figures. The green and orange lines show the pseudolatitudes (PL) used to compute the ArMOC: for one PL, velocities perpendicular to that PL (pseudomeridian velocities) are integrated from America to Europe.

Greenland Sea, where observations indicate a density exceeding 1028.03 kg m^{-3}. On the other hand, the mixed layer density in the Labrador Sea is slightly higher in EC-Earth-PISM than in the observation based climatology. Despite small differences (slightly deeper and broader convective regions), the model represents the overall pattern of deep convection and the formation of dense water masses well. In the following we will study how these features evolve with time.

c. *Weakening and migration of deep convection regions*

The mixed layer changes dramatically from T0 to T4 as the winter sea ice retreats (T1 not shown in this section). This is seen by superimposing the March mixed layer depth with the March sea ice extent for T0, T2, T3, and T4 (Fig. 6). During T0 (Fig. 6a), deep convection is present in the Labrador Sea (>1500 m), in the western Nordic seas (1100 m) and in the Iceland–Scotland region (800 m), similarly to T1 (Fig. 4c). The magnitude of convection cannot be directly compared with Fig. 4c since it is averaged over March only (instead of February, March, April). Still, a similar pattern can be recognized. In general, there is a clear contrast in mixed layer depth between the regions close to the sea ice edge and those covered by sea ice where only shallow (<100 m) mixing occurs. The main difference between T0 and T1 is a northward shift in regions showing the deepest convection. During T0 the mixed layer depths in the southernmost regions (Labrador Sea and Iceland–Scotland) exceed those in the western Nordic seas, which is opposite to what was found for T1 (Fig. 4c).

For T2 (Fig. 6b), there is no active deep-water formation in the Labrador Sea and the Iceland–Scotland region since, in these regions, the maximum mixed layer depth is reduced to 450 m. The remaining active deep-water formation areas are farther north in the western Nordic seas. A decline in the maximum mixed layer depth is also found in the Nordic seas, although to a lesser extent than in the Labrador Sea. Within the western Nordic seas, the location of the deepest mixed layer depth moves north to the south coast of Svalbard, following the retreating winter sea ice edge. This supports the hypothesis that deep-water formation sites are migrating northward, as the climate warms and the winter sea ice edge retreats. Given the reduction in deep-water formation area and mixed layer depth, the amount of deep water formed is also reduced.

The northward migration continues in T3 (Fig. 6c) with 900-m deep convection appearing north of Svalbard at the edge of the winter sea ice cover in the Nansen Basin. Farther south, mixed layers in the three original convective regions are shallower with only one active convection site left in the western Nordic seas. The northward progression stops during T4 (Fig. 6d). Neither the Nordic seas nor the Nansen Basin have convection exceeding 700 m, and the sea ice edge decouples from the deepest mixed layer regions. As a result, the T4 period and the rapid retreat of winter sea ice marks the end of the North Atlantic deep-water formation era.

d. *AMOC weakening at 26°N*

Deep convection is thought to be important for the strength, structure, and variability of the AMOC (Kuhlbrodt et al. 2007). Here, we review the main characteristics of the AMOC in EC-Earth-PISM for easy comparison with other studies.

The AMOC can be seen as the superposition of two cells turning in opposite direction in the depth-latitude space, and visualized via the streamfunction Ψ:

$$\Psi(\lambda, z) = \int_0^z \int_{\text{west}}^{\text{east}} V(\phi', \lambda, z')\, d\phi'\, dz', \tag{1}$$

where V is the meridional velocity, ϕ is the longitude, λ is the latitude, and z is the depth. In the following, we focus on the upper cell that transports warm Atlantic water northward and cooled ventilated water at depth southward.

For T0 in EC-Earth-PISM, the upper cell of the overturning is located between 200- and 2500-m depth (Fig. 7) with a core at 900-m depth and a maximum transport of 15 Sv (1 Sv $\equiv 10^6$ m^3 s^{-1}). The northward flowing Atlantic water returns to depth south of the Greenland–Scotland ridge (60°–68°N), apart from 2 Sv, which sinks north of the ridge before returning southward to merge with the main AMOC cell at 800–1000-m depth (white contour in Fig. 7). The accuracy of the overturning meridional streamfunction north of the Greenland–Scotland ridge will be addressed in section 3e.

For ease of comparison, it is common to compute Ψ at 26°N, which is also the latitude of the 19 moorings deployed in 2004 as part of the RAPID program (Cunningham 2008). The maximum strength of the meridional overturning streamfunction at 26°N is often used as an AMOC index. Based on the RAPID array, McCarthy et al. (2015) evaluated the AMOC index to be 17.2 ± 4.6 Sv between 2004 and 2007. For this same time period, EC-Earth-PISM has a mean AMOC index of 14.4 Sv (Fig. 1), which is within the observed uncertainty range.

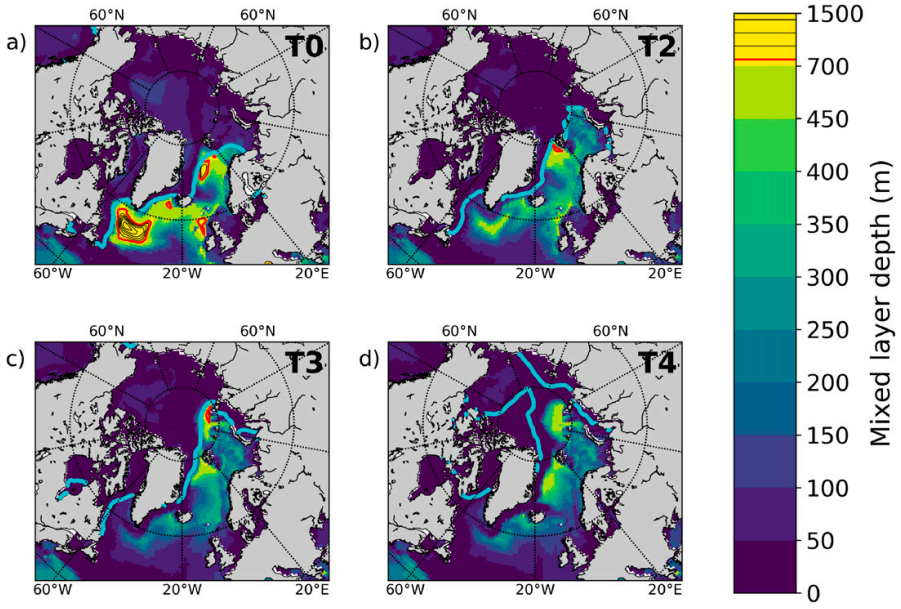

FIG. 6. Mixed layer depth in March for the four different time periods in the EC-Earth-PISM simulation. The blue line indicates the winter sea ice extent and black contour lines indicate mixed layer depths greater than 800 m.

However, following the simulated decline in deep convection, the modeled AMOC is expected to weaken. Similar to 10 other CMIP5 models showing a 15%–60% AMOC index weakening at 30°N by 2100 (Cheng et al. 2013), we record a weakening of 22% by 2100 and 55% by 2200 at 26°N. Following 2200, the AMOC index increases slightly before stabilizing at a mean value of 7 Sv for the remainder of the experiment (until the year 3200, not shown here). The coupled and the uncoupled experiments show the same AMOC changes (blue vs gray in Fig. 1) until 2100. However, Madsen et al. (2020, manuscript submitted to *Climate Dyn.*) show that the recovery following the weakening of the AMOC is reduced in EC-Earth-PISM with respect to EC-Earth.

e. Strengthening of the ArMOC

The meridional overturning streamfunction [Eq. (1)] is a convenient tool to capture the mean water-mass transport in the Atlantic; however, it is not well adapted to the Arctic Basin where integration over longitude is no longer constrained by continents. The result of the integration at 75°N includes for example the transport in the Greenland Sea and the transport in the East Siberian Sea, which are separated by the Eurasian Basin and at opposite longitudes. Hence the transport at 75°N is based on very distinct regions that also have opposite positive meridional velocities. Therefore, the meridional overturning streamfunction may not be a physically correct estimate for the overturning at high latitudes, and the secondary AMOC cell north of 65°N (Fig. 7) may be underestimated.

To further investigate changes in the meridional overturning at high latitudes, we calculate the overturning by integrating the velocities along a transect going from Iceland to the Siberian shelf following Bitz et al. (2006) (see red line in Fig. 5). Here, we use a similar domain of integration by making use of the segment pole of the EC-Earth-PISM's ocean model's ORCA grid (see Madec 2008 for details). On the ORCA grid the variables are defined on pseudolatitudes that flatten close to the North Pole becoming parallel to the Alaska–Siberia segment pole. We integrate v, the velocities normal to the pseudolatitude before the North Pole (green lines in Fig. 5), and continue with $-v$, the velocities normal to the pseudolatitude after the North Pole (yellow lines in Fig. 5) and

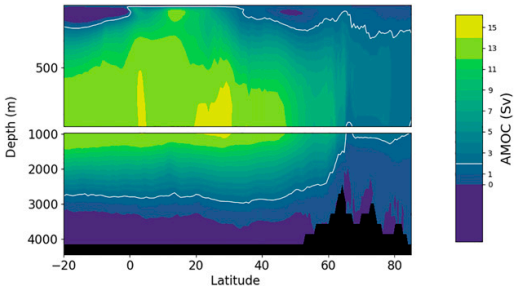

FIG. 7. AMOC during T0: 1970–80 as shown by the meridional overturning streamfunction from 20°S to 90°N in the EC-Earth-PISM simulation. The white contour line (2-Sv transport) stresses a weak northern extension of the AMOC, past the Greenland–Scotland ridge at 65°N.

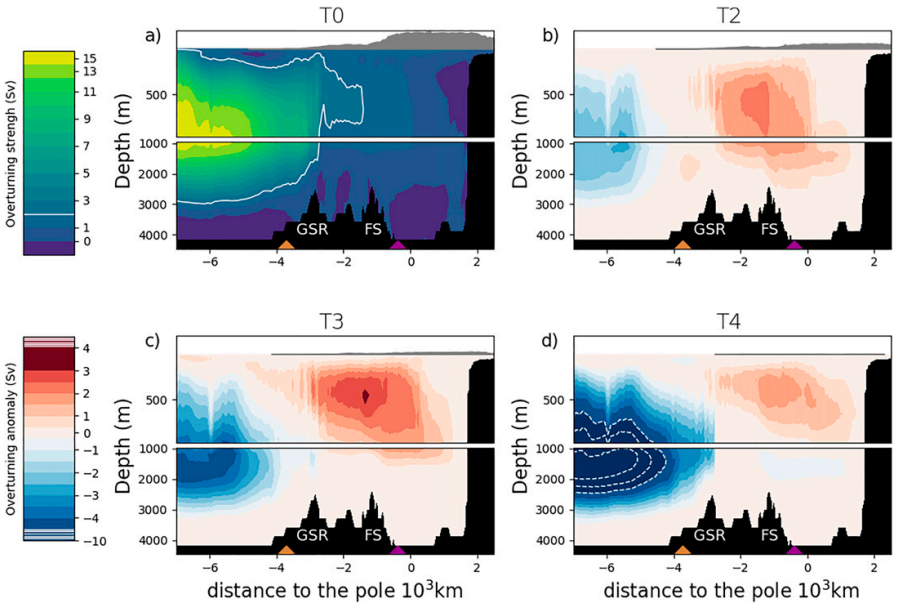

FIG. 8. ArMOC during (a) T0: 1970–80 and anomalies during (b) T2: 2050–60, (c) T3: 2090–2100, and (d) T4: 2130–40 with respect to T0 in the EC-Earth-PISM simulation. Positive anomalies indicate an enhancement of the circulation. In addition to the strengthening of the ArMOC, note the weakening of the AMOC south of the Greenland–Scotland ridge (-7 to -3×10^3 km to the pole). As in Fig. 7, the white contour line at T0 (a) highlights the 2 Sv streamline. For T2, T3, and T4, the white solid (dashed) lines indicate streamlines above 5 Sv (below -5 Sv). The absolute values are shown in Fig. A4. The gray shading at the top of each panel indicates the mean March sea ice thickness as a function of pseudolatitude. The locations of the Greenland–Scotland ridge (GSR) and Fram Strait (FS) are indicated (see also Fig. 5, with matching colors, for the positions of the triangles and a definition of the pseudolatitudes). Note that the bathymetry is a result of a zonal average, which makes the Greenland–Scotland ridge appear deeper than it is.

pointing toward the south. By doing this we ensure that we capture the circulation within the Arctic up to the Siberian shelf in a physically correct manner. The result of this integration can be seen in Fig. 8.

During T0 (Fig. 8a), we observe the typical AMOC cell centered at 900-m depth in the North Atlantic (-6×10^3 km to the pole) and extending to the Greenland–Scotland ridge at 65°N (-3×10^3 km to the pole). This is to be expected, as the integration only differs from the meridional overturning streamfunction north of the Arctic circle at 66°N. North of the Greenland–Scotland ridge, 2 Sv of the AMOC makes its way into the Nordic seas and north to the Fram Strait, and returns at 900-m depth where it merges again with the AMOC. We will from now on refer to the secondary cell north of the Greenland–Scotland ridge as the Arctic meridional overturning circulation (ArMOC).

A clear pattern in the circulation changes can be observed from T2 (Fig. 8b): the AMOC weakens and becomes shallower while the ArMOC strengthens and expands toward the Siberian Shelf. The maximum AMOC is reduced by 2 Sv during T2 and by 4 Sv during T3. In contrast, the maximum strength of the ArMOC increases by about 1.5 Sv during T2, and by 1 to 2.5 Sv during T3. Moreover, positive anomalies of 2.5 Sv are observed at the edge of the Eurasian Basin during T2 and up to the North Pole during T3, which indicates a displacement of the ArMOC toward the interior basin of the Arctic.

While the AMOC at 26°N weakens steadily throughout the twenty-first and twenty-second century, the ArMOC experiences a strengthening until 2100 (T3) followed by a weakening (T4). For comparison with the AMOC index at 26°N through time, the maximal strength with time of the ArMOC in the Nansen Basin (pseudolatitude cutting the red section in Fig. 5 at 87°N, purple diamond) is shown in Fig. 9a. While the AMOC at 26°N weakens, the ArMOC strength almost doubles from 2025 to 2100. After 2100–10 the cell weakens to reach its initial state (1.5 Sv) around year 2225. To link the evolution of the AMOC at 26°N and the ArMOC, Fig. 9a includes a time series of the maximal AMOC strength at 60°N (brown curve), just south of the Greenland–Scotland ridge. Consistent with the AMOC at 26°N, the circulation at 60°N weakens during the twenty-first century but at a much slower rate. However, the weakening at 60°N accelerates around 2100, at the same time as the ArMOC

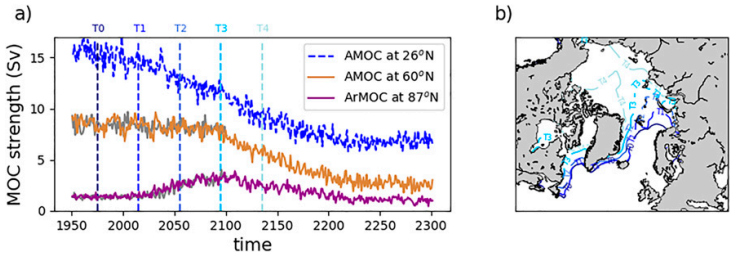

FIG. 9. (a) Time series of the maximal strength of the meridional overturning streamfunction at 26°N in blue (AMOC index), at 60°N in brown, and of the ArMOC at 87°N in purple in the EC-Earth-PISM simulation. Time series for the EC-Earth simulation are superimposed in gray for the AMOC at 60°N and the ArMOC at 87°N. The AMOC at 60°N and ArMOC at 87°N are both computed using the pseudolatitudes outlined in Fig. 5. The main time periods are marked with shades of blue. (b) Map of the ice extent for these time periods with the same colors in (a).

starts to weaken. This suggests that the ArMOC influences the northern overturning circulation in the Atlantic and partly compensates for the early weakening. However, the compensation becomes smaller at lower latitudes and is barely visible in the AMOC strength at 26°N.

This strengthening of the ArMOC until the year 2100 coincides with the northward shift of the ice edge and deep-water formation regions. To investigate this link further, we compute the streamfunction on density surfaces for the ArMOC section. Meridional velocities are collected into potential density bins computed with respect to 2000-m depth and are then integrated throughout the density bins using the cdfmocsig subroutine from the package CDFTOOLS (https://github.com/meom-group/CDFTOOLS).

The result of this integration is shown in Fig. 10a: within the AMOC relatively light water (potential density between 33 and 36.5 kg m^{-3}) travels north and return south 3 × 10^3 km before the pole (~65°N) at density between 36 and 36.8 kg m^{-3}. The ArMOC is also associated with a change in density: 2 Sv travel farther north and become even denser reaching a density of 37 kg m^{-3}. However, when the dense water formed in the Arctic returns toward the Atlantic and joins the AMOC, the high densities are not conserved. From T2 (Fig. 10b) to T4 (Fig. 10d) the streamfunction anomalies

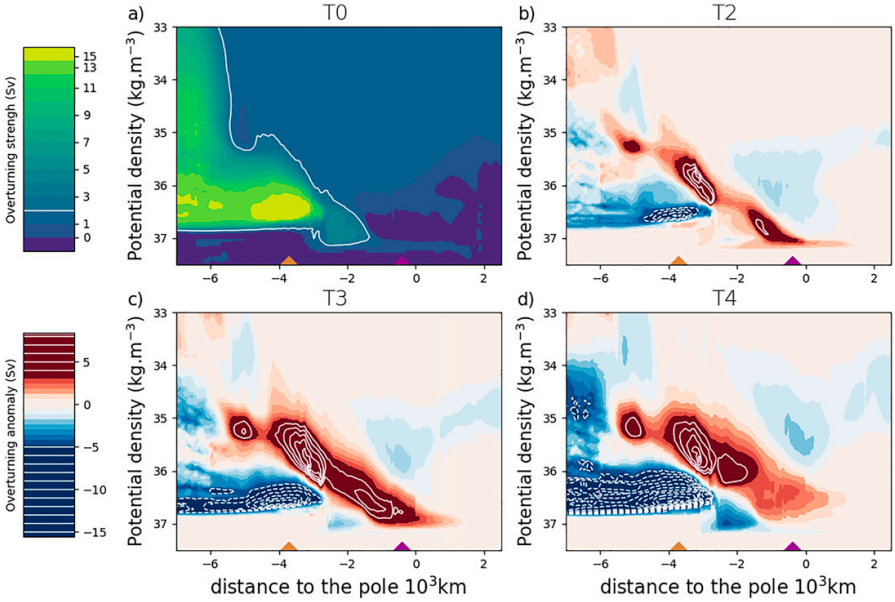

FIG. 10. As in Fig. 8, but in density space. Potential density is computed with respect to the 2000-Pa surface.

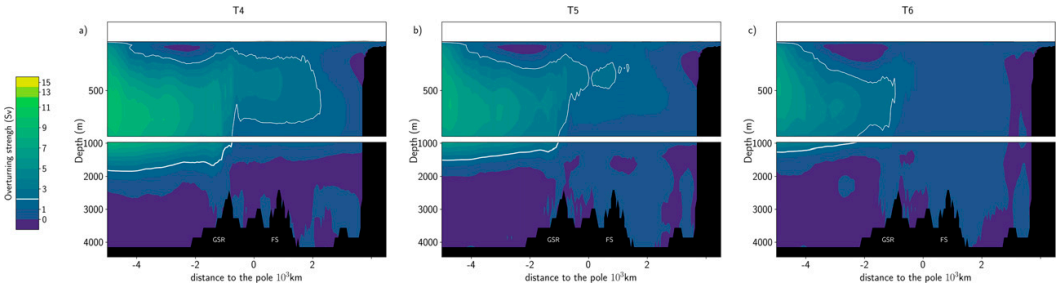

FIG. 11. ArMOC during (a) T4: 2130–40, (b) T5: 2170–80, and (c) T6: 2290–2300 in the EC-Earth-PISM simulation. As in Fig. 7, the white contour lines highlight the 2-Sv streamline.

show two different trends for the AMOC: first the water gets lighter (negative anomaly for the highest densities and positive anomaly for water lighter than 36 kg m^{-3}) and second the overall AMOC weakens. Although more difficult to see than in depth coordinates, it is at least clear during T4 that the circulation has weakened as the weakening in the high density range (10 Sv and more) cannot be compensated by the enhancement observed for the lower densities (5–9 Sv). For the ArMOC, we observe as in Fig. 8 an enhancement of the cell during T2 and T3 together with the development of the cell toward the Siberian Shelf. During T4, Fig. 10d shows that the ArMOC has a weaker core, which is consistent with the streamfunction in depth coordinates.

f. The ice free Arctic Ocean

This section focuses on the changes in the Arctic accompanying the disappearance of the last M km^2 of sea ice. While there is still around 5 M km^2 of winter sea ice during T4, the ocean is ice free by T5 (Fig. 1).

Figure 11 shows that the weakening of the ArMOC initiated between T3 and T4 (Fig. 8) continues after T4: the ArMOC retreats southward between T4 and T5 (Fig. 11b) and the cell is gone by T6 (Fig. 11c). This shows that the simulated weakening of the ArMOC after 2100 (Fig. 9) impacts the entire Arctic overturning cell, from the Greenland–Scotland ridge to the Siberian shelf. The weakening is consistent with the continued reduction in maximum mixed layer depths in the Arctic Basin (not shown).

4. Discussion

Under the most extreme emission scenario from the 5th IPCC report, RCP8.5, Arctic summer sea ice is permanently gone by 2060 in the EC-Earth-PISM simulation (Fig. 1). This timing is independent of the ice sheet coupling: most of the Greenland melting takes place after 2150 (gray line, Fig. A1) when only a small amount of Arctic winter sea ice is left. Additional EC-Earth2.3 experiments by Koenigk et al. (2013) also indicate a summer ice-free ocean from 2060, under the same emission scenario. However, according to Koenigk et al. (2013), the Arctic could be ice free in summer already by 2040 given that the EC-Earth2.3 model overestimates the current observed Arctic sea ice cover, and underestimates the observed retreat rate.

Our coupled simulation also captures the disappearance of winter sea ice, which still covers most of the Canadian and Eurasian Basins by 2100 (T3, Fig. 3). While summer sea ice retreats rapidly from 2035, winter sea ice retreats at a slower rate until the year 2110 (Fig. 1). At this time, the retreat rate increases and the Arctic becomes ice-free all year round from 2165. We focus on the retreat from 1970 to 2130 as the slow winter sea ice retreat appears to be the most relevant for this study.

In addition to the notable sea ice changes in the Arctic, the future of North Atlantic deep convection receives a lot of attention. While many studies focus on the weakening convection in the Labrador and Irminger Seas (Yang et al. 2016; Belonenko et al. 2018), which is forecasted to shut down as a result of increased freshwater fluxes (Jahn and Holland 2013; Wang et al. 2018), it has been suggested that the deep convection could move to higher latitudes, in particular to the interior Arctic Ocean (Nansen Basin; Brodeau and Koenigk 2016; Lique et al. 2018). The latitudinal shift of deep-water formation sites has previously been linked to the winter sea ice retreat by Lique and Thomas (2018) who compared two equilibrium states; one based on preindustrial greenhouse gas concentration with winter sea ice covering the Barents, Greenland, and Iceland Seas, and another based on a 4 × CO_2 increase with respect to preindustrial conditions with the sea ice edge entering the Nansen Basin. More recently, Pérez-Hernández et al. (2019) and Athanase et al. (2020) arrived at the same conclusion after observing deep mixing close to Svalbard in new ice-free areas. Deep convection near Svalbard is a logical intermediate step before it appears in the Nansen Basin; however, the equilibrium simulation by Lique and Thomas (2018) does not allow for an analysis of the changes preceding the emergence of deep convection in the Nansen Basin. Here we opt for an analysis of four time periods of a long coupled experiment covering the different stages of the winter sea ice retreat up to an ice-free Arctic Ocean. Hence, we can test the consistency of deep-water formation changes with winter sea ice retreat in time, and study what happens when the sea ice retreats farther into the Eurasian and Canadian Basins.

We find that as the prevailing deep-water formation sites weaken, new sites appear farther north, closely following the

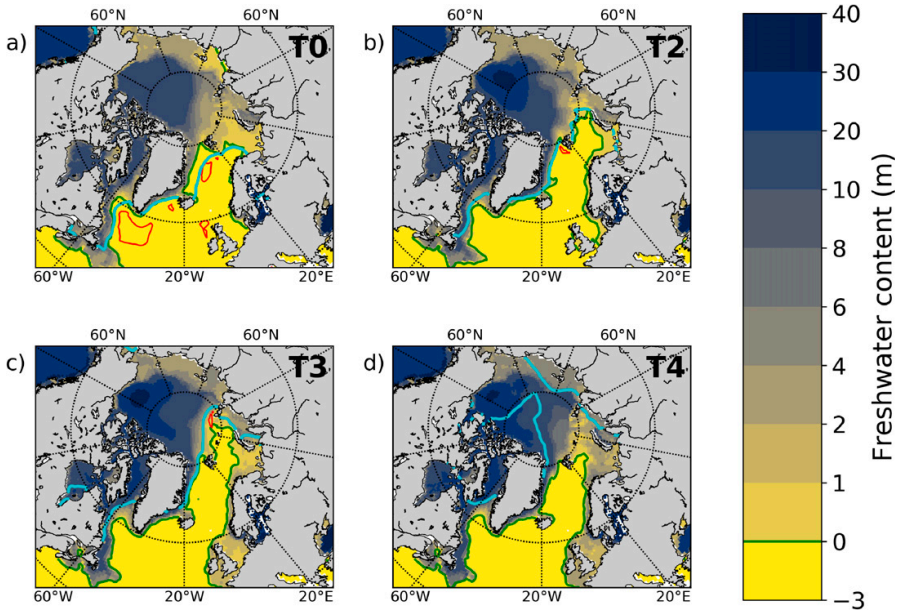

FIG. 12. Freshwater content in the top 800 m during (a) T0: 1970–80, (b) T2: 2050–60, (c) T3: 2090–2100, and (d) T4: 2130–40 in the EC-Earth-PISM simulation. The blue lines indicate the winter (March) sea ice edge, while the red lines indicate the location of deep-water formation.

retreating winter sea ice edge until the sea ice edge reaches the Nansen Basin. At an early stage (T1; 2010–19, Fig. 4c), convection in the Labrador Sea weakens, while convection in the Nordic seas strengthens. In the following years, the core of the convection in the Nordic seas moves farther north to the newly ice free south coast of Svalbard (T2; 2050–60, Fig. 6c), which is consistent with Pérez-Hernández et al. (2019) and Athanase et al. (2020). Finally, the end of the century (T3; 2090–2100, Fig. 6d) is marked by the notable emergence of deep convection in the Nansen Basin at the edge of the winter sea ice cover, as previously described by Brodeau and Koenigk (2016, EC-Earth2.3 with RCP8.5 forcing) and Lique et al. (2018; HiGEM with 4 × CO_2 forcing). Brodeau and Koenigk (2016) show a weakening of the convection in the Nansen Basin toward the end of their simulations (2085 to 2100). What happens after 2100, when the winter sea ice retreats farther into the Eurasian Basin has not been investigated in these previous studies.

According to the long simulations analyzed here, the northward migration of the deep-water formation sites does not continue after 2100. Instead, while the retreat of winter sea ice continues and accelerates, the deepest mixed layers remain within the Nansen Basin and the western Nordic seas during T4 (2130–40, Fig. 6d) and become shallower, consistent with Brodeau and Koenigk (2016). In 2140, 25 years before the Arctic becomes perennially ice free, deep convection (>800 m) is absent in the Atlantic Ocean, in the Nordic seas, as well as farther north in the Nansen Basin. In summary, simulated future reductions in Atlantic deep-water formation is only temporarily and partially compensated by enhanced deep-water formation farther north into the Nordic seas and the Arctic Ocean.

The fact that convection is not initiated in the Canadian Basin can be explained by its high surface freshwater content. The Arctic Ocean, and particularly the Canadian Basin, is known to be very fresh compared to the Atlantic Ocean as a result of river runoff from Siberia and Canada and the inflow of fresh Pacific water through the Bering Strait (Aagaard and Carmack 1989). Here we measure the freshwater content FWC by integrating the salinity anomaly in the upper 800 m, using the reference salinity S_{ref} = 34.8 defined by Aagaard and Carmack (1989) and corresponding to the mean salinity of the Arctic Ocean:

$$\mathrm{FWC} = \int_{-800\,\mathrm{m}}^{0} \frac{S_{\mathrm{ref}} - S(z)}{S_{\mathrm{ref}}} dz .$$

We use a depth of 800 m for the integration and the mean salinity in March to compare the freshwater content with the location of deep-water formation. In EC-Earth-PISM, most of the Arctic Basin has an upper ocean freshwater content larger than 10 m (Fig. 12d). In fact, the presence of freshwater in the top layer indicates that the ocean is highly stratified, hence stable. During T4 (2130–40) the sea ice edge meets this very stable region and the increased air–sea heat flux, in this newly ice-free area, is not sufficient to trigger convection. In contrast, during T3, deep convection in the Nansen Basin was made

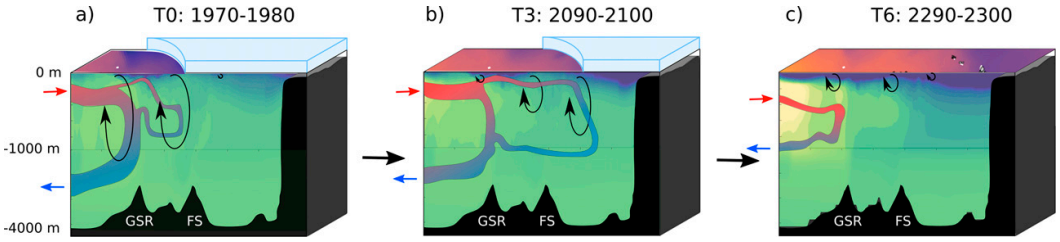

FIG. 13. Sketch summarizing the evolution of the deep mixing and the ArMOC under the retreat of the sea ice edge. (a) During T0: 1970–80 there is deep convection on both sides of the Greenland–Scotland ridge. Both AMOC and ArMOC are present, but the ArMOC extent is limited by the sea ice edge. (b) During T3: 2090–2100 the sea ice edge retreats and the surface ocean warms, which result in shallower (weaker) convection. The ArMOC develops as deep convection moves northward, while the AMOC weakens. Finally, (c) during T6: 2290–2300 there is no more winter sea ice or deep convection, which is linked to the warming of the surface and the freshening of the upper ocean. The AMOC is strongly weakened but still present by opposition to the ArMOC, which has shut down. In this sketch, the ArMOC circulation and the bathymetry are based on Figs. A4a and A4c for T0 and T3 and on Fig. 11 for T6.

possible by a concomitant retreat of freshwater, or intrusion of saline Atlantic water (Fig. 12c). The strengthening of the ArMOC could be responsible for this saline intrusion, which acts as a positive feedback on the ArMOC by weakening the stratification (see the negative Brunt–Väisälä frequency anomaly in the Barents Sea and Nansen Basin; Fig. A2c) and enhancing the convection. However, the saline Atlantic water does not make its way to the central Arctic Basin (Figs. 12d and A3). Most of the Arctic Basin becomes fresher and more stable through time (positive anomaly in Figs. A2b–d). Lique et al. (2018) also obtain stability differences between the Canadian and the Eurasian Basins under the sea ice retreat. They suggest that surface circulation changes in the Arctic Ocean are responsible for the changes in freshwater distribution. Aagaard and Carmack (1989) already suggested that the Eurasian and Canadian Basins could answer differently to the climate change due to their differences in freshwater sources and sinks.

In this study, we find that the changes in deep-water formation in the Nordic seas and Arctic Basin have consequences for the northern extension of the AMOC and introduce the term ArMOC. The ArMOC is shallower than the AMOC and is represented by an overturning of 2–3 Sv (Fig. 8a). However, the ArMOC is associated with a further densification of the Atlantic water (Fig. 10a). As the sea ice and deep-water formation sites retreat northward, the ArMOC strengthens and migrates north (T2, T3, Fig. 8). Moreover, the maximum strength of the ArMOC around 2100 (Fig. 9a) coincides with the disappearance of the northernmost convection site in the Nansen Basin. Bitz et al. (2006) show similar enhancement of an Arctic cell in a CO_2 ramping experiment with CCSM3. However, in this previous study the enhancement is linked to increasing sea ice formation on the Siberian shelf as a consequence of increased seasonality. The timing of increased sea ice formation and the enhanced ArMOC do not coincide in our simulation. Instead, we suggest that open-water convection is the main driver of the Arctic cell.

The strengthening of the ArMOC during the twenty-first century contrasts with the forecasted AMOC weakening. The weakening of the AMOC at 26°N is found in most climate models (Cheng et al. 2013) and is consistent with the reduction in North Atlantic deep convection (Jahn and Holland 2013; Brodeau and Koenigk 2016). However, the observed reduction in deep-water formation has not yet been linked to a consistent observed weakening of the AMOC at 26°N (Smeed et al. 2018). In the long EC-Earth-PISM simulation, the AMOC strength at 26°N steadily decreases from 15.5 Sv in 1950 to 7 Sv in 2200 (Fig. 9a). We find that the ArMOC strengthens due to the simulated enhanced deep-water formation north of the Greenland–Scotland ridge, while the AMOC weakens because of the overall deep-water formation reduction. In particular, the enhanced deep-water formation north of the Greenland–Scotland ridge seems to compensate the AMOC weakening at 60°N according to the kink at 2100 present in Fig. 9a coinciding with the ArMOC maximum. However, the intermittent ArMOC strengthening (~1.8 Sv) is small compared to the overall 8.5-Sv reduction of the AMOC at 26°N in the period from 1950 to 2200, hence the delay is unnoticed at 26°N. Similarly, Lique et al. (2018) estimate an increase of the Arctic contribution to the AMOC of only 0.7 Sv when convection reaches the Eurasian Basin.

We suggest that the enhanced convection in the Arctic Ocean and the strengthening of the ArMOC slows down the weakening of the AMOC. This hypothesis is supported by recent observations highlighting a more active role of the region north of the Greenland–Scotland ridge in determining AMOC variability (Chafik et al. 2019) and water mass transformation (Chafik and Rossby 2019). Further, the Overturning in the Subpolar North Atlantic Programme (OSNAP) array, consisting of moorings from Labrador to the tip of Greenland (OSNAP West), and from the tip of Greenland to Scotland (OSNAP East), makes it possible to separate the impact of deep-water formation in the Labrador Sea, Iceland–Scotland region, and Nordic seas (Lozier et al. 2017). Based on the first 21 months of observations, Lozier et al. (2019) find that the AMOC variability is driven by water mass transformation north of the OSNAP East line (i.e., in the Iceland–Scotland region, Nordic seas, and farther north).

According to Heuzé et al. (2013), CMIP5 models overestimate deep-water formation resulting from open-water convection in the Southern Ocean at the expense of shelf processes not resolved by the models. In the North Atlantic, the simulated

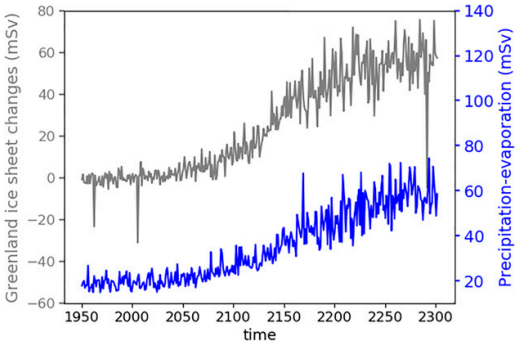

FIG. A1. Time series of the freshwater resulting from the Greenland ice sheet melting (gray line) and the rainfall (precipitation − evaporation) over the Arctic Basins and Nordic seas (blue line) in EC-Earth-PISM. The reduction in Greenland ice volume from around 2100 (Fig. 2) results in an increase in freshwater flux to the ocean. This freshwater flux is comparable to the rainfall over the Arctic Basins and Nordic seas from around 2200 (40 mSv) and stabilizes close to 60 mSv. However, part of the Greenland meltwater is transported southward (not studied here).

dense water produces a reasonable AMOC strength at 26°N, although the amount of open convection is unrealistically high in the models (Heuzé 2017). In fact, the cascading of dense shelf water off continental shelves has been described as one of the main mechanisms generating Arctic deep water (Aagaard et al. 1985). If dense shelf water were to be represented, we would expect the dynamics of the ArMOC, and its simulated strength over the next century, to be altered. In particular, the Arctic summer sea ice retreat and enhanced seasonality could lead to a strengthened ArMOC, as suggested by Bitz et al. (2006). In this hypothesis, the asymmetry between summer and winter sea ice reduction results in more winter sea ice formation and more brine rejection, enhancing dense-water formation on the shelves. On the other hand, reducing the importance of open water convection could imply a smaller impact of the northward shift of Arctic sea ice on the ArMOC.

5. Conclusions

The two simulations analyzed in this study show that accelerated melt of the Greenland ice sheet occurs after the simulated abrupt reduction in Arctic sea ice. This suggests that the additional freshwater input to the ocean, originating from the coupling with the Greenland ice sheet (PISM), does not significantly slow down the sea ice reduction in the EC-Earth-PISM model. The meltwater flux from Greenland exceeds 30 mSv by 2150, when the Arctic Ocean is nearly ice free, and reaches its mean maximal value of 53 mSv by 2200. At this point, the Greenland melt contributes by freshening and stabilizing the Arctic Basins, thereby promoting the weakening the Arctic meridional overturning circulation (ArMOC) north of the Greenland–Scotland ridge.

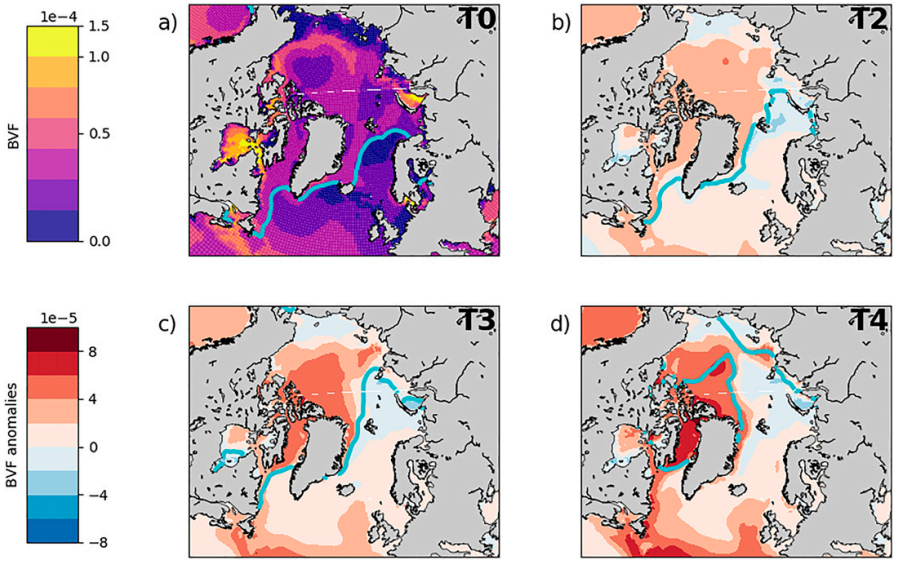

FIG. A2. Yearly mean Brunt–Väisälä frequencies in the top 800 m for the period (a) T0: 1970–80 in the EC-Earth-PISM simulation and anomalies during (b) T2: 2050–60, (c) T3: 2090–2100, and (d) T4: 2130–40 with respect to T0. The winter sea ice edge is plotted with the blue contour line. The blue color at the edge of the winter sea ice (Barents Sea and Nansen Basin) shows a weakening of the stratification while the rest of the ocean, and in particular the Arctic Basins and Nansen Basin excluded, becomes more stable.

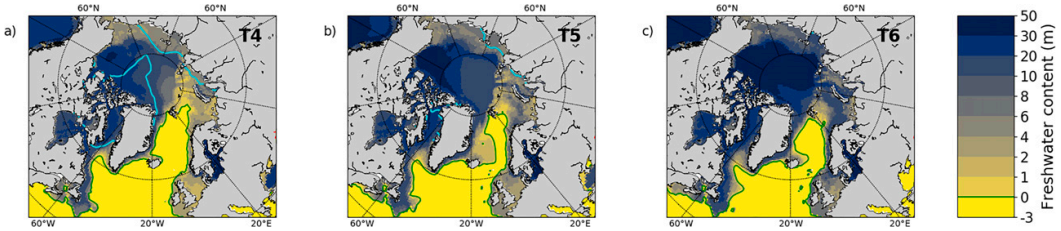

FIG. A3. Freshwater content as in Fig. 12, but during (a) T4: 2130–40, (b) T5: 2170–80, and (c) T6: 2290–2300. After T4, the Arctic Basins get consistently fresher, which can be linked to the water cycle acceleration and the ArMOC weakening that brings less saline Atlantic water to the Arctic.

Our key findings, related to the Arctic meridional overturning circulation (ArMOC), a new metric introduced to study the overturning changes north of the Greenland–Scotland ridge and into the central Arctic, are as follows:

- As the winter sea ice edge retreats into the interior Arctic Ocean from 1970 (Fig. 13a) to 2100 (Fig. 13b), the deep-water sites migrate north, enhancing the ArMOC.
- The simulated ArMOC strengthening contributes to a slowdown of the AMOC weakening at 26°N by 0.01 Sv yr^{-1} until 2100.
- After 2100, as the Arctic interior becomes ice free, there is a decoupling between the winter sea ice edge and deep-water formation. The upper ocean is strongly stratified due to large freshwater fluxes. Deep convection weakens in all basins, and the ArMOC is reduced, becoming negligible by 2200.
- In contrast to the ArMOC, the AMOC at 26°N is steadily reduced from 2000 to 2200. Hence, the AMOC and ArMOC appear decoupled in a warming climate, which warrants the need to study them separately.

Acknowledgments. The research leading to these results is part of the ice2ice project funded by the European Research Council under the European Community Seventh Framework Programme (FP7/2007-2013)/ERC Grant Agreement 610055. The research was supported by the Centre for Climate Dynamics at the Bjerknes Centre for Climate Research and the Trond Mohn Foundation under Grant Agreement BFS2016REK01 (A.B.).

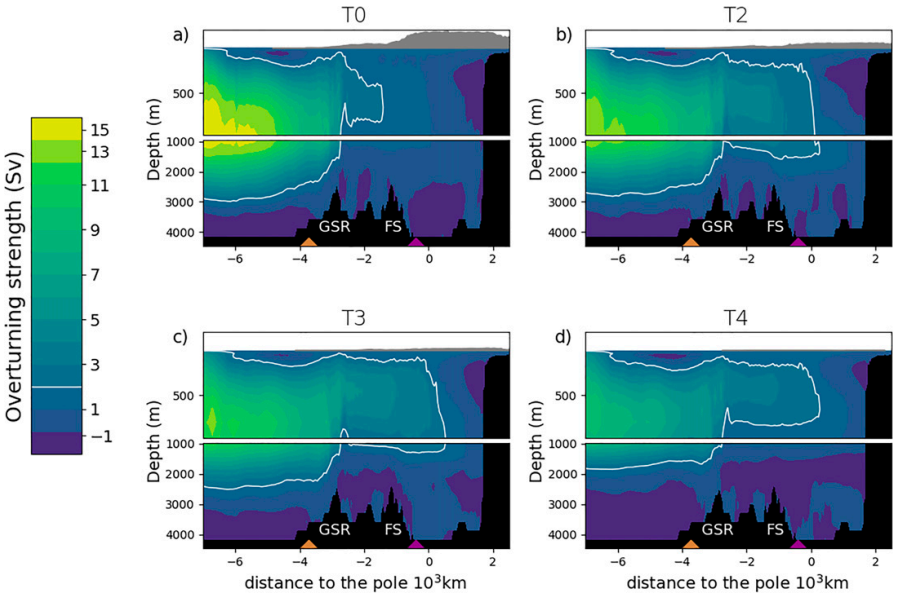

FIG. A4. ArMOC during (a) T0: 1970–80, (b) T2: 2050–60, (c) T3: 2090–2100, and (d) T4: 2130–40 in the EC-Earth-PISM simulation. As in Fig. 7, the white contour lines highlight the 2-Sv streamline and shows nicely the development of the ArMOC: its expansion from T0 to T3 and its reduction after T3.

We are grateful to Julian Mak for adapting functions of the CDFTOOLS program, in particular, cdfmocsig, into Python and sharing them on GitHub (https://github.com/julianmak/NEMO-related?files=1; personal website: https://nemo-related.readthedocs.io/en/latest/). Finally, we wish to thank Ida Margrethe Ringgaard for her help with the model outputs, Helene Asbjørnsen for her friendly review, and three anonymous reviewers for good suggestions that improved the manuscript.

Data availability statement. The Argo mixed layer database used in this study is available online at http://mixedlayer.ucsd.edu (see also Holte et al. 2017). The hydrographic dataset from Huang et al. (2020) consists of observations from several archives that can be accessed as listed in their Supplementary Table 1. The combined hydrographic dataset is available on request from A.B. (Ailin.Brakstad@uib.no).

APPENDIX

Complementary Figures

Figure A1 is a complement to Fig. 2: the ice volume change of Greenland is converted into freshwater fluxes and compared to the increase in rainfall over the Arctic region. Figure A2 shows the stability of the top 500 m of the water column as a complement to the freshwater content displayed in Fig. 12. Figure A3 shows that the Arctic Basins and Barents and Kara Seas only get fresher after T4, which is consistent with the ArMOC weakening in Fig. 11. Finally, Fig. A4 intends to better show the ArMOC spatial extension in time, as a complement to Fig. 8. . . .

REFERENCES

Aagaard, K., and E. C. Carmack, 1989: The role of sea ice and other fresh water in the Arctic circulation. *J. Geophys. Res.*, **94**, 14485, https://doi.org/10.1029/JC094iC10p14485.

——, J. H. Swift, and E. C. Carmack, 1985: Thermohaline circulation in the Arctic Mediterranean Seas. *J. Geophys. Res.*, **90**, 4833, https://doi.org/10.1029/JC090iC03p04833.

Athanase, M., C. Provost, M. D. Pérez-Hernández, N. Sennéchael, C. Bertosio, C. Artana, G. Garric, and J.-M. Lellouche, 2020: Atlantic water modification north of Svalbard in the Mercator physical system from 2007 to 2020. *J. Geophys. Res. Oceans*, **125**, e2020JC016463, https://doi.org/10.1029/2020JC016463.

Belonenko, T. V., A. M. Fedorov, I. L. Bashmachnikov, and V. R. Foux, 2018: Current intensity trends in the Labrador and Irminger Seas based on satellite altimetry data. *Izv. Atmos. Ocean. Phys.*, **54**, 1031–1038, https://doi.org/10.1134/S0001433818090074.

Bitz, C. M., P. R. Gent, R. A. Woodgate, M. M. Holland, and R. Lindsay, 2006: The influence of sea ice on ocean heat uptake in response to increasing CO_2. *J. Climate*, **19**, 2437–2450, https://doi.org/10.1175/JCLI3756.1.

Böning, C. W., E. Behrens, A. Biastoch, K. Getzlaff, and J. L. Bamber, 2016: Emerging impact of Greenland meltwater on deepwater formation in the North Atlantic Ocean. *Nat. Geosci.*, **9**, 523–527, https://doi.org/10.1038/ngeo2740.

Brakstad, A., K. Våge, L. Håvik, and G. W. K. Moore, 2019: Water mass transformation in the Greenland Sea during the period 1986–2016. *J. Phys. Oceanogr.*, **49**, 121–140, https://doi.org/10.1175/JPO-D-17-0273.1.

Brodeau, L., and T. Koenigk, 2016: Extinction of the northern oceanic deep convection in an ensemble of climate model simulations of the 20th and 21st centuries. *Climate Dyn.*, **46**, 2863–2882, https://doi.org/10.1007/s00382-015-2736-5.

Broecker, W., G. Bond, M. Klas, E. Clark, and J. McManus, 1992: Origin of the northern Atlantic's Heinrich events. *Climate Dyn.*, **6**, 265–273, https://doi.org/10.1007/BF00193540.

Bueler, E., and J. Brown, 2009: Shallow shelf approximation as a "sliding law" in a thermomechanically coupled ice sheet model. *J. Geophys. Res.*, **114**, F03008, https://doi.org/10.1029/2008JF001179.

Chafik, L., and T. Rossby, 2019: Volume, heat, and freshwater divergences in the subpolar North Atlantic suggest the Nordic Seas as key to the state of the meridional overturning circulation. *Geophys. Res. Lett.*, **46**, 4799–4808, https://doi.org/10.1029/2019GL082110.

——, J. E. Øie Nilsen, S. Dangendorf, G. Reverdin, and T. Frederikse, 2019: North Atlantic Ocean circulation and decadal sea level change during the altimetry era. *Sci. Rep.*, **9**, 1041, https://doi.org/10.1038/s41598-018-37603-6.

Cheng, W., J. C. Chiang, and D. Zhang, 2013: Atlantic meridional overturning circulation (AMOC) in CMIP5 models: RCP and historical simulations. *J. Climate*, **26**, 7187–7197, https://doi.org/10.1175/JCLI-D-12-00496.1.

Cunningham, S., 2008: Monitoring the Atlantic meridional overturning circulation at 26.5°N: Rapid-watch. National Oceanography Centre Southampton Research and Consultancy Rep. 59, 18 pp., http://nora.nerc.ac.uk/id/eprint/165106/1/NOCS_R%26C_59.pdf.

Davis, P. E., C. Lique, H. L. Johnson, and J. D. Guthrie, 2016: Competing effects of elevated vertical mixing and increased freshwater input on the stratification and sea ice cover in a changing Arctic Ocean. *J. Phys. Oceanogr.*, **46**, 1531–1553, https://doi.org/10.1175/JPO-D-15-0174.1.

de Boyer Montégut, C., G. Madec, A. S. Fischer, A. Lazar, and D. Iudicone, 2004: Mixed layer depth over the global ocean: An examination of profile data and a profile-based climatology. *J. Geophys. Res.*, **109**, C12003, https://doi.org/10.1029/2004JC002378.

de Jong, M. F., and L. de Steur, 2016: Strong winter cooling over the Irminger Sea in winter 2014–2015, exceptional deep convection, and the emergence of anomalously low SST. *Geophys. Res. Lett.*, **43**, 7106–7113, https://doi.org/10.1002/2016GL069596.

Fairbanks, R. G., 1990: The age and origin of the "Younger Dryas climate event" in Greenland ice cores. *Paleoceanography*, **5**, 937–948, https://doi.org/10.1029/PA005i006p00937.

Fichefet, T., and M. A. M. Maqueda, 1997: Sensitivity of a global sea ice model to the treatment of ice thermodynamics and dynamics. *J. Geophys. Res.*, **102**, 12 609–12 646, https://doi.org/10.1029/97JC00480.

——, C. Poncin, H. Goosse, P. Huybrechts, I. Janssens, and H. L. Treut, 2003: Implications of changes in freshwater flux from the Greenland ice sheet for the climate of the 21st century. *Geophys. Res. Lett.*, **30**, 1911, https://doi.org/10.1029/2003GL017826.

Hazeleger, W., and Coauthors, 2012: EC-Earth V2.2: Description and validation of a new seamless earth system prediction model. *Climate Dyn.*, **39**, 2611–2629, https://doi.org/10.1007/s00382-011-1228-5.

Heuzé, C., 2017: North Atlantic deep water formation and AMOC in CMIP5 models. *Ocean Sci.*, **13**, 609–622, https://doi.org/10.5194/os-13-609-2017.

——, K. J. Heywood, D. P. Stevens, and J. K. Ridley, 2013: Southern Ocean bottom water characteristics in CMIP5 models. *Geophys. Res. Lett.*, **40**, 1409–1414, https://doi.org/10.1002/grl.50287.

Hillaire-Marcel, C., A. D. Vernal, G. Bilodeau, and A. J. Weaver, 2001: Absence of deep-water formation in the Labrador Sea during the last interglacial period. *Nature*, **410**, 1073–1077, https://doi.org/10.1038/35074059.

Holte, J., L. D. Talley, J. Gilson, and D. Roemmich, 2017: An Argo mixed layer climatology and database. *Geophys. Res. Lett.*, **44**, 5618–5626, https://doi.org/10.1002/2017GL073426.

Huang, J., R. S. Pickart, R. X. Huang, P. Lin, A. Brakstad, and F. Xu, 2020: Sources and upstream pathways of the densest overflow water in the Nordic Seas. *Nat. Commun.*, **11**, 5389, https://doi.org/10.1038/s41467-020-19050-y.

Jahn, A., and M. M. Holland, 2013: Implications of Arctic sea ice changes for North Atlantic deep convection and the meridional overturning circulation in CCSM4-CMIP5 simulations. *Geophys. Res. Lett.*, **40**, 1206–1211, https://doi.org/10.1002/grl.50183.

Kim, W. M., S. Yeager, and G. Danabasoglu, 2020: Revisiting the causal connection between the great salinity anomaly of the 1970s and the shutdown of Labrador Sea deep convection. *J. Climate*, **34**, 675–696, https://doi.org/10.1175/JCLI-D-20-0327.1.

Koenigk, T., L. Brodeau, R. G. Graversen, J. Karlsson, G. Svensson, M. Tjernström, U. Willén, and K. Wyser, 2013: Arctic climate change in 21st century CMIP5 simulations with EC-Earth. *Climate Dyn.*, **40**, 2719–2743, https://doi.org/10.1007/s00382-012-1505-y.

Kuhlbrodt, T., A. Griesel, M. Montoya, A. Levermann, M. Hofmann, and S. Rahmstorf, 2007: On the driving processes of the Atlantic meridional overturning circulation. *Rev. Geophys.*, **45**, RG2001, https://doi.org/10.1029/2004RG000166.

Lique, C., and M. D. Thomas, 2018: Latitudinal shift of the Atlantic meridional overturning circulation source regions under a warming climate. *Nat. Climate Change*, **8**, 1013–1020, https://doi.org/10.1038/s41558-018-0316-5.

——, H. L. Johnson, and Y. Plancherel, 2018: Emergence of deep convection in the Arctic Ocean under a warming climate. *Climate Dyn.*, **50**, 3833–3847, https://doi.org/10.1007/s00382-017-3849-9.

Lozier, M. S., and Coauthors, 2017: Overturning in the subpolar North Atlantic program: A new international ocean observing system. *Bull. Amer. Meteor. Soc.*, **98**, 737–752, https://doi.org/10.1175/BAMS-D-16-0057.1.

——, and Coauthors, 2019: A sea change in our view of overturning in the subpolar North Atlantic. *Science*, **363**, 516–521, https://doi.org/10.1126/science.aau6592.

Madec, G., 2008: NEMO ocean engine. IPSL Note du Pôle de Modélisation 27, 209 pp.

McCarthy, G. D., and Coauthors, 2015: Measuring the Atlantic meridional overturning circulation at 26°N. *Prog. Oceanogr.*, **130**, 91–111, https://doi.org/10.1016/j.pocean.2014.10.006.

Nghiem, S. V., I. G. Rigor, D. K. Perovich, P. Clemente-Colón, J. W. Weatherly, and G. Neumann, 2007: Rapid reduction of Arctic perennial sea ice. *Geophys. Res. Lett.*, **34**, L19504, https://doi.org/10.1029/2007GL031138.

Notz, D., and J. Stroeve, 2016: Observed Arctic sea-ice loss directly follows anthropogenic CO_2 emission. *Science*, **354**, 747–750, https://doi.org/10.1126/science.aag2345.

——, and Coauthors, 2020: Arctic sea ice in CMIP6. *Geophys. Res. Lett.*, **47**, e2019GL086749, https://doi.org/10.1029/2019GL086749.

Nummelin, A., C. Li, and L. H. Smedsrud, 2015: Response of Arctic Ocean stratification to changing river runoff in a column model. *J. Geophys. Res. Oceans*, **120**, 2655–2675, https://doi.org/10.1002/2014JC010571.

Pérez-Hernández, M. D., and Coauthors, 2019: Structure, transport, and seasonality of the Atlantic water boundary current north of Svalbard: Results from a yearlong mooring array. *J. Geophys. Res. Oceans*, **124**, 1679–1698, https://doi.org/10.1029/2018JC014759.

Rawlins, M. A., and Coauthors, 2010: Analysis of the Arctic system for freshwater cycle intensification: Observations and expectations. *J. Climate*, **23**, 5715–5737, https://doi.org/10.1175/2010JCLI3421.1.

Smeed, D. A., and Coauthors, 2018: The North Atlantic Ocean is in a state of reduced overturning. *Geophys. Res. Lett.*, **45**, 1527–1533, https://doi.org/10.1002/2017GL076350.

Smith, R. S., and J. M. Gregory, 2009: A study of the sensitivity of ocean overturning circulation and climate to freshwater input in different regions of the North Atlantic. *Geophys. Res. Lett.*, **36**, L15701, https://doi.org/10.1029/2009GL038607.

Stroeve, J., and D. Notz, 2018: Changing state of Arctic sea ice across all seasons. *Environ. Res. Lett.*, **13**, 103001, https://doi.org/10.1088/1748-9326/aade56.

Taylor, K. E., R. J. Stouffer, and G. A. Meehl, 2012: An overview of CMIP5 and the experiment design. *Bull. Amer. Meteor. Soc.*, **93**, 485–498, https://doi.org/10.1175/BAMS-D-11-00094.1.

Våge, K., and Coauthors, 2009: Surprising return of deep convection to the subpolar North Atlantic Ocean in winter 2007–2008. *Nat. Geosci.*, **2**, 67–72, https://doi.org/10.1038/ngeo382.

Valcke, S., 2006: OASIS3 user guide. PRISM Project Tech. Rep. 3, 64 pp.

van Vuuren, D. P., and Coauthors, 2011: The representative concentration pathways: An overview. *Climatic Change*, **109**, 5–31, https://doi.org/10.1007/s10584-011-0148-z.

Wang, H., S. Legg, and R. Hallberg, 2018: The effect of Arctic freshwater pathways on North Atlantic convection and the Atlantic meridional overturning circulation. *J. Climate*, **31**, 5165–5188, https://doi.org/10.1175/JCLI-D-17-0629.1.

Winkelmann, R., M. A. Martin, M. Haseloff, T. Albrecht, E. Bueler, C. Khroulev, and A. Levermann, 2011: The Potsdam Parallel Ice Sheet Model (PISM-PIK)—Part 1: Model description. *Cryosphere*, **5**, 715–726, https://doi.org/10.5194/tc-5-715-2011.

Yang, Q., T. H. Dixon, P. G. Myers, J. Bonin, D. Chambers, and M. R. V. D. Broeke, 2016: Correction: Corrigendum: Recent increases in Arctic freshwater flux affects Labrador Sea convection and Atlantic overturning circulation. *Nat. Commun.*, **7**, 13545, https://doi.org/10.1038/ncomms13545.

Yashayaev, I., and J. W. Loder, 2017: Further intensification of deep convection in the Labrador Sea in 2016. *Geophys. Res. Lett.*, **44**, 1429–1438, https://doi.org/10.1002/2016GL071668.

Paper II

4.2 Arctic Overturning Circulation (ArMOC) strengthening in CMIP6 models

Anaïs Bretones, Aleksi Nummelin, Kerim H. Nisancioglu, Morven Muilwijk
submitted to *Journal of Climate*

Paper III

4.3 Arctic circulation changes accompanying the transition from Heinrich Stadial to Greenland Interstadial (in NorESM1-F)

Anaïs Bretones, Chuncheng Guo, Yvan Romé, Kerim H. Nisancioglu

Manuscript prepared for submission

Chapter 5

Perspectives and outlook

In this dissertation, I provide a new way to study the Arctic overturning, by making use of the meridional overturning streamfunction and the geometry of tripolar grids in state-of-the-art climate models. The streamfunction north of the GSR is adapted and named the Arctic Meridional Overturning Circulation (ArMOC), providing a means of comparing the strength and extent of the circulation throughout the Nordic Seas and Arctic basins. This metric, the ArMOC, proves to be invaluable for investigating the mechanism driving the overturning variability in the Arctic and assessing the Arctic overturning strength in climate models. Despite recent attention (*Weijer et al.*, 2022), the Arctic overturning has mostly been assessed via observation of volume transport at the main gateways (*Østerhus et al.*, 2019) and its drivers have been studied using idealized models (*Eldevik and Nilsen*, 2013; *Haine*, 2021). To date, only one other study has looked into the Arctic overturning in a state-of-the-art climate model (*Bitz et al.*, 2006). This dissertation thus provides novel insight about an important component of the global ocean circulation.

5.1 The ArMOC framework

One downside of our method applied to studying the Arctic overturning is that it can only be applied to models with a tripolar grid, therefore reducing the number of models that can be analyzed. In particular, it favors models using NEMO as the ocean component. Recent results indicate intensified Arctic changes in this family of models (*Pan et al.*, 2023) which could reflect on the ArMOC strength (see section 4.2 for further discussion).

Another potential weakness of the applied method is that the section used to calculate ArMOC (yellow line, Fig. 2.4) does not fully capture the circulation in the domain, which could result in an underestimation of the changes. The method could be improved by using

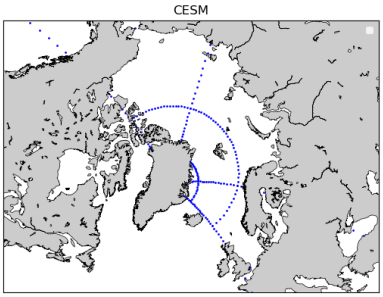

Figure 5.1: CESM's grid characteristics in the Arctic highlighted through 2 parallels and 4 meridians. The parallels encircle Greenland, following the Arctic Ocean along its central axis, with one meridian aligning with the GSR.

an axis of integration that is perpendicular to the GSR and to the Fram Strait and Barents Sea Opening. In CESM2, pseudo-latitudes satisfy these conditions (Fig. 5.1), making this grid a promising alternative to study the overturning in this model. In this case, the overturning would be obtained by integrating zonal velocities u along "pseudo-parallels" starting from the GSR and ending in the Canadian archipelago. An effective approach for improving the ArMOC investigation would involve projecting the data from each CMIP6 model onto the CESM2 grid. This would allow a systematic evaluation of the ArMOC in CMIP6 models and a better representation of the circulation. The transformation and analysis should then also be applied to Ocean state estimate products, which would provide a means of evaluating model performance.

Other methods exist that could have been used to calculate the Arctic overturning. The streamfunction in thermohaline coordinates (e.g., *Zika et al.*, 2012), which describes the volume flow in temperature-salinity coordinates and shows the conversion of temperature and salinity through the whole ocean interior, could potentially offer an accurate estimate of the total volume transport associated with the transformation of Atlantic water. The velocities are then integrated for specific combinations of temperature and salinity, and the circulation provided in T-S space. This method effectively prevents biases originating from model grid considerations, but it comes at the expense of losing the spatial dimension, and should therefore be used as a complementary diagnostic.

5.2 ArMOC dependency on dense-water formation

Through an analysis of the ArMOC in different models, and under different forcing conditions, I have highlighted the dependency between the overturning and dense-water formation, suggesting a minor role of the wind in driving the overturning circulation in the Arctic. Notably, in the scenario where extensive sea-ice cover inhibits dense-water formation (stadial; Paper III), the Arctic overturning cell is inactive. Conversely, the overturning cell becomes operational as soon as the Nordic Seas are ice-free. However, the location of dense-water formation (Paper I) and its intensity (Paper II) significantly influence the extent and strength of the overturning. Meanwhile, dense-water formation is pre-conditioned by the position of the sea-ice edge and the prevailing background stratification (see section 4.4).

Jackson and Petit (2023) have earlier shown good correlations between the subpolar overturning strength in density coordinates and the watermass transformation from surface buoyancy forcing north of 45°N, with or without including the Nordic Seas, suggesting that the subpolar overturning and the ArMOC are disconnected. However, the maximum overturning strength in the subpolar North Atlantic is found at shallower depths/lower densities than that impacted by the Nordic Seas overflow and *Årthun* (2023) find the trends in overturning in the Nordic Seas correlate with the lower limb (1500-2000 m) of the subpolar overturning. Further studies are warranted to understand the relationship between future ArMOC and overturning changes in the North Atlantic.

I hypothesized that the ArMOC is primarily driven by dense-water formation in the Arctic Ocean. However, it could also be that dense-water formation increases as a result of a strengthened circulation which weakens the stratification. As an example, changes in the horizontal circulation can influence the zonal density gradient in the Arctic, and consequently the ArMOC (*Zhang and Thomas*, 2021; *Årthun et al.*, 2023). In fact, *Lique et al.* (2015) find a strengthening of the wind-driven circulation in the Greenland Sea under a $4\times CO_2$ forcing. To rule out the wind as a driver of the Arctic overturning strengthening, and to further test our hypothesis, a cross-correlation analysis should be performed between the ArMOC strength, the wind-stress curl, and the dense-water formation in the Nordic Seas, as a future extension to this study.

One of the difficulties encountered in this dissertation was to evaluate dense-water formation. In Paper I, we defined dense-water formation sites as regions with a mixed-layer depth exceeding 800 m. Changes in the maximum mixed-layer depth, and in the area and location of the dense-water formation, are then compared and discussed with respect to changes in ArMOC strength. This method, however, does not allow for a systematic and quantitative evaluation, especially given the large differences in mixed layers among the models. In Paper II, we overcome this issue by computing watermass transformation from surface buoyancy fluxes.

Dense-water formation is then assessed by evaluating the watermass transformation toward a high range of densities during the winter months only. However, this method does not take into account the fact that the overturning water is becoming lighter in the future, nor a change in the length of the dense-water formation season. In conclusion, additional work is required to be able to relate watermass transformation via buoyancy flux to mixed-layer depth, and dense-water formation.

5.3 ArMOC strengthening in the future

Considering the ongoing sea-ice retreat, I believe that the ArMOC could become stronger in the future. This hypothesis builds upon the dependency of the ArMOC on dense-water formation (section 4.2) and the understanding that a retreat of the sea ice leads to increased watermass transformation and a shift in location of dense-water formation (*Lique and Thomas*, 2018; *Våge et al.*, 2009; *Koenigk et al.*, 2013; see Figure 5.2, left panel). In Paper I, we identified a strengthening of the ArMOC in EC-Earth-PISM continuing till the end of this century together with a northward shift of dense-water formation sites. This relationship is further supported by 4 climate models in Paper II. In these models, a stronger ArMOC in the mid-century is concurrent with an increase in dense-water formation in the Nordic Seas.

These results stress the need to study the ArMOC and how its state relates to the dense overflow at the GSR, and consequently to the AMOC. It is not unlikely that a strengthening of the ArMOC could partly compensate for the observed AMOC weakening (*Årthun*, 2023). The ArMOC strengthening also lends new insights into the ongoing Atlantification of the Arctic.

Although the hypothesis of a stronger future ArMOC is supported by several models, the large spread of model responses in the Arctic identified in Paper II needs to be discussed further. As described, 4 models show no sign of ArMOC strengthening (referred to as "weak-ArMOC models") and the amplitude and timing of the ArMOC strengthening in the 4 "strong-ArMOC models" (CanESM5, EC-Earth3, MRI-ESM2-0, and UKESEM1-0-LL) vary considerably. As of yet, there is no clear evidence to rule out either of these models, and the reason behind the different simulated responses to a warming Arctic is unclear. The strengthening could be linked to intensified changes in the Arctic detected in the NEMO-family of models; however one of the strong-ArMOC models does not use NEMO (MRI-ESM2-0) while two weak-ArMOC models do use NEMO (CNRM-CM6-1 and IPS6-CM6A-LR, see Table 2.2).

An ArMOC strengthening could be expected in models with a lower horizontal resolution; a

lower resolution has been linked with strong vertical mixing and strong overturning at the expense of eddy mixing and a stronger horizontal circulation (*Hirschi et al.*, 2020). However, two models with similarly low horizontal resolution give a weak ArMOC. Further, it should be noted that all the strong-ArMOC models use the same turbulent closure scheme in the parametrization of vertical mixing. If this mixing scheme tends to induce more convection, this could explain the dense-water formation increase and ArMOC strengthening in those models.

According to *Levermann et al.* (2007), models with a weak AMOC present a reduced AMOC weakening which is due to the presence of a more extensive sea-ice cover. Under radiative forcing, these models present more sea-ice reduction which leads to enhanced heat loss and dense-water formation in the Nordic Seas. In light of our results, this would imply an ArMOC strengthening. If this is the case, the strong-ArMOC models should be the models with an extensive winter sea-ice cover. However, it appears not to be the case in our subset of models (Table 2.2.2). In addition, there is no indication that the strong-ArMOC models have a weaker AMOC decline (Table 2.2.2).

It should be noted that the ArMOC strength does not exceed 4 Sv for the historical period in most models, which is only 2/3 of the value estimated from observations (*Østerhus et al.*, 2019). According to *Cai et al.* (2021), an underestimation of the overturning in the Arctic region, and associated heat transport, could explain the cold bias present in the models in the Arctic. As a consequence of underestimating the ArMOC, we could also be underestimating any potential future ArMOC enhancements.

These results highlight the sensitivity of the simulated ArMOC to model details. Further in-depth studies are needed to better understand and constrain the mechanisms driving overturning changes in the Arctic, in order to produce more reliable projections of the ArMOC in climate models.

According to *Heuzé* (2017) and *Heuzé et al.* (2023), CMIP models overestimate dense-water formation resulting from deep convection because they do not resolve dense-water formation on the shelves. In addition, *Aagaard et al.* (1985) consider the cascading of dense shelf water off continental shelves to be one of the main mechanisms generating dense water in the Arctic. As the Arctic Overturning depends on dense-water formation, as shown in Papers II and III, a misrepresentation of dense shelf-waters could partly explain the present underestimation of the Arctic overturning in models. In addition, dense-water formation on the shelves is expected to increase under increased seasonality, which offers another possible mechanism for a transient ArMOC strengthening (*Bitz et al.*, 2006).

5.4 ArMOC, freshwater and the estuarine circulation

Throughout this dissertation, it has become clear that the dynamics of the ArMOC strongly depend on the distribution of freshwater at the surface, and consequently on the estuarine circulation. Notably, in paper III, a strong estuarine cell develops in the transition from a stadial to an interstadial climate state. This sets the stage for the onset of convection in the Nordic Seas, ultimately leading to the activation of the ArMOC. An active estuarine circulation is necessary to flush out the anomalous freshwater present in the Nordic Seas during the stadial. It is worth noting that the estuarine cell has opposite effects in the Labrador Sea where deep convection is inhibited by the increased freshwater export from the Nordic Seas.

In addition, in Paper I we find that the northward shift in deep convection, and the ArMOC strengthening, stop at the end of this century due to the high freshwater content in the Arctic basins. A stronger estuarine cell would be necessary to dissipate the freshwater anomaly present in the Arctic basins, which is also increasing as a result of a strengthened hydrological cycle. Meanwhile, the anomalous freshwater fluxes from a melting Greenland ice sheet are not found to affect the convection and overturning in the Arctic, including the Nordic Seas. This is probably due to the fact that the increase in meltwater occurs later in time when deep convection is already reduced.

There seems to be a fundamental mechanism linking the overturning and the estuarine circulation in the Arctic; however, the meridional overturning streamfunction is the sum of both and does not lend itself to separating the two. Although we know that the estuarine circulation is present in the models analyzed in Papers I and II, we can not measure its strength since it is hindered by the strong overturning. On the other hand, in Paper III, the estuarine cell is initially stronger than the overturning and can be assessed. This implies that the estuarine and overturning circulations partly cancel each other, resulting in an underestimation of their individual strength. In Paper III, we could be missing the early development of the ArMOC as it is hidden by the strong estuarine cell.

With the results from Papers I, II, and III, I can only offer speculative insights into how the estuarine and overturning circulation are coupled, as summarized in Figure 5.2 (right panels). I propose that the estuarine circulation and the ArMOC are both enhanced initially and have positive feedback on each other in the ongoing sea-ice retreat (Papers I&II). The increased Atlantic inflow enhances the estuarine cell, which results in an increase in freshwater export, a weakening of the stratification, increased heat loss, and a strengthening of the ArMOC. In turn, a stronger ArMOC imports more Atlantic water, which can then mix with freshwater and enhance the estuarine cell.

However, the overturning and estuarine circulations respond differently to forcing depending on key parameters such as the temperature of the inflowing Atlantic water, or the freshwater input to the Arctic (*Haine*, 2021). The system could reach a so-called heat crisis anticipated by *Haine* (2021) leading to the weakening of the estuarine cell during the second half of the century, and the subsequent weakening of the ArMOC. In Paper III, it is also likely that the estuarine cell is activated by the enhanced inflow of Atlantic water. Since there is no active convection in the Nordic Seas at this point, it would mean that other forcings (e.g. wind) also play a significant role in influencing the overturning and estuarine circulations.

In conclusion, there is a need to separate the circulation into its overturning and estuarine components. This could be achieved by combining our diagnostic with an analysis of the circulation in thermohaline coordinates (*Zika et al.*, 2012). As an example, using this coordinate system would allow for separating the enhancement of the thermally-driven cell from a weakening of the salinity-driven cell. Further work could compare the sensitivity of ArMOC to heat and freshwater forcing with that inferred from the analytical model of *Haine* (2021).

5.5 The ArMOC during a D-O event

Based on the D-O event simulation in Paper III, it can be inferred that the abrupt warming in Greenland is predominantly influenced by the interplay between the estuarine and ArMOC circulations. The Greenland warming correlates with the sea-ice retreat in the Nordic Seas, which follows the activation of the estuarine circulation. The timing of the transition can be explained through the following mechanism: the strengthening of the AMOC results in an increase in Atlantic water transport in the subpolar region. This water mixes with surface freshwater, weakening the stratification in the eastern subpolar region and activating an estuarine cell, which ultimately delays the sea-ice retreat. This mechanism is repeated when the Atlantic water makes its way to the Nordic Seas. Part of the water mixes with the anomalous freshwater in the Nordic Seas, sustaining the strong estuarine circulation and further inhibiting convection in the Labrador Sea. The remaining (minor) part of the inflowing Atlantic water is cooled at the surface in the eastern Nordic Seas until convection is activated. Deep convection enhances the ArMOC and further heat loss to the atmosphere, which results in rapid Greenland warming. In conclusion, the ArMOC is intimately linked to the abrupt warming observed during D-O events in Greenland.

The simulation presented here is meant to mimic a H-stadial to D-O interstadial transition. However, freshwater input is highly uncertain for the glacial period. In order to get a strong response in the model, the freshwater flux applied is exaggerated. Based on model sensitivity studies and reconstructions, such as *Roche et al.*, 2010; *Hemming*, 2004, the freshwater

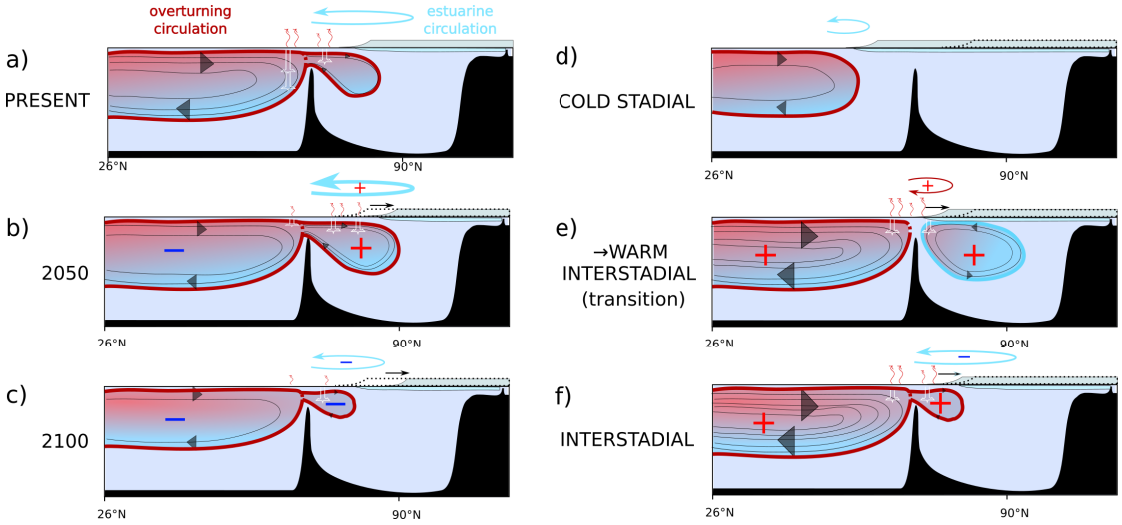

Figure 5.2: Development of the overturning (dark red) and estuarine circulation (light blue) under future and past sea-ice retreat, as illustrated by the meridional overturning streamfunction. In the Arctic, the streamfunction only captures the dominant circulation, which in practice is the overturning cell. Here, we suggest how the secondary circulation evolves (i.e. the estuarine circulation, see blue arrows in a,b,c,d, and f).
With the current sea-ice cover (left panels), the retreat of the sea ice is accompanied by a weakening of the AMOC (b, c, -), a heat loss increase in the Arctic, and a strengthening of the ArMOC and estuarine circulation (b, +) until the mid-century. The collapse of the estuarine cell and the accumulation of freshwater in the Arctic prevent further heat loss increase and result in the final ArMOC weakening (c). Under a very extensive sea-ice cover (d), the ArMOC is inactive. As the sea ice retreats and the Atlantic inflow increases (e), the estuarine cell strengthens, preconditioning the heat loss increase in the Nordic Seas and the activation of the ArMOC (f).

release is expected to have been smaller in magnitude and located further south in the subpolar gyre. However, the sensitivity to surface freshwater forcing is highly model-dependent, and the simulation presented in this study sheds light on the potential of the estuarine circulation in driving changes. My stated hypothesis is that the ArMOC and estuarine circulation are regulating each other. In this context, the transition between cold and warm conditions (weak and strong AMOC, inactive and active ArMOC) could be triggered by the collapse or activation of the estuarine cell (*Haine*, 2021).

To further investigate the role of overturning changes during D-O events, it would be advantageous to analyze simulations with unforced D-O like oscillations, such as those found in the model studies of *Vettoretti et al.* (2022) or *Klockmann et al.* (2020). In light of my results showing the importance of the estuarine circulation, I recommend including an analysis in thermohaline coordinates in future studies. If possible, it would also be valuable to reproduce the experiments of *Haine* (2021) using forcing consistent with MIS3 and D-O conditions.

Bibliography

Aagaard, K., J. H. Swift, and E. C. Carmack (1985), Thermohaline circulation in the arctic mediterranean seas, *Journal of Geophysical Research: Oceans*, *90*(C3), 4833–4846, doi:https://doi.org/10.1029/JC090iC03p04833.

Asbjørnsen, H., and M. Årthun (2023), Deconstructing future amoc decline at 26.5°n, *Geophysical Research Letters*, *50*(14), e2023GL103,515, doi:https://doi.org/10.1029/2023GL103515, e2023GL103515 2023GL103515.

Barnhart, K. R., C. R. Miller, I. Overeem, and J. E. Kay (2016), Mapping the future expansion of arctic open water, *Nature Climate Change*, *6*, doi:10.1038/nclimate2848.

Bassis, J. N., S. V. Petersen, and L. Mac Cathles (2017), Heinrich events triggered by ocean forcing and modulated by isostatic adjustment, *Nature*, *542*(7641), 332–334, doi:10.1038/nature21069.

Bentsen, M., I. Bethke, J. B. Debernard, T. Iversen, A. Kirkevåg, Ø. Seland, H. Drange, C. Roelandt, I. A. Seierstad, C. Hoose, and J. E. Kristjánsson (2013), The Norwegian Earth System Model, NorESM1-M – Part 1: Description and basic evaluation of the physical climate, *Geoscientific Model Development*, *6*(3), 687–720, doi:10.5194/gmd-6-687-2013.

Bingham, R. J., C. W. Hughes, V. Roussenov, and R. G. Williams (2007), Meridional coherence of the north atlantic meridional overturning circulation, *Geophysical Research Letters*, *34*, doi:10.1029/2007GL031731.

Birchfield, E. G., H. Wang, and J. J. Rich (1994), Century/millennium internal climate oscillations in an ocean-atmosphere-continental ice sheet model, *Journal of Geophysical Research: Oceans*, *99*(C6), 12,459–12,470, doi:10.1029/94JC00523, important - Abstract.

Bitz, C. M., P. R. Gent, R. A. Woodgate, M. M. Holland, and R. Lindsay (2006), The influence of sea ice on ocean heat uptake in response to increasing co2, *Journal of Climate*, *19*, 2437–2450, doi:10.1175/JCLI3756.1.

Bluhm, B., K. Kosobokova, and E. Carmack (2015), A tale of two basins: An integrated physical and biological perspective of the deep arctic ocean, *Progress in Oceanography*, *139*,

89–121, doi:https://doi.org/10.1016/j.pocean.2015.07.011, overarching perspectives of contemporary and future ecosystems in the Arctic Ocean.

Bond, G., W. Broecker, S. Johnsen, J. McManus, L. Labeyrie, J. Jouzel, and G. Bonani (1993), Correlations between climate records from North Atlantic sediments and Greenland ice, *Nature*, *365*(6442), 143–147, doi:10.1038/365143a0, number: 6442 Publisher: Nature Publishing Group.

Brakstad, A., K. Våge, L. Håvik, and G. W. K. Moore (2019), Water mass transformation in the greenland sea during the period 1986–2016, *Journal of Physical Oceanography*, *49*(1), 121 – 140, doi:10.1175/JPO-D-17-0273.1.

Brodeau, L., and T. Koenigk (2016), Extinction of the northern oceanic deep convection in an ensemble of climate model simulations of the 20th and 21st centuries, *Climate Dynamics*, *46*, 2863–2882, doi:10.1007/s00382-015-2736-5.

Buckley, M. W., and J. Marshall (2016), Observations, inferences, and mechanisms of the atlantic meridional overturning circulation: A review, *Reviews of Geophysics*, *54*(1), 5–63, doi:https://doi.org/10.1002/2015RG000493.

Böhm, E., J. Lippold, M. Gutjahr, M. Frank, P. Blaser, B. Antz, J. Fohlmeister, N. Frank, M. B. Andersen, and M. Deininger (2015), Strong and deep Atlantic meridional overturning circulation during the last glacial cycle, *Nature*, *517*(7532), 73–76, doi:10.1038/nature14059.

Caesar, L., G. D. McCarthy, D. J. Thornalley, N. Cahill, and S. Rahmstorf (2021), Current atlantic meridional overturning circulation weakest in last millennium, *Nature Geoscience*, *14*, doi:10.1038/s41561-021-00699-z.

Cai, Z., Q. You, F. Wu, H. W. Chen, D. Chen, and J. Cohen (2021), Arctic warming revealed by multiple cmip6 models: Evaluation of historical simulations and quantification of future projection uncertainties, *Journal of Climate*, *34*(12), 4871 – 4892, doi:10.1175/JCLI-D-20-0791.1.

Carmack, E., and P. Wassmann (2006), Food webs and physical-biological coupling on pan-arctic shelves: Unifying concepts and comprehensive perspectives, *Progress in Oceanography*, *71*, doi:10.1016/j.pocean.2006.10.004.

Chafik, L., J. E. Øie Nilsen, S. Dangendorf, G. Reverdin, and T. Frederikse (2019), North atlantic ocean circulation and decadal sea level change during the altimetry era, *Scientific Reports*, *9*, 1–9, doi:10.1038/s41598-018-37603-6.

Comiso, J. C., W. N. Meier, and R. Gersten (2017), Variability and trends in the arctic sea ice cover: Results from different techniques, *Journal of Geophysical Research: Oceans*, *122*, doi:10.1002/2017JC012768.

Cunningham, S. (2008), Monitoring the atlantic meridional overturning circulation at 26.5°n: Rapid-watch, *Report*.

Davy, R., and S. Outten (2020), The arctic surface climate in cmip6: Status and developments since cmip5, *Journal of Climate*, *33*, 8047–8068, doi:10.1175/JCLI-D-19-0990.1.

de Boyer Montégut, C., G. Madec, A. S. Fischer, A. Lazar, and D. Iudicone (2004), Mixed layer depth over the global ocean: An examination of profile data and a profile-based climatology, *Journal of Geophysical Research C: Oceans*, *109*, 1–20, doi:10.1029/2004JC002378.

de Jong, M. F., and L. de Steur (2016), Strong winter cooling over the irminger sea in winter 2014-2015, exceptional deep convection, and the emergence of anomalously low sst, *Geophysical Research Letters*, *43*, 7106–7113, doi:10.1002/2016GL069596.

Desbruyères, D. G., H. Mercier, G. Maze, and N. Daniault (2019), Surface predictor of overturning circulation and heat content change in the subpolar north atlantic, *Ocean Science*, *15*(3), 809–817, doi:10.5194/os-15-809-2019.

Ding, Q., A. Schweiger, M. L'Heureux, D. S. Battisti, S. Po-Chedley, N. C. Johnson, E. Blanchard-Wrigglesworth, K. Harnos, Q. Zhang, R. Eastman, and E. J. Steig (2017), Influence of high-latitude atmospheric circulation changes on summertime arctic sea ice, *Nature Climate Change*, *7*, doi:10.1038/nclimate3241.

Ditlevsen, P., and S. Ditlevsen (2023), Warning of a forthcoming collapse of the atlantic meridional overturning circulation, *Nature Communications*, *14*(1), 4254, doi:10.1038/s41467-023-39810-w.

Dokken, T. M., K. H. Nisancioglu, C. Li, D. S. Battisti, and C. Kissel (2013), Dansgaard-oeschger cycles: Interactions between ocean and sea ice intrinsic to the nordic seas, *Paleoceanography*, *28*, doi:10.1002/palo.20042.

Döscher, R., M. Acosta, A. Alessandri, P. Anthoni, T. Arsouze, T. Bergman, R. Bernardello, S. Boussetta, L.-P. Caron, G. Carver, M. Castrillo, F. Catalano, I. Cvijanovic, P. Davini, E. Dekker, F. J. Doblas-Reyes, D. Docquier, P. Echevarria, U. Fladrich, R. Fuentes-Franco, M. Gröger, J. v. Hardenberg, J. Hieronymus, M. P. Karami, J.-P. Keskinen, T. Koenigk, R. Makkonen, F. Massonnet, M. Ménégoz, P. A. Miller, E. Moreno-Chamarro, L. Nieradzik, T. van Noije, P. Nolan, D. O'Donnell, P. Ollinaho, G. van den Oord, P. Ortega, O. T. Prims, A. Ramos, T. Reerink, C. Rousset, Y. Ruprich-Robert, P. Le Sager, T. Schmith,

R. Schrödner, F. Serva, V. Sicardi, M. Sloth Madsen, B. Smith, T. Tian, E. Tourigny, P. Uotila, M. Vancoppenolle, S. Wang, D. Wårlind, U. Willén, K. Wyser, S. Yang, X. Yepes-Arbós, and Q. Zhang (2022), The ec-earth3 earth system model for the coupled model intercomparison project 6, *Geoscientific Model Development*, *15*(7), 2973–3020, doi:10.5194/gmd-15-2973-2022.

Eldevik, T., and J. E. Nilsen (2013), The arctic–atlantic thermohaline circulation, *Journal of Climate*, *26*, 8698–8705, doi:10.1175/JCLI-D-13-00305.1.

Eyring, V., S. Bony, G. A. Meehl, C. A. Senior, B. Stevens, R. J. Stouffer, and K. E. Taylor (2016), Overview of the coupled model intercomparison project phase 6 (cmip6) experimental design and organization, *Geoscientific Model Development*, *9*, 1937–1958, doi:10.5194/GMD-9-1937-2016.

Ganachaud, A., and C. Wunsch (2003), Large-scale ocean heat and freshwater transports during the world ocean circulation experiment, *Journal of Climate*, *16*, doi:10.1175/1520-0442(2003)016⟨0696:LSOHAF⟩2.0.CO;2.

Gräwe, U., G. Flöser, T. Gerkema, M. Duran-Matute, T. H. Badewien, E. Schulz, and H. Burchard (2016), A numerical model for the entire wadden sea: Skill assessment and analysis of hydrodynamics, *Journal of Geophysical Research: Oceans*, *121*(7), 5231–5251, doi:https://doi.org/10.1002/2016JC011655.

Guo, C., M. Bentsen, I. Bethke, M. Ilicak, J. Tjiputra, T. Toniazzo, J. Schwinger, and O. H. Otterå (2019a), Description and evaluation of noresm1-f: a fast version of the norwegian earth system model (noresm), *Geoscientific Model Development*, *12*(1), 343–362, doi:10.5194/gmd-12-343-2019.

Guo, C., K. H. Nisancioglu, M. Bentsen, I. Bethke, and Z. Zhang (2019b), Equilibrium simulations of marine isotope stage 3 climate, *Climate of the Past*, *15*(3), 1133–1151, doi:10.5194/cp-15-1133-2019.

Haine, T. W. (2021), A conceptual model of polar overturning circulations, *Journal of Physical Oceanography*, *51*, 727–744, doi:10.1175/JPO-D-20-0139.1.

Hazeleger, W., X. Wang, C. Severijns, S. Ştefănescu, R. Bintanja, A. Sterl, K. Wyser, T. Semmler, S. Yang, B. van den Hurk, T. van Noije, E. van der Linden, and K. van der Wiel (2012), Ec-earth v2.2: Description and validation of a new seamless earth system prediction model, *Climate Dynamics*, *39*, doi:10.1007/s00382-011-1228-5.

Heinrich, H. (1988), Origin and consequences of cyclic ice rafting in the northeast atlantic ocean during the past 130,000 years, *Quaternary Research*, *29*, doi:10.1016/0033-5894(88)90057-9.

Hemming, S. R. (2004), Heinrich events: Massive late Pleistocene detritus layers of the North Atlantic and their global climate imprint, *Reviews of Geophysics*, *42*(1), doi:10.1029/2003RG000128.

Heuzé, C. (2021), Antarctic bottom water and north atlantic deep water in cmip6 models, *Ocean Science*, *17*(1), 59–90, doi:10.5194/os-17-59-2021.

Heuzé, C. (2017), North atlantic deep water formation and amoc in cmip5 models, *Ocean Science*, *13*, doi:10.5194/os-13-609-2017.

Heuzé, C., K. J. Heywood, D. P. Stevens, and J. K. Ridley (2013), Southern ocean bottom water characteristics in CMIP5 models, *Geophysical Research Letters*, *40*, 1409–1414, doi:10.1002/grl.50287.

Heuzé, C., H. Zanowski, S. Karam, and M. Muilwijk (2023), The deep arctic ocean and fram strait in cmip6 models, *Journal of Climate*, *36*(8), 2551 – 2584, doi:https://doi.org/10.1175/JCLI-D-22-0194.1.

Heuzé, C., and M. Årthun (2019), The atlantic inflow across the greenland-scotland ridge in global climate models (cmip5), *Elementa*, *7*, doi:10.1525/ELEMENTA.354/112488.

Hirschi, J. J., B. Barnier, C. Böning, A. Biastoch, A. T. Blaker, A. Coward, S. Danilov, S. Drijfhout, K. Getzlaff, S. M. Griffies, H. Hasumi, H. Hewitt, D. Iovino, T. Kawasaki, A. E. Kiss, N. Koldunov, A. Marzocchi, J. V. Mecking, B. Moat, J. M. Molines, P. G. Myers, T. Penduff, M. Roberts, A. M. Treguier, D. V. Sein, D. Sidorenko, J. Small, P. Spence, L. A. Thompson, W. Weijer, and X. Xu (2020), The atlantic meridional overturning circulation in high-resolution models, *Journal of Geophysical Research: Oceans*, *125*, e2019JC015,522, doi:10.1029/2019JC015522.

Hoff, U., T. L. Rasmussen, R. Stein, M. M. Ezat, and K. Fahl (2016), Sea ice and millennial-scale climate variability in the nordic seas 90 kyr ago to present, *Nature Communications*, *7*, doi:10.1038/ncomms12247.

Huang, J., R. S. Pickart, R. X. Huang, P. Lin, A. Brakstad, and F. Xu (2020), Sources and upstream pathways of the densest overflow water in the nordic seas, *Nature Communications*, *11*, 1–9, doi:10.1038/s41467-020-19050-y.

Ingvaldsen, R. B., K. M. Assmann, R. Primicerio, M. Fossheim, I. V. Polyakov, and A. V. Dolgov (2021), Physical manifestations and ecological implications of arctic atlantification, doi:10.1038/s43017-021-00228-x.

Jackson, L. C., and T. Petit (2023), North atlantic overturning and water mass transformation in cmip6 models, *Climate Dynamics*, *60*, doi:10.1007/s00382-022-06448-1.

Jansen, E., J. H. Christensen, T. Dokken, K. H. Nisancioglu, B. M. Vinther, E. Capron, C. Guo, M. F. Jensen, P. L. Langen, R. A. Pedersen, S. Yang, M. Bentsen, H. A. Kjær, H. Sadatzki, E. Sessford, and M. Stendel (2020), Past perspectives on the present era of abrupt arctic climate change, *Nature Climate Change*, *10*, doi:10.1038/s41558-020-0860-7.

Johnson, H. L., P. Cessi, D. P. Marshall, F. Schloesser, and M. A. Spall (2019), Recent contributions of theory to our understanding of the atlantic meridional overturning circulation, *Journal of Geophysical Research: Oceans*, *124*, 5376–5399, doi:10.1029/2019JC015330.

Kageyama, M., A. Paul, D. M. Roche, and C. J. Van Meerbeeck (2010), Modelling glacial climatic millennial-scale variability related to changes in the Atlantic meridional overturning circulation: a review, *Quaternary Science Reviews*, *29*(21), 2931–2956, doi:10.1016/j.quascirev.2010.05.029.

Khosravi, N., Q. Wang, N. Koldunov, C. Hinrichs, T. Semmler, S. Danilov, and T. Jung (2022), The arctic ocean in cmip6 models: Biases and projected changes in temperature and salinity, *Earth's Future*, *10*(2), e2021EF002,282, doi:https://doi.org/10.1029/2021EF002282, e2021EF002282 2021EF002282.

Kindler, P., M. Guillevic, M. Baumgartner, J. Schwander, A. Landais, and M. Leuenberger (2014), Temperature reconstruction from 10 to 120 kyr b2k from the ngrip ice core, *Climate of the Past*, *10*, doi:10.5194/cp-10-887-2014.

Klockmann, M., U. Mikolajewicz, H. Kleppin, and J. Marotzke (2020), Coupling of the subpolar gyre and the overturning circulation during abrupt glacial climate transitions, *Geophysical Research Letters*, *47*(21), e2020GL090,361, doi:https://doi.org/10.1029/2020GL090361, vettoretti2020.

Koenigk, T., L. Brodeau, R. G. Graversen, J. Karlsson, G. Svensson, M. Tjernström, U. Willén, and K. Wyser (2013), Arctic climate change in 21st century CMIP5 simulations with ec-earth, *Climate Dynamics*, *40*, 2719–2743, doi:10.1007/s00382-012-1505-y.

Kostov, Y., H. L. Johnson, D. P. Marshall, P. Heimbach, G. Forget, N. P. Holliday, M. S. Lozier, F. Li, H. R. Pillar, and T. Smith (2021), Distinct sources of interannual subtropical and subpolar atlantic overturning variability, *Nature Geoscience*, *14*, doi:10.1038/s41561-021-00759-4.

Kwok, R. (2018), Arctic sea ice thickness, volume, and multiyear ice coverage: Losses and coupled variability (1958-2018), doi:10.1088/1748-9326/aae3ec.

Landrum, L., and M. M. Holland (2020), Extremes become routine in an emerging new arctic, *Nature Climate Change*, *10*, doi:10.1038/s41558-020-0892-z.

Langehaug, H. R., P. B. Rhines, T. Eldevik, J. Mignot, and K. Lohmann (2012), Water mass transformation and the north atlantic current in three multicentury climate model simulations, *Journal of Geophysical Research: Oceans*, *117*(C11), doi:https://doi.org/10.1029/2012JC008021.

Laxon, S., H. Peacock, and D. Smith (2003), High interannual variability of sea ice thickness in the arctic region, *Nature 2003 425:6961*, *425*, 947–950, doi:10.1038/nature02050.

Levermann, A., J. Mignot, S. Nawrath, and S. Rahmstorf (2007), The role of northern sea ice cover for the weakening of the thermohaline circulation under global warming, *Journal of Climate*, *20*(16), 4160 – 4171, doi:https://doi.org/10.1175/JCLI4232.1.

Li, C., and A. Born (2019), Coupled atmosphere-ice-ocean dynamics in dansgaard-oeschger events, *Quaternary Science Reviews*, *203*, 1–20, doi:10.1016/J.QUASCIREV.2018.10.031.

Lind, S., R. B. Ingvaldsen, and T. Furevik (2018), Arctic warming hotspot in the northern barents sea linked to declining sea-ice import, *Nature Climate Change 2018 8:7*, *8*, 634–639, doi:10.1038/s41558-018-0205-y.

Lindsay, R., and A. Schweiger (2015), Arctic sea ice thickness loss determined using subsurface, aircraft, and satellite observations, *Cryosphere*, *9*, 269–283, doi:10.5194/TC-9-269-2015.

Lique, C., and M. D. Thomas (2018), Latitudinal shift of the atlantic meridional overturning circulation source regions under a warming climate, *Nature Climate Change 2018 8:11*, *8*, 1013–1020, doi:10.1038/s41558-018-0316-5.

Lique, C., H. L. Johnson, Y. Plancherel, and R. Flanders (2015), Ocean change around greenland under a warming climate, *Climate Dynamics*, *45*, doi:10.1007/s00382-014-2373-4.

Lohmann, J., and P. D. Ditlevsen (2019), Objective extraction and analysis of statistical features of Dansgaard–Oeschger events, *Climate of the Past*, *15*(5), 1771–1792, doi:https://doi.org/10.5194/cp-15-1771-2019, publisher: Copernicus GmbH.

Lozier, M. S., F. Li, S. Bacon, F. Bahr, A. S. Bower, S. A. Cunningham, M. F. D. Jong, L. D. Steur, B. DeYoung, J. Fischer, S. F. Gary, B. J. Greenan, N. P. Holliday, A. Houk, L. Houpert, M. E. Inall, W. E. Johns, H. L. Johnson, C. Johnson, J. Karstensen, G. Koman, I. A. L. Bras, X. Lin, N. Mackay, D. P. Marshall, H. Mercier, M. Oltmanns, R. S. Pickart, A. L. Ramsey, D. Rayner, F. Straneo, V. Thierry, D. J. Torres, R. G. Williams, C. Wilson, J. Yang, I. Yashayaev, and J. Zhao (2019), A sea change in our view of overturning in the subpolar north atlantic, *Science*, *363*, 516–521, doi:10.1126/science.aau6592.

Lurton, T., Y. Balkanski, V. Bastrikov, S. Bekki, L. Bopp, P. Braconnot, P. Brockmann, P. Cadule, C. Contoux, A. Cozic, D. Cugnet, J. L. Dufresne, C. Éthé, M. A. Foujols, J. Ghattas, D. Hauglustaine, R. M. Hu, M. Kageyama, M. Khodri, N. Lebas, G. Levavasseur, M. Marchand, C. Ottlé, P. Peylin, A. Sima, S. Szopa, R. Thiéblemont, N. Vuichard, and O. Boucher (2020), Implementation of the cmip6 forcing data in the ipsl-cm6a-lr model, *Journal of Advances in Modeling Earth Systems*, *12*, e2019MS001,940, doi:10.1029/2019MS001940.

Lynch-Stieglitz, J. (2017), The atlantic meridional overturning circulation and abrupt climate change, *Annual Review of Marine Science*, *9*(1), 83–104, doi:10.1146/annurev-marine-010816-060415, pMID: 27814029.

Madec, G., P. Delecluse, M. Imbard, and C. Levy (1998), Opa version 8. ocean general circulation model reference manual, *Tech. rep.*

Madonna, E., and A. B. Sandø (2022), Understanding differences in north atlantic poleward ocean heat transport and its variability in global climate models, *Geophysical Research Letters*, *49*(1), e2021GL096,683, doi:https://doi.org/10.1029/2021GL096683, e2021GL096683 2021GL096683.

Madsen, M. S., S. Yang, G. Aalgeirsdóttir, S. H. Svendsen, C. B. Rodehacke, and I. M. Ringgaard (2022), The role of an interactive greenland ice sheet in the coupled climate-ice sheet model ec-earth-pism, *Climate Dynamics*, *59*, doi:10.1007/s00382-022-06184-6.

Manabe, S., and R. J. Stouffer (1995), Simulation of abrupt climate change induced by freshwater input to the North Atlantic Ocean, *Nature*, *378*(6553), 165–167, doi:10.1038/378165a0, number: 6553 Publisher: Nature Publishing Group.

Manabe, S., and R. J. Stouffer (1997), Coupled ocean-atmosphere model response to freshwater input: Comparison to younger dryas event, *Paleoceanography*, *12*(2), 321–336, doi:https://doi.org/10.1029/96PA03932.

Marcott, S. A., P. U. Clark, L. Padman, G. P. Klinkhammer, S. R. Springer, Z. Liu, B. L. Otto-Bliesner, A. E. Carlson, A. Ungerer, J. Padman, F. He, J. Cheng, and A. Schmittner (2011), Ice-shelf collapse from subsurface warming as a trigger for heinrich events, *Proceedings of the National Academy of Sciences of the United States of America*, *108*, doi:10.1073/pnas.1104772108.

Muchowski, J. C., M. Jakobsson, L. Umlauf, L. Arneborg, B. Gustafsson, P. Holtermann, C. Humborg, and C. Stranne (2023), Observations of strong turbulence and mixing impacting water exchange between two basins in the baltic sea, *EGUsphere*, *2023*, 1–28, doi:10.5194/egusphere-2023-920.

Muilwijk, M., L. H. Smedsrud, M. Ilicak, and H. Drange (2018), Atlantic water heat transport variability in the 20th century arctic ocean from a global ocean model and observations, *Journal of Geophysical Research: Oceans*, *123*, 8159–8179, doi:10.1029/2018JC014327.

Muilwijk, M., A. Nummelin, L. H. Smedsrud, I. V. Polyakov, H. Zanowski, and C. Heuzé (2023), Divergence in climate model projections of arctic atlantification, doi:10.31223/X55D2V.

Murray, R. J. (1996), Explicit generation of orthogonal grids for ocean models, *Journal of Computational Physics*, *126*(2), 251–273, doi:https://doi.org/10.1006/jcph.1996.0136.

Notz, D., and SIMIP Community (2020), Arctic sea ice in CMIP6, *Geophysical Research Letters*, *47*, e2019GL086,749, doi:10.1029/2019GL086749.

Nummelin, A., C. Li, and P. J. Hezel (2017), Connecting ocean heat transport changes from the midlatitudes to the arctic ocean, *Geophysical Research Letters*, *44*(4), 1899–1908, doi:https://doi.org/10.1002/2016GL071333.

Obase, T., and A. Abe-Ouchi (2019), Abrupt Bølling-Allerød Warming Simulated under Gradual Forcing of the Last Deglaciation, *Geophysical Research Letters*, *46*(20), 11,397–11,405, doi:10.1029/2019GL084675, _eprint: https://onlinelibrary.wiley.com/doi/pdf/10.1029/2019GL084675.

Onarheim, I. H., L. H. Smedsrud, R. B. Ingvaldsen, and F. Nilsen (2014), Loss of sea ice during winter north of svalbard, *Tellus, Series A: Dynamic Meteorology and Oceanography*, *66*, doi:10.3402/tellusa.v66.23933.

Onarheim, I. H., T. Eldevik, L. H. Smedsrud, and J. C. Stroeve (2018), Seasonal and regional manifestation of arctic sea ice loss, *Journal of Climate*, *31*, doi:10.1175/JCLI-D-17-0427.1.

Østerhus, S., R. Woodgate, H. Valdimarsson, B. Turrell, L. de Steur, D. Quadfasel, S. M. Olsen, M. Moritz, C. M. Lee, K. M. H. Larsen, S. Jónsson, C. Johnson, K. Jochumsen, B. Hansen, B. Curry, S. Cunningham, and B. Berx (2019), Arctic mediterranean exchanges: a consistent volume budget and trends in transports from two decades of observations, *Ocean Science*, *15*(2), 379–399, doi:10.5194/os-15-379-2019.

Pan, R., Q. Shu, Q. Wang, S. Wang, Z. Song, Y. He, and F. Qiao (2023), Future arctic climate change in cmip6 strikingly intensified by nemo-family climate models, *Geophysical Research Letters*, *50*, doi:10.1029/2022GL102077.

Petit, T., M. S. Lozier, S. A. Josey, and S. A. Cunningham (2020), Atlantic deep water formation occurs primarily in the iceland basin and irminger sea by local buoyancy forcing, *Geophysical Research Letters*, *47*, doi:10.1029/2020GL091028.

Polyakov, I. V., A. V. Pnyushkov, M. B. Alkire, I. M. Ashik, T. M. Baumann, E. C. Carmack, I. Goszczko, J. Guthrie, V. V. Ivanov, T. Kanzow, R. Krishfield, R. Kwok, A. Sundfjord, J. Morison, R. Rember, and A. Yulin (2017), Greater role for atlantic inflows on sea-ice loss in the eurasian basin of the arctic ocean, *Science*, *356*, 285–291, doi:10.1126/SCIENCE.AAI8204/SUPPL_FILE/POLYAKOV-SM.PDF.

Pérez-Hernández, M. D., R. S. Pickart, D. J. Torres, F. Bahr, A. Sundfjord, R. Ingvaldsen, A. H. Renner, A. Beszczynska-Möller, W. J. von Appen, and V. Pavlov (2019), Structure, transport, and seasonality of the atlantic water boundary current north of svalbard: Results from a yearlong mooring array, *Journal of Geophysical Research: Oceans*, *124*, doi:10.1029/2018JC014759.

Rahmstorf, S. (2002), Ocean circulation and climate during the past 120,000 years, *Nature*, *419*(1), 207–204, doi:10.1038/nature01090.

Rantanen, M., A. Y. Karpechko, A. Lipponen, K. Nordling, O. Hyvärinen, K. Ruosteenoja, T. Vihma, and A. Laaksonen (2022), The arctic has warmed nearly four times faster than the globe since 1979, *Communications Earth Environment 2022 3:1*, *3*, 1–10, doi:10.1038/s43247-022-00498-3.

Roche, D. M., A. P. Wiersma, and H. Renssen (2010), A systematic study of the impact of freshwater pulses with respect to different geographical locations, *Climate Dynamics*, *34*(7), 997–1013, doi:10.1007/s00382-009-0578-8.

Romé, Y. M., R. F. Ivanovic, L. J. Gregoire, S. Sherriff-Tadano, and P. J. Valdes (2022), Millennial-Scale Climate Oscillations Triggered by Deglacial Meltwater Discharge in Last Glacial Maximum Simulations, *Paleoceanography and Paleoclimatology*, *37*(10), e2022PA004,451, doi:10.1029/2022PA004451.

Rudels, B. (2010), Constraints on exchanges in the arctic mediterranean—do they exist and can they be of use?, *Tellus*, *62A*, 109–122.

Rudels, B. (2015), Arctic ocean circulation, processes and water masses: A description of observations and ideas with focus on the period prior to the international polar year 2007-2009, *Progress in Oceanography*, *132*, doi:10.1016/j.pocean.2013.11.006.

Rudels, B., and E. Carmack (2022), Arctic ocean water mass structure and circulation, *Oceanography*, *35*(3/4), pp. 52–65.

Rudels, B., and D. Quadfasel (1991), Convection and deep water formation in the arctic ocean-greenland sea system, *Journal of Marine Systems*, *2*(3), 435–450, doi:https://doi.org/10.1016/0924-7963(91)90045-V.

Sadatzki, H., T. M. Dokken, S. M. P. Berben, F. Muschitiello, R. Stein, K. Fahl, L. Menviel, A. Timmermann, and E. Jansen (2019), Sea ice variability in the southern norwegian sea during glacial dansgaard-oeschger climate cycles, *Science Advances*, *5*(3), eaau6174, doi:10.1126/sciadv.aau6174.

Seland, Ø., M. Bentsen, D. Olivié, T. Toniazzo, A. Gjermundsen, L. S. Graff, J. B. Debernard, A. K. Gupta, Y. C. He, A. Kirkevåg, J. Schwinger, J. Tjiputra, K. S. Aas, I. Bethke, Y. Fan, J. Griesfeller, A. Grini, C. Guo, M. Ilicak, I. H. H. Karset, O. Landgren, J. Liakka, K. O. Moseid, A. Nummelin, C. Spensberger, H. Tang, Z. Zhang, C. Heinze, T. Iversen, and M. Schulz (2020), Overview of the norwegian earth system model (noresm2) and key climate response of cmip6 deck, historical, and scenario simulations, *Geoscientific Model Development*, *13*, 6165–6200, doi:10.5194/GMD-13-6165-2020.

Sellar, A. A., J. Walton, C. G. Jones, R. Wood, N. L. Abraham, M. Andrejczuk, M. B. Andrews, T. Andrews, A. T. Archibald, L. de Mora, H. Dyson, M. Elkington, R. Ellis, P. Florek, P. Good, L. Gohar, S. Haddad, S. C. Hardiman, E. Hogan, A. Iwi, C. D. Jones, B. Johnson, D. I. Kelley, J. Kettleborough, J. R. Knight, M. O. Köhler, T. Kuhlbrodt, S. Liddicoat, I. Linova-Pavlova, M. S. Mizielinski, O. Morgenstern, J. Mulcahy, E. Neininger, F. M. O'Connor, R. Petrie, J. Ridley, J. C. Rioual, M. Roberts, E. Robertson, S. Rumbold, J. Seddon, H. Shepherd, S. Shim, A. Stephens, J. C. Teixiera, Y. Tang, J. Williams, A. Wiltshire, and P. T. Griffiths (2020), Implementation of u.k. earth system models for cmip6, *Journal of Advances in Modeling Earth Systems*, *12*, e2019MS001,946, doi:10.1029/2019MS001946.

Shen, Z., A. Duan, D. Li, and J. Li (2021), Assessment and ranking of climate models in arctic sea ice cover simulation: From cmip5 to cmip6, *Journal of Climate*, *34*(9), 3609 – 3627, doi:https://doi.org/10.1175/JCLI-D-20-0294.1.

Shu, Q., Q. Wang, M. Årthun, S. Wang, Z. Song, M. Zhang, and F. Qiao (2022), Arctic ocean amplification in a warming climate in cmip6 models, *Science Advances*, *8*, 9755, doi:10.1126/SCIADV.ABN9755/SUPPL_FILE/SCIADV.ABN9755_SM.PDF.

Smedsrud, L. H., I. Esau, R. B. Ingvaldsen, T. Eldevik, P. M. Haugan, C. Li, V. S. Lien, A. Olsen, A. M. Omar, B. Risebrobakken, A. B. Sandø, V. A. Semenov, and S. A. Sorokina (2013), The role of the barents sea in the arctic climate system, *Reviews of Geophysics*, *51*, doi:10.1002/rog.20017.

Smedsrud, L. H., M. Muilwijk, A. Brakstad, E. Madonna, S. K. Lauvset, C. Spensberger, A. Born, T. Eldevik, H. Drange, E. Jeansson, C. Li, A. Olsen, Øystein Skagseth, D. A. Slater, F. Straneo, K. Våge, and M. Årthun (2022), Nordic seas heat loss, atlantic inflow, and arctic sea ice cover over the last century, doi:10.1029/2020RG000725.

Swart, N. C., J. N. Cole, V. V. Kharin, M. Lazare, J. F. Scinocca, N. P. Gillett, J. Anstey, V. Arora, J. R. Christian, S. Hanna, Y. Jiao, W. G. Lee, F. Majaess, O. A. Saenko, C. Seiler,

C. Seinen, A. Shao, M. Sigmond, L. Solheim, K. V. Salzen, D. Yang, and B. Winter (2019), The canadian earth system model version 5 (canesm5.0.3), *Geoscientific Model Development*, *12*, 4823–4873, doi:10.5194/GMD-12-4823-2019.

Taylor, K. E., R. J. Stouffer, and G. A. Meehl (2012), An overview of CMIP5 and the experiment design, doi:10.1175/BAMS-D-11-00094.1.

Tsubouchi, T., K. Våge, B. Hansen, K. M. H. Larsen, S. Østerhus, C. Johnson, S. Jónsson, and H. Valdimarsson (2020), Increased ocean heat transport into the nordic seas and arctic ocean over the period 1993–2016, *Nature Climate Change 2020 11:1*, *11*, 21–26, doi:10.1038/s41558-020-00941-3.

Tsubouchi, T., W.-J. von Appen, T. Kanzow, and L. de Steur (2023), Temporal variability of the overturning circulation in the arctic ocean and the associated heat and freshwater transports during 2004-2010, *Journal of Physical Oceanography*, doi:https://doi.org/10.1175/JPO-D-23-0056.1.

Uenzelmann-Neben, G., and J. Gruetzner (2018), Chronology of greenland scotland ridge overflow: What do we really know?, *Marine Geology*, *406*, 109–118, doi:https://doi.org/10.1016/j.margeo.2018.09.008.

Van Meerbeeck, C. J., H. Renssen, and D. M. Roche (2009), How did marine isotope stage 3 and last glacial maximum climates differ? – perspectives from equilibrium simulations, *Climate of the Past*, *5*(1), 33–51, doi:10.5194/cp-5-33-2009.

Vettoretti, G., P. Ditlevsen, M. Jochum, and S. O. Rasmussen (2022), Atmospheric co2 control of spontaneous millennial-scale ice age climate oscillations, *Nature Geoscience 2022 15:4*, *15*, 300–306, doi:10.1038/s41561-022-00920-7.

Voldoire, A., D. Saint-Martin, S. Sénési, B. Decharme, A. Alias, M. Chevallier, J. Colin, J.-F. Guérémy, M. Michou, M.-P. Moine, P. Nabat, R. Roehrig, D. Salas y Mélia, R. Séférian, S. Valcke, I. Beau, S. Belamari, S. Berthet, C. Cassou, J. Cattiaux, J. Deshayes, H. Douville, C. Ethé, L. Franchistéguy, O. Geoffroy, C. Lévy, G. Madec, Y. Meurdesoif, R. Msadek, A. Ribes, E. Sanchez-Gomez, L. Terray, and R. Waldman (2019), Evaluation of cmip6 deck experiments with cnrm-cm6-1, *Journal of Advances in Modeling Earth Systems*, *11*(7), 2177–2213, doi:https://doi.org/10.1029/2019MS001683.

Våge, K., R. S. Pickart, V. Thierry, G. Reverdin, C. M. Lee, B. Petrie, T. A. Agnew, A. Wong, and M. H. Ribergaard (2009), Surprising return of deep convection to the subpolar north atlantic ocean in winter 2007-2008, *Nature Geoscience*, *2*, 67–72, doi:10.1038/ngeo382.

Våge, K., L. Papritz, L. Håvik, M. A. Spall, and G. W. Moore (2018), Ocean convection linked to the recent ice edge retreat along east greenland, *Nature Communications*, *9*, doi:10.1038/s41467-018-03468-6.

Weijer, W., W. Cheng, O. A. Garuba, A. Hu, and B. T. Nadiga (2020), Cmip6 models predict significant 21st century decline of the atlantic meridional overturning circulation, *Geophysical Research Letters*, *47*, doi:10.1029/2019GL086075.

Weijer, W., T. W. N. Haine, A. H. Siddiqui, W. Cheng, M. Veneziani, and P. Kurtakoti (2022), Interactions between the arctic mediterranean and the atlantic meridional overturning circulation, *SPECIAL ISSUE ON THE NEW ARCTIC OCEAN*, *35*, 118–127, doi:10.2307/2182704.

Wettstein, J. J., and C. Deser (2014), Internal variability in projections of twenty-first-century arctic sea ice loss: Role of the large-scale atmospheric circulation, *Journal of Climate*, *27*, doi:10.1175/JCLI-D-12-00839.1.

Wilson, N. J., and F. Straneo (2015), Water exchange between the continental shelf and the cavity beneath nioghalvfjerdsbræ (79 north glacier), *Geophysical Research Letters*, *42*(18), 7648–7654, doi:https://doi.org/10.1002/2015GL064944.

Wolff, E. W., J. Chappellaz, T. Blunier, S. O. Rasmussen, and A. Svensson (2010), Millennial-scale variability during the last glacial: The ice core record, *Quaternary Science Reviews*, *29*, doi:10.1016/j.quascirev.2009.10.013.

Woodgate, R. A. (2018), Increases in the pacific inflow to the arctic from 1990 to 2015, and insights into seasonal trends and driving mechanisms from year-round bering strait mooring data, *Progress in Oceanography*, *160*, 124–154, doi:https://doi.org/10.1016/j.pocean.2017.12.007.

Yukimoto, S., H. Kawai, T. Koshiro, N. Oshima, K. Yoshida, S. Urakawa, H. Tsujino, M. Deushi, T. Tanaka, M. Hosaka, S. Yabu, H. Yoshimura, E. Shindo, R. Mizuta, A. Obata, Y. Adachi, and M. Ishii (2019), The meteorological research institute earth system model version 2.0, mri-esm2.0: Description and basic evaluation of the physical component, *Journal of the Meteorological Society of Japan. Ser. II*, *97*, 2019–051, doi:10.2151/JMSJ.2019-051.

Zhang, R. (2010), Latitudinal dependence of atlantic meridional overturning circulation (amoc) variations, *Geophysical Research Letters*, *37*(16), doi:https://doi.org/10.1029/2010GL044474.

Zhang, R., and M. Thomas (2021), Horizontal circulation across density surfaces contributes substantially to the long-term mean northern atlantic meridional overturning circulation, *Communications Earth and Environment*, *2*, doi:10.1038/s43247-021-00182-y.

Zhang, R., R. Sutton, G. Danabasoglu, Y.-O. Kwon, R. Marsh, S. G. Yeager, D. E. Amrhein, and C. M. Little (2019), A review of the role of the atlantic meridional overturning

circulation in atlantic multidecadal variability and associated climate impacts, *Reviews of Geophysics*, *57*(2), 316–375, doi:https://doi.org/10.1029/2019RG000644.

Ziehn, T., M. A. Chamberlain, R. M. Law, A. Lenton, R. W. Bodman, M. Dix, L. Stevens, Y.-P. Wang, J. Srbinovsky, T. Ziehn, M. A. Chamberlain, R. M. Law, A. Lenton, R. W. Bodman, M. Dix, L. Stevens, Y.-P. Wang, and J. Srbinovsky (2020), The australian earth system model: Access-esm1.5, *Journal of Southern Hemisphere Earth Systems Science*, *70*, 193–214, doi:10.1071/ES19035.

Zika, J. D., M. H. England, and W. P. Sijp (2012), The ocean circulation in thermohaline coordinates, *Journal of Physical Oceanography*, *42*(5), 708 – 724, doi:10.1175/JPO-D-11-0139.1.

Årthun, M. (2023), Surface-forced variability in the nordic seas overturning circulation and overflows, *Geophysical Research Letters*, *50*(15), e2023GL104,158, doi:https://doi.org/10.1029/2023GL104158, e2023GL104158 2023GL104158.

Årthun, M., T. Eldevik, L. H. Smedsrud, Skagseth, and R. B. Ingvaldsen (2012), Quantifying the influence of atlantic heat on barents sea ice variability and retreat, *Journal of Climate*, *25*, 4736–4743, doi:10.1175/JCLI-D-11-00466.1.

Årthun, M., T. Eldevik, and L. H. Smedsrud (2019), The role of atlantic heat transport in future arctic winter sea ice loss, *Journal of Climate*, *32*, 3327–3341, doi:10.1175/JCLI-D-18-0750.1.

Årthun, M., I. H. Onarheim, J. Dörr, and T. Eldevik (2021), The seasonal and regional transition to an ice-free arctic, doi:10.1029/2020GL090825.

Årthun, M., H. Asbjørnsen, L. Chafik, H. L. Johnson, and K. Våge (2023), Future strengthening of the nordic seas overturning circulation, *Nature Communications*, *14*, doi:10.1038/s41467-023-37846-6.

Errata for
The overturning circulation in a changing Arctic

Anaïs Bretones

Thesis for the degree philosophiae doctor (PhD)
at the University of Bergen

*25/10/23, Anaïs Bretones*___ _27/10/2023__ Ingrid Sollhoy

(date and sign. of candidate) (date and sign. of faculty)

Errata

Acknowledgments:

Missing names… “Johanne, Mats, Vår”

Paper III:

Page 2 Lines 29 and 43 Missing year in the reference Broecker et al. (1990)

Page 5 Line 138 typo: Figure 3a corrected to Figure 2a

Page 5 Line 147 typo: fresherwater corrected to freshwater

Page 7 caption of Figure 2 wrong reference: the caption refers to a section that is not presented in this paper, therefore I added a reference to a previous paper “across the Atlantic and Arctic oceans (as computed in Bretones et al., 2022)” instead of “along the section defined in Figure …”

Page 7 Line 162 typo: Fig 3.1.1b corrected to Fig 2b

Page 8 Line 189 typo: Figure 3c corrected to Figure 3b

Page 11 Line 229 typo: Figure 3.1.1.b corrected to Figure 2b

Graphic design: Communication Division, UiB / Print: Skipnes Kommunikasjon AS

uib.no

ISBN: 9788230844861 (print)
9788230859612 (PDF)